University of Alberta

Structural Elucidation of Thuricin CD, Thurincin H and a Leucocin A Mutant

by

Clarissa Sau-Wei Sit

A thesis submitted to the Faculty of Graduate Studies and Research
in partial fulfillment of the requirements for the degree of

Doctor of Philosophy

Department of Chemistry

Fall, 2011
Edmonton, Alberta

Dedication

For my family

Abstract

Thuricin CD, a two-component bacteriocin produced by *Bacillus thuringiensis* DPC 6431, exhibits potent activity against the hospital superbug *Clostridium difficile* ribotype O27. The two peptides (Trn-α and Trn-β) that constitute thuricin CD operate synergistically to kill sensitive bacteria at nanomolar concentrations. Characterization of Trn-α and Trn-β by mass spectrometry established that each peptide is 6 mass units lighter than predicted from the sequence of its structural gene, suggesting that the peptides undergo post-translational modification. Analysis of nuclear Overhauser effect (NOE) data from NMR experiments run on [^{13}C, ^{15}N]Trn-α and [^{13}C, ^{15}N]Trn-β indicate that each peptide features three sulfur to α-carbon (S-Cα) thioether bridges between Cys5 and residue 28, Cys9 and residue 25, and Cys13 and residue 21. To elucidate the stereochemistry of these bridges, the 3D structures of the eight possible stereoisomers for each peptide were calculated and compared to determine which stereoisomer best fit the NOE data. The most representative structures of Trn-α and Trn-β both feature L-stereochemistry at residue 21 (α-*R*), L-stereochemistry at residue 25 (α-*R*), and D-stereochemistry at residue 28 (α-*S*).

Thurincin H is a single-component bacteriocin produced by *B. thuringiensis* SF361 that is highly active against the human pathogen *Listeria monocytogenes*. Mass spectrometry analysis revealed that thurincin H is 8 mass units lighter than expected from its genetic sequence. NOE experiments on [^{13}C, ^{15}N]thurincin H provided evidence for the presence of four S-Cα bridges in the peptide. Out of the 16 possible stereoisomers, the stereoisomer that features D-

stereochemistry (α-*S*) at all four sulfur-linked α-carbons gave the most representative 3D solution structure of thurincin H.

Leucocin A is an antilisterial bacteriocin with a disulfide bridge between Cys9 and Cys14. Previous studies showed that replacement of the cysteines with phenylalanines had no effect on the peptide's activity, while replacement with serines resulted in complete loss of activity. [^{13}C, ^{15}N]-(C9S, C14S)-leucocin A, produced by heterologous expression, gave an elongated C-terminal α-helix and a disordered N-terminus compared to the 3D structure of wild-type leucocin A, thus providing a potential explanation for the loss in activity. Studies are underway to determine the 3D structure of (C9F, C14F)-leucocin A.

Acknowledgments

The work presented in this thesis is not the result of individual merit, but the culmination of much assistance, kindness and encouragement from many people. I would like to thank my supervisor, Professor John Vederas, for providing me with continual guidance, wisdom and inspiration. Thank you for teaching me to grow and excel beyond even my own expectations. I would also like to thank all the Vederas group members, past and present, for creating an amazing environment to work in. The atmosphere of support, mentorship, camaraderie and good humor has made the lab a truly enjoyable experience, and I will come away from the group with many life-long friends.

I am extremely grateful to Dr. David Dietrich and Dr. Marco van Belkum for their assistance in proofreading this manuscript and offering helpful suggestions. I am indebted to Dr. Leah Martin-Visscher for her incredible patience, time and generosity in teaching me the techniques involved in protein NMR. A very big thank you goes to Dr. Ryan McKay, Mark Miskolzie, and Dr. Pascal Mercier for their kind advice and assistance regarding NMR experiments and structure calculations. I would also like to thank Dr. Randy Whittal, Jing Zheng, and Bela Reiz for their help with mass spectrometry, as well as Dr. Wayne Moffat, David Zinz, and Craig Turk for their assistance with circular dichroism experiments. I would also like to acknowledge Dr. Marco van Belkum and Gareth Lambkin for their advice regarding biological and genetic experiments.

Many other individuals have influenced my growth as a scientist, including the undergraduate students whom I had the great pleasure to supervise.

Thank you to Anna Wiersma, Maude Giroud, Landon Kymson, and Erika Steels for your enthusiasm, optimism, and companionship – you inspire my sense of creativity and remind me of my love for teaching. Thank you also to Dr. Sabesan Yoganathan and Chris Lohans for their work on collaborative research projects not described in this thesis.

Outside of the scientific work, I have also received tremendous assistance from administrative and support staff over the years. Thank you to Christine Otter and Susan Fleming for taking such good care of our group. Through stress and strain, flood and fire, there are always staff to rely on: Sarah Magee, Joe Fiorillo, Laura Pham, Ryan Lewis, Jill Bagwe, Karen McKinley, Bernie Hippel, Andrew Yeung, Marcel Munroe, and Matt Kingston. Thank you for seeing me through the most trying times outside of research. To my friends within and outside of the department, thanks for always listening and believing in me.

Lastly, but most importantly, thank you to my family for their unconditional love and support. To Dad and Mom, you have made my education and my dreams possible, and I will never forget that. Dad, you have inspired me to be inquisitive, confident and curious, and Mom, you have taught me stamina and resilience through your quiet example. Jeremy, thanks for being the best big brother – you have encouraged me to stand on my own feet whenever possible, but you always protect me when I need it. Timothy, thank you for all your sweet kindness and teaching me to see from a different perspective. Matthew, thank you for teaching me more about myself than I thought possible and for motivating me to be the best I can be. Thank you.

Table of Contents

Chapter 1. Sulfur-containing bacteriocins 1

1.1. Significance of bacteriocins 1

1.1.1. Definition and biological importance 1

1.1.2. Use in food preservation and therapeutic applications 3

1.2. Structural classification of bacteriocins 7

1.3. Sulfur-containing bacteriocins 9

1.4. Nisin A 11

1.4.1. Biosynthesis 11

1.4.2. Structure-activity relationship studies 15

1.5. Subtilosin A 17

1.5.1. Biosynthesis 17

1.5.2. Structure-activity relationship studies 23

1.6. Pediocin PA-1 25

1.6.1. Biosynthesis 25

1.6.2. Structure-activity relationship studies 27

1.7. Overview of projects 29

Chapter 2. Thuricin CD 31

2.1. Background 31

2.1.1. Isolation and initial characterization of thuricin CD 31

2.1.2. Significance of thuricin CD activity 33

2.1.3. Biosynthetic gene cluster of thuricin CD 35

2.1.4. Project objectives 37

2.2. Results and discussion 37

2.2.1. Purification of Trn-α and Trn-β 37
2.2.2. Characterization by mass spectrometry 39
2.2.2.a. MS/MS sequencing 39
2.2.2.b. FTICR 40
2.2.3. Production of [^{13}C, ^{15}N]Trn-α and [^{13}C, ^{15}N]Trn-β for NMR 41
2.2.4. Secondary structure prediction via CD and ^{15}N HSQC 43
2.2.5. Structural elucidation of post-translational modifications 44
2.2.5.a. Chemical shift assignments 44
2.2.5.b. Comparison with the chemical shifts of subtilosin A 45
2.2.5.c. NOE analysis of modified residues 46
2.2.5.d. Justification of mass spectrometry findings 48
2.2.6. 3D NMR solution structures of Trn-α and Trn-β 49
2.2.6.a. Design of a modified residue library for CYANA 50
2.2.6.b. Constraints used to create sulfur to α-carbon linkages 54
2.2.6.c. Structure calculations and comparison of stereoisomers 55
2.2.6.d. Trn-α and Trn-β solution structures 59
2.2.6.e. Structural features of Trn-α and Trn-β 62
2.3. Conclusion and future directions 65

Chapter 3. Thurincin H 67

3.1. Background 67
3.1.1. Isolation and initial characterization of thurincin H 67
3.1.2. Biological significance of thurincin H 68
3.1.3. Biosynthetic gene cluster of thurincin H 69
3.1.4. Project objectives 70
3.2. Results and discussion 71
3.2.1. Purification of thurincin H 71

3.2.2. Characterization by FTICR MS and MS/MS sequencing 72

3.2.3. Production of [^{13}C, ^{15}N]thurincin H 72

3.2.4. Secondary structure prediction via CD and ^{15}N HSQC 74

3.2.5. Structural elucidation of post-translational modifications 76

3.2.5.a. Chemical shift assignments 76

3.2.5.b. NOE analysis of modified residues 76

3.2.6. NMR solution structure of thurincin H 77

3.2.6.a. Structure calculations and comparison of stereoisomers 77

3.2.6.b. Structural features of thurincin H 82

3.3. Conclusion and future directions 84

Chapter 4. Double serine mutant of leucocin A 86

4.1. Background 86

4.1.1. Structure and biological activity of leucocin A 86

4.1.2. Biosynthetic gene cluster of leucocin A 87

4.1.3. NMR structure of leucocin A 88

4.1.4. Structure-activity relationship studies of leucocin A 90

4.1.5. Project objectives 92

4.2. Results and discussion 92

4.2.1. Heterologous expression of (C9S, C14S)-leucocin A 92

4.2.2. Purification of unlabeled and [^{13}C, ^{15}N]-labeled (C9S, C14S)-leucocin A 96

4.2.3. Activity testing of (C9S, C14S)-leucocin A 100

4.2.4. 3D NMR solution structure of (C9S, C14S)-leucocin A 101

4.2.4. Chemical shift assignments and structure calculations 101

4.2.4.b. Structural features 104

4.2.4.c. Structural comparison with wild-type leucocin A 105

4.3. Conclusions and future directions 106

Chapter 5. Future perspectives 108

Chapter 6. Experimental procedures 110

6.1. General methods..... 110

6.1.1. Culture conditions..... 110

6.1.2. Instrumentation used for protein purification 110

6.1.3. Instrumentation used for genetic manipulations..... 111

6.1.4. Peptide characterization..... 112

6.1.4.a. MALDI-TOF MS..... 112

6.1.4.b. Circular dichroism 112

6.1.4.c. NMR..... 113

6.2. Experimental procedures for the structural studies of thuricin CD 113

6.2.1. Purification of Trn-α and Trn-β..... 113

6.2.2. Activity testing of Trn-α and Trn-β..... 115

6.2.3. MS/MS sequencing and MALDI FTICR MS analysis..... 116

6.2.4. Production of [^{13}C, ^{15}N]Trn-α and [^{13}C, ^{15}N]Trn-β 116

6.2.5. Circular dichroism analysis of Trn-α and Trn-β 118

6.2.6. NMR spectroscopy of [^{13}C, ^{15}N]Trn-α and [^{13}C, ^{15}N]Trn-β..... 118

6.2.7. Modification of CYANA program 121

6.2.8. Structure calculations..... 122

6.3. Experimental procedures for the structural studies of thurincin H..... 123

6.3.1. Purification of thurincin H..... 123

6.3.2. Activity testing of thurincin H..... 124

6.3.3. MS/MS sequencing and MALDI FTICR MS analysis..... 124

6.3.4. Production of [^{13}C, ^{15}N]thurincin H..... 125

6.3.5. Circular dichroism analysis of thurincin H..... 126

6.3.6. NMR spectroscopy of [^{13}C, ^{15}N]thurincin H 126

6.3.7. Modification of CYANA program 127

6.3.8. Structure calculations 128

6.4. Experimental procedures for the production and structural elucidation of a double serine mutant of leucocin A 129

6.4.1. Construction of pMAL.FXA.(C9S, C14S)LeuA 129

6.4.2. Screening for desired clones in transformed *E. coli* JM109 131

6.4.3. Overexpression and isolation of (C9S, C14S)-leucocin A 133

6.4.4. Factor Xa digestion pilot study 134

6.4.5. Purification of (C9S, C14S)-leucocin A 135

6.4.6. Activity testing of (C9S, C14S)-leucocin A 136

6.4.7. Test growth of *E. coli* JM109 transformants in M9 minimal media 136

6.4.8. Transformation of *E. coli* BL21(DE3) 137

6.4.9. Production of [^{13}C, ^{15}N]-(C9S, C14S)-leucocin A 138

6.4.10. NMR spectroscopy of [^{13}C, ^{15}N]-(C9S, C14S)-leucocin A 138

6.4.11. Structure calculations 139

Chapter 7. References 141

Appendix A. Thuricin CD NMR data and CYANA files 162

Appendix B. Thurincin H MS, NMR data and CYANA files 172

Appendix C. (C9S, C14S)-leucocin A NMR data 179

List of Tables

Table 1: Classification scheme for bacteriocins suggested by Cotter *et al*. 8

Table 2: Exact masses and proposed formulae for Trn-α and its fragments 40

Table 3: Exact masses and proposed formulae for Trn-β and its fragments 41

Table 4: ^{13}C and ^{1}H chemical shift assignments of the Trn-α modified residues 45

Table 5: ^{13}C and ^{1}H chemical shift assignments of the Trn-β modified residues. 45

Table 6: Chemical shifts of modified Thr from Trn-α, Trn-β, and subtilosin A.. 46

Table 7: Comparison of statistics generated by the 8 stereoisomers of Trn-α..... 58

Table 8: Comparison of statistics generated by the 8 stereoisomers of Trn-β 59

Table 9: Structural statistics for Trn-α LLD and Trn-β LLD 60

Table 10: Chemical shifts of the modified residues in thurincin H..... 76

Table 11: Constraint violations generated by each stereoisomer of thurincin H . 79

Table 12: Comparison of statistics generated by stereoisomers of thurincin H ... 80

Table 13: Structural statistics for thurincin H (DDDD) 81

Table 14: Primers used for constructing the (C9S, C14S)-leucocin A gene insert 95

Table 15: Structural statistics for (C9S, C14S)-leucocin A 103

Table 16: Experimental parameters used to acquire NMR spectra on [^{13}C, ^{15}N]Trn-α to obtain chemical shift assignments, coupling constants, and NOE restraints..... 119

Table 17: Experimental parameters used to acquire NMR spectra on [^{13}C, ^{15}N]Trn-β to obtain chemical shift assignments, coupling constants, and NOE restraints..... 120

Table 18: Experimental parameters used to acquire NMR spectra on [^{13}C, ^{15}N]thurincin H to obtain chemical shift assignments, coupling constants, and NOE restraints..... 127

Table 19: Experimental parameters used to acquire NMR spectra on [^{13}C, ^{15}N]-(C9S, C14S)-leucocin A to obtain chemical shift assignments, coupling constants, and NOE restraints..... 139

Table A1: ^{1}H Chemical shift assignments of Trn-α……...162

Table A2: ^{1}H Chemical shift assignments of Trn-β……163

Table A3: Nitrogen and carbon chemical shift assignments of Trn-α……164

Table A4: Nitrogen and carbon chemical shift assignments of Trn-β……165

Table A5: NOE correlations between the Cys and modified residues of Trn-α.166

Table A6: NOE correlations between the Cys and modified residues of Trn-β.166

Table B1: MS/MS sequencing results for thurincin H……172

Table B2: ^{1}H Chemical shift assignments of thurincin H……...173

Table B3: Nitrogen and carbon chemical shift assignments of thurincin H…...174

Table B4: NOEs between the Cys and modified residues of thurincin H……...175

Table C1: ^{1}H Chemical shift assignments of (C9S, C14S)-leucocin A……..179

Table C2: Nitrogen and carbon chemical shift assignments of (C9S, C14S)-leucocin A……...180

List of Figures

Figure 1. Two examples of structurally diverse bacteriocins. (A) A diagram representing nisin A. 3

Figure 2. Diagrams representing the structures of lacticin 3147, gallidermin, and cinnamycin. 6

Figure 3. Intramolecular bridges found in sulfur-containing bacteriocins. 10

Figure 4. The eleven genes involved in the biosynthesis of nisin. 11

Figure 5. A schematic illustrating the biosynthesis of nisin. 12

Figure 6. A depiction of the enzymatic dehydration and cyclization of the precursor peptide to form the N-terminal Dhb, Dha and Lan residues of nisin. 13

Figure 7. Diagram representing the structure of subtilosin. 17

Figure 8. The biosynthetic gene cluster of subtilosin. 18

Figure 9. A possible mechanism for the reductive cleavage of SAM. 19

Figure 10. A proposed mechanism for the formation of sulfur to α-carbon thioether linkages by AlbA.. 20

Figure 11. A cartoon representation of the 3D solution structure of subtilosin A.. 21

Figure 12. The biosynthetic gene cluster of pediocin PA-1. 26

Figure 13. A schematic representing the biosynthesis of pediocin PA-1 26

Figure 14. The biosynthetic gene cluster of thuricin CD. 36

Figure 15. MALDI-TOF spectrum of Trn-α and Trn-β. 38

Figure 16. Activity testing of Trn-α and Trn-β against an indicator strain. 39

Figure 17. The sequences of Trn-α and Trn-β, as determined by infusion MS/MS. 40

Figure 18: MALDI-TOF spectrum of [^{13}C, ^{15}N]Trn-α and [^{13}C, ^{15}N]Trn-β..... 42

Figure 19. CD spectra of Trn-α and Trn-β in 80% TFE/ 10% MeOH/ 10% H_2O. 43

Figure 20. ^{15}N HSQC of Trn-α and Trn-β. 44

Figure 21. (A) Two strips of ^{1}H-^{1}H data taken from a ^{13}C HSQC-NOESY experiment of Trn-β. (B) Diagram indicating the NOE correlations observed between protons. 47

Figure 22: Diagram representing the proposed connectivity of residues in Trn-α and Trn-β. 48

Figure 23: A proposed mechanism for the cleavage of a sulfur to α-carbon linkage during MS/MS fragmentation 49

Figure 24. Nomenclature used by CYANA to define the atoms in a serine residue, and alteration of that nomenclature to reflect the loss of the Hα in the modified serine. 51

Figure 25. Diagram showing the dihedral angles that orient the backbone and side chain atoms of a serine residue. 51

Figure 26. A description of serine in the residue library of CYANA. 52

Figure 27. A description of modified serine with L-stereochemistry (MSER) that was added to the residue library of CYANA. 53

Figure 28. A description of modified serine with D-stereochemistry (DSER) that was added to the residue library of CYANA. 53

Figure 29. Creation of sulfur to α-carbon linkages in CYANA..... 55

Figure 30. The chemical structures of Trn-α and Trn-β 56

Figure 31. Cartoon representation of the three-dimensional solution structures of Trn-α (LLD isomer) and Trn-β (LLD isomer). 60

Figure 32. Backbone overlay of the 20 lowest energy conformers of Trn-α LLD and Trn-β LLD..... 62

Figure 33. Stick representation of Trn-α LLD and Trn-β LLD, illustrating most of the side chains pointing outward. 63

Figure 34. Surface hydrophobicity of Trn-α LLD and Trn-β LLD. 64

Figure 35. Electrostatic surface potential of Trn-α LLD and Trn-β LLD. 65

Figure 36. The biosynthetic gene cluster of thurincin H. 69

Figure 37. Characterization of thurincin H by MALDI-TOF MS and activity testing. 71

Figure 38. The sequence of thurincin H, as determined by infusion nanoESI MS/MS and MALDI MS/MS.. 72

Figure 39. MALDI-TOF spectrum of partially [^{13}C, ^{15}N]-labeled thurincin H.... 74

Figure 40. CD spectrum of thurincin H in 100% MeOH. 75

Figure 41. ^{15}N HSQC spectrum of thurincin H. 75

Figure 42. Diagram representing the connectivity of residues in thurincin H. 77

Figure 43. The chemical structure of thurincin H 78

Figure 44. Cartoon representation of the 3D solution structure of thurincin H (DDDD isomer). 81

Figure 45. Backbone overlay of the 20 lowest energy conformers of thurincin H (DDDD isomer). 81

Figure 46. Stick representation of thurincin H, illustrating most of the side chains pointing outward 82

Figure 47. Cartoon representation of thurincin H, showing the interaction of Thr29 with Trp5. 83

Figure 48. Electrostatic surface potential and surface hydrophobicity of thurincin H 84

Figure 49. Diagram representing the structure of leucocin A. 86

Figure 50. The biosynthetic gene cluster of leucocin A 88

Figure 51. The 3D NMR structure of leucocin A in TFE. 89

Figure 52. (A) Diagram representing the structure of carba-leucocin A; (B) Structures of serine, phenylalanine, allylglycine, and norvaline used to replace Cys9 and Cys14 to generate (C9S, C14S)-leucocin A, (C9F, C14F)-leucocin A, diallyl-leucocin A, and norvaline-leucocin A, respectively. 91

Figure 53. A diagram representing the desired sequence for the (C9S, C14S)-leucocin A gene of interest and a schematic representing the use of two long, overlapping primers to construct the full-length template of the gene of interest. 94

Figure 54. A schematic of the procedure to build the MalE–(C9S, C14S)-LeuA construct. 96

Figure 55. SDS-PAGE gel showing expression of protein in transformed JM109 cells before and up to 3 h after induction. 97

Figure 56. SDS-PAGE gel of a FXa digest of MBP–(C9S, C14S)-leucocin A during different time points 98

Figure 57. MALDI-TOF spectrum of (C9S, C14S)-leucocin A 99

Figure 58. MALDI-TOF spectrum of [^{13}C, ^{15}N]-(C9S, C14S)-leucocin A..... 100

Figure 59. Activity testing (by spot-on-lawn assay) of (C9S, C14S)-leucocin A against *C. maltaromaticum* UAL26, *C. divergens* LV13, *L. lactis* cremoris HP, and *L. monocytogenes* ATCC 43256. 101

Figure 60. ^{15}N HSQC spectrum of (C9S, C14S)-leucocin A. 102

Figure 61. Cartoon representation of the 3D solution structure of (C9S, C14S)-leucocin A.. 103

Figure 62. Backbone overlay of the 20 lowest energy conformers of (C9S, C14S)-leucocin A 104

Figure 63. Electrostatic surface potential and surface hydrophobicity of (C9S, C14S)-leucocin A 105

Figure A1. A description of modified alanine with L-stereochemistry (MALA) that was added to the residue library of CYANA……...167

Figure A2. A description of modified alanine with D-stereochemistry (DALA) that was added to the residue library of CYANA……...167

Figure A3. A description of modified threonine with L-stereochemistry (MTHR) that was added to the residue library of CYANA……...168

Figure A4. A description of modified threonine with D-stereochemistry (DTHR) that was added to the residue library of CYANA……...168

Figure A5. A description of modified tyrosine with L-stereochemistry (MTYR) that was added to the residue library of CYANA……...169

Figure A6. A description of modified tyrosine with D-stereochemistry (DTYR) that was added to the residue library of CYANA……...170

Figure A7. An example of a complete sequence file used in the structure calculations of a Trn-β stereoisomer……..171

Figure B1. A description of modified asparagine with L-stereochemistry (MASN) that was added to the residue library of CYANA……...176

Figure B2. A description of modified asparagine with D-stereochemistry (DASN) that was added to the residue library of CYANA……...176

Figure B3. The lower limit constraints files of a thurincin H isomer…….177

Figure B4. The upper limit constraints files of a thurincin H isomer…….177

Figure B5. An example of a complete sequence file used in the structure calculations of a thurincin H stereoisomer…….178

List of Abbreviations

3D	three-dimensional
A or Ala	alanine
aa	amino acid
ABC	ATP-binding cassette
AEBSF	4-(2-aminoethyl) benzenesulfonyl fluoride hydrochloride
amp	ampicillin
APT	all purpose tween
ATCC	American Type Culture Collection
ATP	adenosine triphosphate
BHI	brain heart infusion
C or Cys	cysteine
CD	circular dichroism
CDI	*Clostridium difficile* infection
CFS	cell-free supernatant
D or Asp	aspartic acid / aspartate
***d_3*-TFE**	deuterated trifluoroethanol (CF_3CD_2OD)
DNA	deoxyribonucleic acid
dNTP	deoxynucleotide triphosphate
DSS	2,2-dimethyl-2-silapentane-5-sulfonate sodium salt
DTT	± dithiothreitol
E or Glu	glutamic acid / glutamate

EDTA	ethylenediaminetetraacetic acid
EII_t^{man}	mannose permease complex of the man-PTS system
EtOH	ethanol
F or Phe	phenylalanine
FTICR	Fourier transform ion cyclotron resonance
FXa	Factor Xa
G or Gly	glycine
H or His	histidine
HCCA	α-cyano-4-hydroxycinamic acid
HSQC	heteronuclear single quantum coherence
I or Ile	isoleucine
IPA	2-propanol / isopropyl alcohol
IPTG	isopropyl-β-D-thiogalactopyranoside
K or Lys	lysine
L or Leu	leucine
LAB	lactic acid bacteria
LB	Luria-Bertani
LeuA	leucocin A
M or Met	methionine
MALDI-TOF	matrix assisted laser desorption ionization time of flight
malE	maltose binding protein gene
man-PTS	mannose phosphotransferase system
MeOH	methanol

mptAB	structural gene for the IIAB protein of the EII_t^{man} permease
mptC	structural gene for the IIC protein of the EII_t^{man} permease
mptD	structural gene for the IID protein of the EII_t^{man} permease
MRSA	methicillin resistant *Staphylococcus aureus*
MS	mass spectrometry
MS/MS	tandem mass spectrometry
MW	molecular weight
MWCO	molecular weight cut-off
N or Asn	asparagine
NMR	nuclear magnetic resonance
NOE	nuclear Overhauser effect / enhancement
NOESY	NOE spectroscopy
OD_{600}	optical density measured at 600 nm
P or Pro	proline
PAGE	polyacrylamide gel electrophoresis
PCR	polymerase chain reaction
PDB	Protein Data Bank
Q or Gln	glutamine
R or Arg	arginine
rmsd	root mean square deviation
RP-HPLC	reverse phase high performance liquid chromatography
rpm	revolutions per minute
S or Ser	serine

S-Cα	sulfur to α-carbon thioether bridge
SDS	sodium dodecyl sulfate
SDS-PAGE	sodium dodecyl sulfate poly acrylamide gel electrophoresis
SPE	solid phase extraction
T or Thr	threonine
TBE	tris-borate EDTA
TFA	trifluoroacetic acid
TFE	trifluoroethanol
TOCSY	total correlation spectroscopy
Tris-HCl	tris(hydroxymethyl)aminomethane hydrochloride
TSB	tryptic soy broth
V or Val	valine
VRE	vancomycin resistant enterococci
W or Trp	tryptophan
WDA	well diffusion assay
Y or Tyr	tyrosine

Chapter 1. Sulfur-containing bacteriocins

1.1. Significance of bacteriocins

1.1.1. Definition and biological importance

Bacteriocins are ribosomally synthesized antimicrobial peptides produced by bacteria as a method to compete against other organisms in their immediate environment. Many bacteriocins bind to specific receptors within or on the cell surface of sensitive bacteria, giving each bacteriocin a defined spectrum of activity.[1, 2] The producer will typically synthesize bacteriocins that kill closely related strains of bacteria in a bid to out-compete them for limited environmental resources. To protect itself, the producer will concomitantly generate immunity proteins against its own bacteriocins.[2-6]

To maintain the sensitivity of other bacteria towards its bacteriocins, many producer strains will only synthesize the peptides under conditions of high cell-density. Specifically, a bacterium will make use of signaling molecules to detect the presence of other bacteria and, as bacterial cell-density rises, will induce the production of its bacteriocins.[7, 8] By controlling the amount of time that sensitive strains are exposed to specific bacteriocins, it may limit the development of resistance mechanisms.

In spite of this controlled production, resistance against bacteriocins can still develop. For example, some bacteria can produce proteolytic enzymes that degrade bacteriocins, while others produce cell surface transporters that remove the peptides from the cell membrane.[9, 10] These microorganisms will also change the lipid composition of its cell membranes to alter the net charge of some of its

phospholipids, thus decreasing the electrostatic attraction of the bacteriocins to its cell surface.[11] As such, bacteria are constantly evolving new bacteriocins to counteract the resistance mechanisms established by their competitors. To date, hundreds of structurally diverse peptides comprise the class of known bacteriocins, with many others yet to be isolated and characterized (**Figure 1**). Since most bacteriocins are able to exhibit a well-defined spectrum of activity, often at nanomolar concentrations, they possess great potential for use in food preservation and human therapeutics.

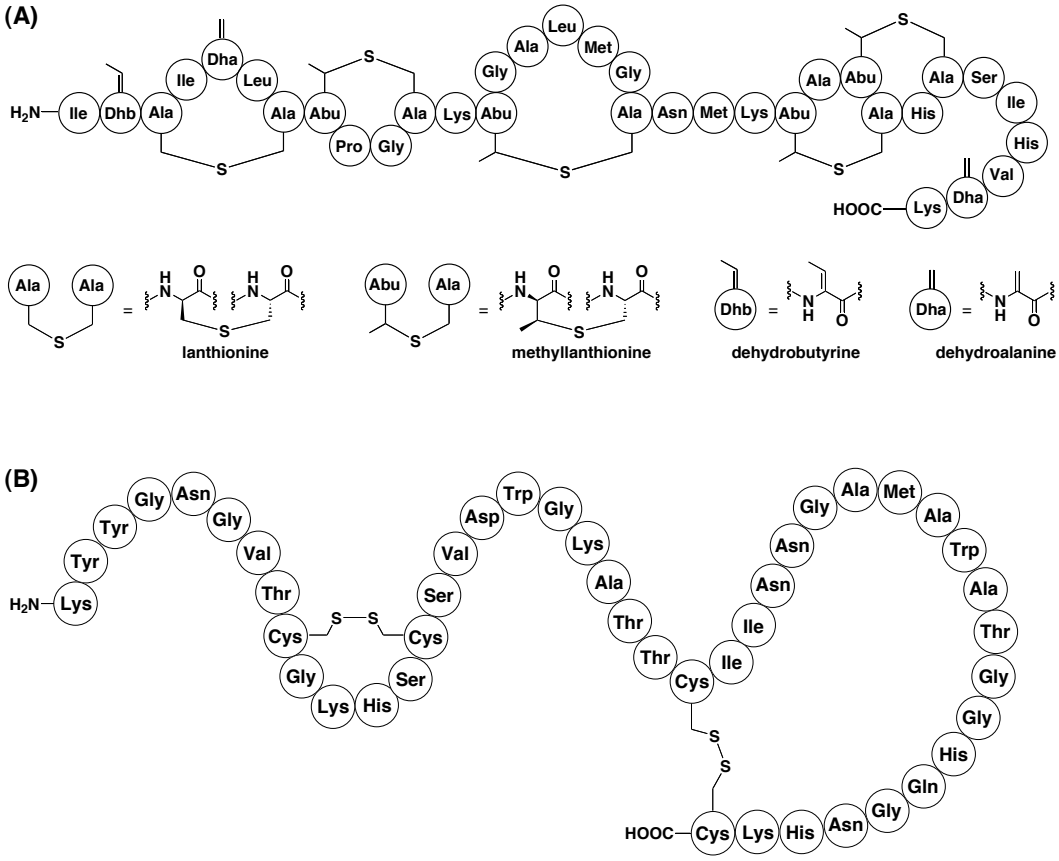

Figure 1. Two examples of structurally diverse bacteriocins. (A) A diagram representing nisin A. The chemical structures of its unusual amino acid residues (lanthionine, methyllanthionine, dehydrobutyrine and dehydroalanine) are also shown. (B) A diagram representing pediocin PA-1, which features two disulfide bridges in its structure.

1.1.2. Use in food preservation and therapeutic applications

Many bacteriocins have been found to exhibit desirable traits for applications in food preservation: they are heat stable, highly active against specific strains of food-borne pathogens, and are non-toxic to humans when ingested.[1] These traits make them compatible with pasteurization, canning, and fermentation, amongst other food processing techniques. One of the most widely used bacteriocins in food preservation is nisin A (**Figure 1A**), a peptide produced

by the food-grade organism *Lactococcus lactis*. Approved for use in over 50 countries, nisin or its producer organism is frequently added to dairy products such as yogurt, milk and cheese to inhibit a wide range of harmful Gram-positive bacteria, including *Staphylococcus aureus*.[1,12] Another bacteriocin, pediocin PA-1 (**Figure 1B**), from *Pediococcus acidilactici*, is commonly used in food products to prevent the growth of *Listeria monocytogenes*, a pathogen that can cause miscarriages in pregnant women and fatal infections in immunocompromised individuals.[1] One drawback of the food-grade bacteriocins is that many of these peptides cannot penetrate the outer membrane of Gram-negative bacteria, rendering them inactive against organisms such as *Escherichia coli* and *Salmonella enterica*. In spite of this disadvantage, numerous studies have found that addition of chelating agents such as ethylenediaminetetraacetic acid (EDTA) can weaken the outer membrane, allowing nisin and other bacteriocins to pass through, bind to specific targets in the inner membrane, and kill the Gram-negative bacteria.[13-16] These findings suggest that co-treatment with other agents or structural modification of the bacteriocins themselves could confer Gram-negative activity to these peptides and expand their utility as food preservatives.[17]

A number of bacteriocins also exhibit activity against drug-resistant strains of bacteria, making them highly attractive as potential therapeutic agents. Nisin is known to inhibit methicillin-resistant *Staphylococcus aureus* (MRSA), while lacticin 3147, a structurally related two-component bacteriocin (**Figure 2**), can kill multidrug-resistant *Clostridium difficile*.[12, 18] Since most front-line antibiotics have been exhausted against MRSA and *C. difficile*, both of which are highly

contagious and cause infections associated with high mortality rates, nisin and lacticin serve as appealing candidates for alternative therapy. In order to develop these bacteriocins into drugs, however, several issues still need to be addressed, including the peptides' susceptibility to proteolytic degradation, pH instability, and potential toxicities toward epithelial cells.[19, 20] To circumvent these problems, researchers are actively investigating methods to encapsulate the bacteriocins for targeted delivery to the sites of infection.[18, 21]

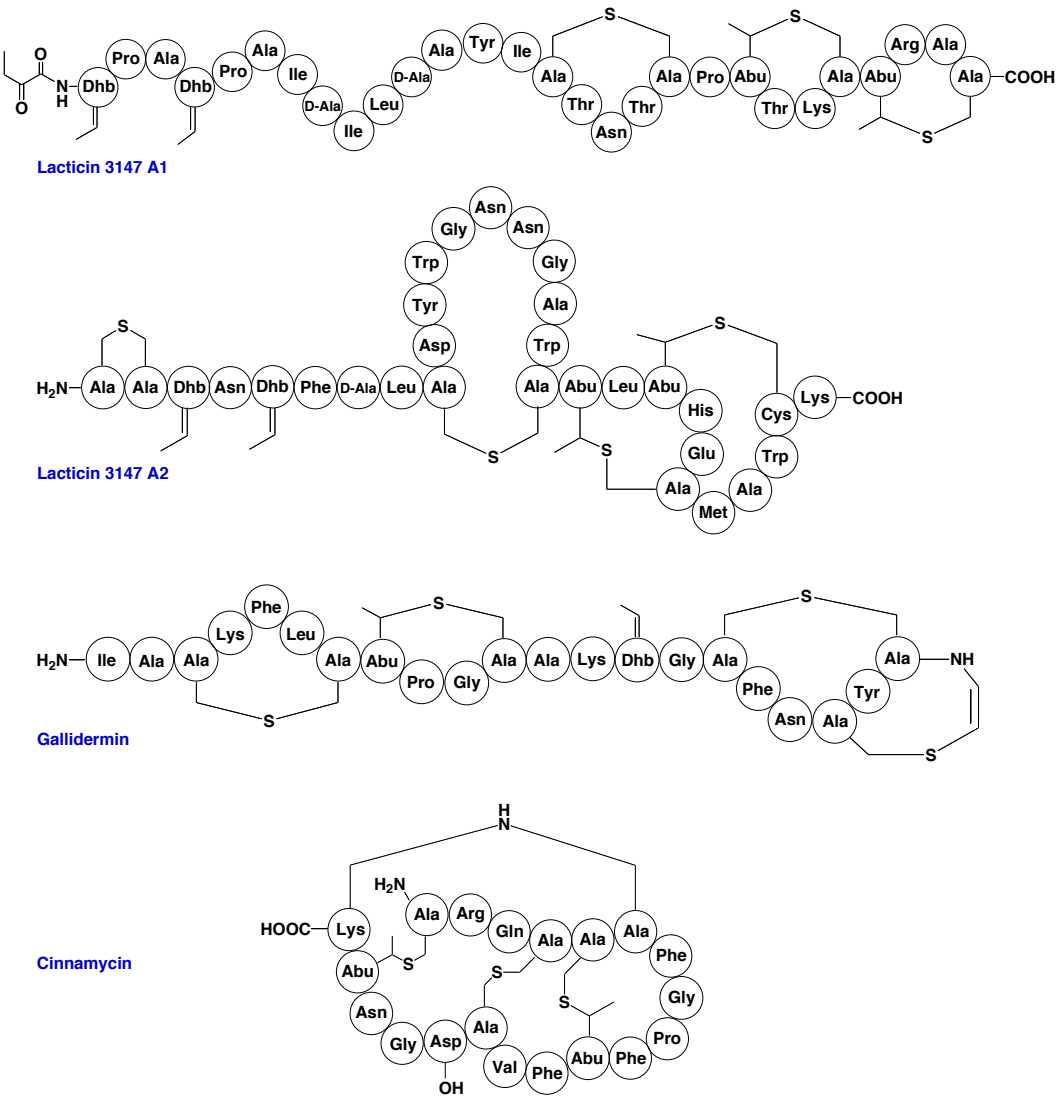

Figure 2. Diagrams representing the structures of lacticin 3147 (which consists of two components named A1 and A2), gallidermin, and cinnamycin.

Another bacteriocin that shows greater promise as a human therapeutic is gallidermin (**Figure 2**), which is produced by *Staphylococcus gallinarum*. It is non-toxic to mammalian cells, stable at skin pH (5.4), and active against staphylococci, streptococci and *Propionibacterium acnes*, making gallidermin ideal as a topical treatment for acne.[12, 19, 22]

Beyond antimicrobial activity, some bacteriocins exhibit other useful physiological effects. Cinnamycin (**Figure 2**) can inhibit human phospholipase A2 and angiotensin converting enzyme, making it potentially useful in the treatment of inflammation and high blood pressure.[12, 23] In addition to its antibacterial activity, lacticin 3147 has been found to be spermicidal. It can immobilize mammalian sperm in less than 30 s during *in vitro* assays, suggesting that it could serve as an effective contraceptive agent.[24]

Collectively, the full potential of bacteriocins has yet to be realized in human and agricultural applications. Although most bacteriocins exhibit potent and unique biological activities, the physical and pharmacological properties of these peptides need to be optimized in order to improve their utility. Since the chemical structure of a bacteriocin governs its biological activity and physical stability, there is a fundamental need to elucidate the native structures of bacteriocins. Once the structure of a bacteriocin is established, it can be selectively modified by chemical synthesis, genetic mutation, or *in vitro* biosynthesis to alter its natural properties, with the eventual goal of developing the peptide into an effective drug.[25, 26]

1.2. Structural classification of bacteriocins

Bacteriocins are a structurally diverse class of molecules. Produced by both Gram-positive and Gram-negative bacteria, bacteriocins can range in size from 2 kDa to upwards of 70 kDa.[25, 27] Some bacteriocins feature only standard amino acids encoded by the universal genetic code, while other bacteriocins feature unusual amino acids that arise from post-translational modification. The

remaining sections of this chapter will focus on a subset of Gram-positive produced bacteriocins that exhibit clinically useful biological activity.

Several schemes had been proposed in the literature for the classification of bacteriocins produced by Gram-positive bacteria. Most of these schemes divided the peptides into different groups according to their structures (**Table 1**). Traditionally, the lantibiotics, peptides that feature lanthionine (Lan) and methyllanthionine (MeLan) residues, constituted the class of post-translationally modified bacteriocins (class I), while all other bacteriocins were loosely classified as unmodified peptides (class II).[1, 28]

Table 1: Classification scheme for bacteriocins suggested by Cotter *et al*.[1]

Classification	Description	Examples
Class I	Lanthionine-containing bacteriocins (lantibiotics)	Nisin A Lacticin 3147 Gallidermin Cinnamycin
Class II	Non-lanthionine containing bacteriocins	Pediocin PA-1 Leucocin A Carnocyclin A Subtilosin A

Over time, as new bacteriocins were discovered, it became clear that certain peptides did not fit into the classification scheme. For example, circular bacteriocins, such as carnocyclin A, do not feature any unusual amino acids, but have their backbones cyclized at the N and C-termini through a post-translational modification.[29-31] The lack of Lan or MeLan residues in circular bacteriocins precludes the peptides from being included into the class I lantibiotics; at the same

time, the formation of the cyclized backbone suggests that the circular bacteriocins do not belong in class II. The circular bacteriocins, along with other newly characterized bacteriocins, challenge the currently established classification systems. With the huge diversity of structure and biosynthetic pathways that typify the bacteriocins, future attempts to classify these peptides into different categories may need to be based on a combination of structural features and on phylogenetic studies: grouping bacteriocins together according to their evolutionary relatedness as well as their common structural features may provide a more meaningful and robust classification scheme.

1.3. Sulfur-containing bacteriocins

All classifications aside, much scientific interest has developed regarding the study of sulfur-containing bacteriocins produced by Gram-positive bacteria. Most of the sulfur-containing bacteriocins characterized to date exhibit potent activity against medically significant pathogens, such as MRSA, *C. difficile* and *L. monocytogenes*. Interestingly, outside of methionine residues, the sulfur atoms in these bacteriocins are able to form intramolecular bridges that play a key role in shaping the mechanisms of action of these peptides. As a result, extensive research has been devoted towards understanding how these sulfur bridges are biosynthesized and how altering their structures will affect the bacteriocins' biological activity.

The intramolecular bridges in sulfur-containing bacteriocins can be divided into three distinct motifs: lanthionine-like bridges, sulfur to α-carbon

bridges, and disulfide bridges (**Figure 3**).[2, 3, 22, 32] By definition, lanthionine-like bridges are featured exclusively in the lantibiotics. However, in addition to Lan and MeLan residues, certain lantibiotics are known to contain disulfide bridges as well.[33-36] The sulfur to α-carbon bridge is a relatively rare crosslink that has, thus far, been discovered in only one bacteriocin, subtilosin A.[32, 37] In comparison, disulfide bridges are more common, featuring prominently in the non-lantibiotic, pediocin-like bacteriocins. The pediocin class is a group of unmodified peptides that rely heavily on the presence of disulfide bonds to effect its antimicrobial activity.

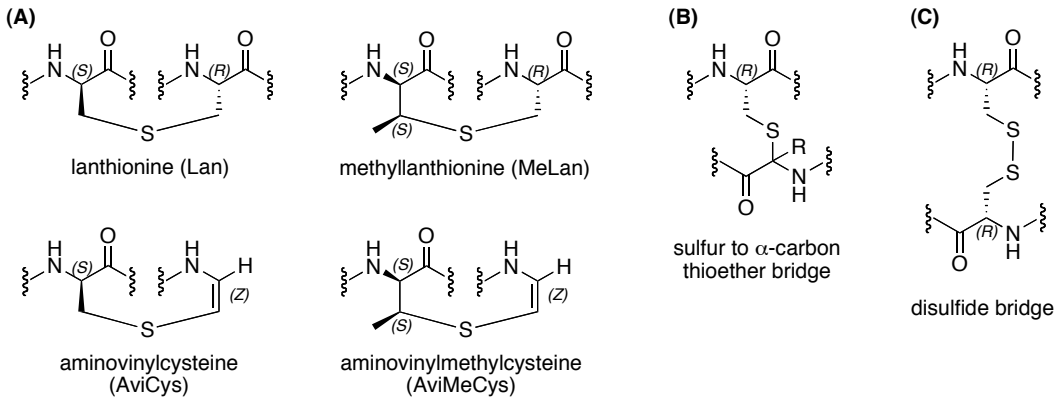

Figure 3. Intramolecular bridges found in sulfur-containing bacteriocins: (A) lanthionine-like bridges, (B) a sulfur to α-carbon bridge, where R represents the side chain of an amino acid residue, and (C) a disulfide bridge.

In the subsequent sections of this chapter, an example of a bacteriocin containing each type of intramolecular sulfur bridge will be discussed. An overview of the biosynthesis and structure activity-relationship (SAR) studies of nisin A, subtilosin A and pediocin PA-1 will be presented.

1.4. Nisin A

1.4.1. Biosynthesis

Nisin A is the most well studied example of the lantibiotics. The biosynthesis of its one Lan and four MeLan rings, as well as its dehydrobutyrine (Dhb) and two dehydroalanine (Dha) residues, has been thoroughly investigated. The genes that encode for the production of nisin are clustered together along a stretch of DNA that has been organized into operon-like structures (**Figure 4**).[3, 5, 38, 39] Operon-like structures are functional units of DNA that contain multiple genes under the control of a single regulatory DNA sequence called a promoter. When the promoter is activated, all genes within the operon will be transcribed and, thus, expressed together.

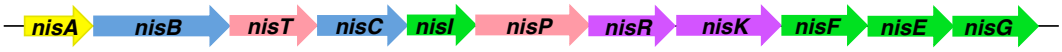

Figure 4. The eleven genes involved in the biosynthesis of nisin: *nisA* (yellow) encodes for the precursor peptide; *nisB*, *nisC* (blue) lead to the formation of unusual amino acids in the precursor; *nisT*, *nisP* (pink) are involved in the cleavage of the leader peptide and secretion of nisin; *nisI*, *nisFEG* (green) afford immunity to the producer organism; and *nisR*, *nisK* (purple) regulate nisin production.

The biosynthesis of nisin begins with the production of a linear precursor peptide from the *nisA* gene. The precursor consists of an N-terminal 23 amino acid leader preceding the C-terminal 34-residue propeptide that will eventually form the structure of nisin (**Figure 5**). The leader has several proposed functions, including serving as a recognition sequence for the machinery that post-

translationally modifies the precursor peptide, as well as maintaining the bacteriocin in an inactive state until final processing and secretion occurs.[40]

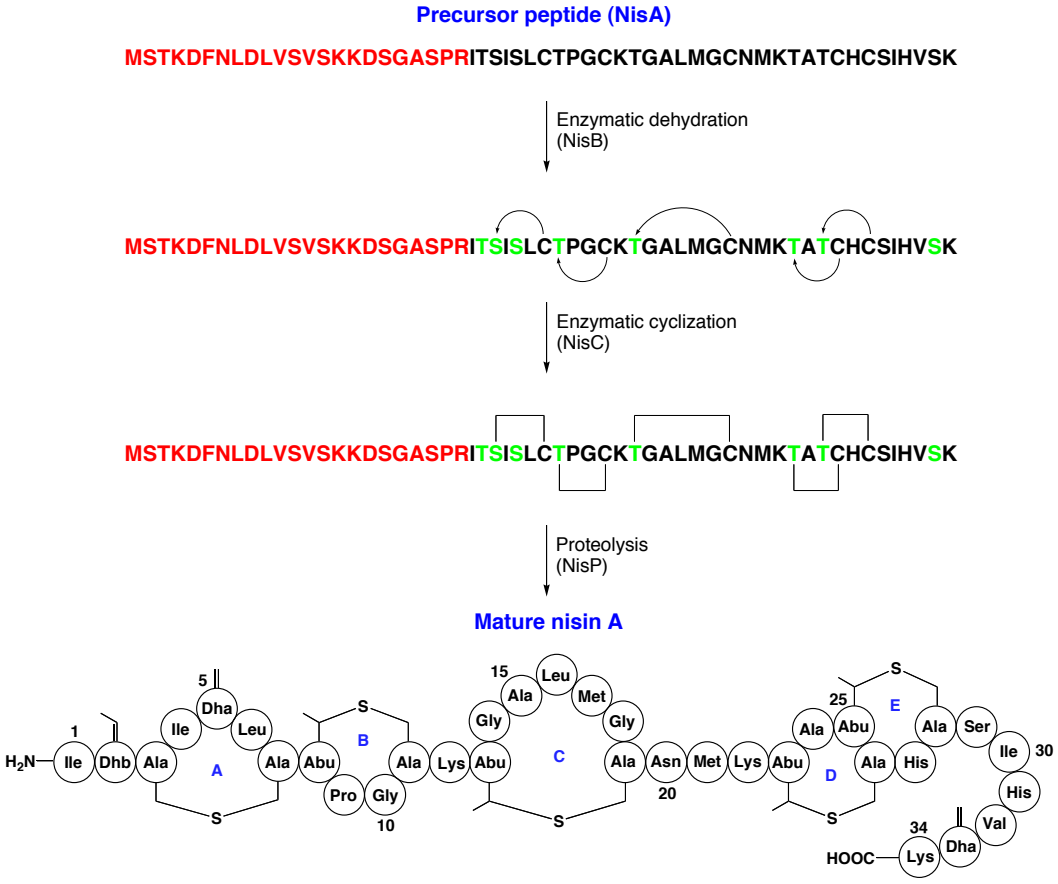

Figure 5. A schematic illustrating the biosynthesis of nisin. The precursor peptide NisA, which consists of a leader portion (red) and propeptide portion (black), undergoes processing by NisB to dehydrate selected Thr and Ser residues to Dhb and Dha residues (green). Cyclization of Cys residues onto specific Dha and Dhb residues by NisC forms the Lan and MeLan rings in the propeptide. Proteolytic cleavage by NisP subsequently removes the leader peptide to produce mature nisin (the Lan ring is labeled as "A" while the four MeLan rings are labeled "B" through "E") (figure adapted from Chatterjee *et al.*[3]).

The precursor peptide undergoes its first set of post-translational modifications when it binds to NisB, the enzyme encoded by the *nisB* gene. NisB is a dehydratase that selectively dehydrates some of the Ser and Thr residues of

the propeptide into Dha and Dhb residues, respectively. The NisC cyclase then catalyzes the stereo- and regioselective Michael addition of cysteine thiol groups onto Dha or Dhb to form the five Lan or MeLan rings of nisin (**Figure 6**).[41] The specific binding of the leader peptide to NisB and NisC is thought to guide the sequence recognition and selectivity exhibited by both enzymes.[3]

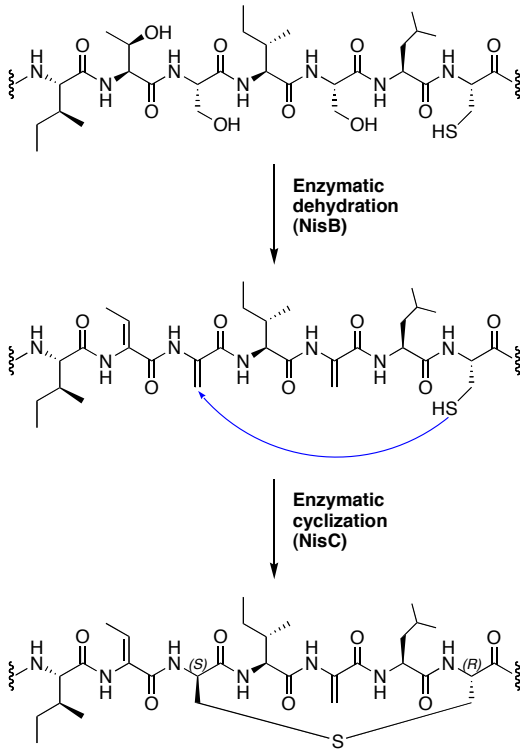

Figure 6. A depiction of the enzymatic dehydration and cyclization of the precursor peptide to form the N-terminal Dhb, Dha and Lan residues of nisin.

After the unusual amino acid residues have been formed in the precursor peptide, the leader sequence is cleaved off as the mature bacteriocin is exported from the bacterial cell. These final stages of processing are carried out by the gene products of *nisT* and *nisP*. NisP is a serine protease that removes the leader

peptide, while NisT is an ATP-binding cassette (ABC) transporter that hydrolyzes adenosine-5′-triphosphate (ATP) as it transports nisin out of the cell.[3]

To protect itself from the bactericidal activity of nisin, the *L. lactis* producer organism employs two different immunity mechanisms that are encoded for by the *nisI* and *nisFEG* genes.[6, 42] NisI is an immunity protein that operates extracellularly: it is either secreted as a soluble protein or anchored to the external face of the lipid membrane.[43, 44] It acts by physically binding to nisin, effectively sequestering the bacteriocin away from the cell surface. NisFEG forms the three domains of an ABC-transporter, which provides an alternate mechanism of immunity by actively removing any nisin molecules that have inserted into the cytoplasmic membrane.

The biosynthetic gene cluster of nisin also encodes for two proteins, NisK and NisR, that help regulate the production of the bacteriocin. Both of these proteins are constitutively expressed and upregulate the transcription of *nisABTCIP* (and possibly *nisFEG* as well) upon the detection of extracellular nisin. NisK is a histidine protein kinase (HPK) sensor that spans the cytoplasmic membrane of the producer organism. When the extracellular domain of NisK detects the presence of nisin, its intracellular HPK domain autophosphorylates a histidine residue in its C-terminus. It then transfers this phosphoryl group to an aspartate residue on the intracellular NisR protein, which serves as a response regulator (RR). Once phosphorylated, NisR will bind to the promoter that controls *nisABTCIP* transcription, thus activating the expression of these genes. The mechanism of this sensory response system indicates that nisin not only acts as a

bacteriocin, but also functions as an autoinducing hormone to stimulate its own production.[6, 45]

Understanding the structure and biosynthesis of nisin has, in turn, led to extensive SAR studies on the bacteriocin to determine which residues are essential for antimicrobial activity. Using techniques such as directed mutagenesis and chemical modification, a large number of nisin analogues have been generated with the aim of isolating peptides with increased potencies, increased stability, and broader spectra of activity.

1.4.2. Structure-activity relationship studies

The antimicrobial activity of nisin is guided by its specific binding to a receptor molecule on the surface of sensitive bacteria. Nisin binds to lipid II, a precursor for cell wall biosynthesis.[46] In Gram-positive bacteria, the cell wall forms the outermost layer, enveloping the cytoplasmic membrane of the cells. The proposed mode of action for nisin begins with the peptide docking to lipid II through its N-terminal Lan and MeLan rings (rings A and B), followed by insertion of its C-terminal half into the cytoplasmic membrane.[47] Upon binding of additional molecules of nisin, several lipid II/bacteriocin complexes can come together to form pores in the cytoplasmic membrane. Nisin can thus stop the growth of bacteria by sequestering lipid II and inhibiting cell wall biosynthesis, and it can kill bacteria by forming pores and causing leakage of cytoplasmic contents.[3]

Numerous SAR studies have been carried out on nisin, many of which have been previously reviewed in depth.[3, 12, 42, 48, 49] In brief, it was found that

removal of the five C-terminal residues of nisin resulted in a 10-fold reduction in potency. Further removal of rings D and E by enzymatic digestion caused a 100-fold decrease in potency. If ring C was also cut off, leaving the N-terminal rings A and B intact, the peptide lost all antimicrobial activity and became antagonistic to full-length nisin due to competition for lipid II binding sites.[50]

The most successful variants of nisin generated by directed mutagenesis contained mutations in the residues of ring A. Introduction of aromatic residues and positively charged lysine into the ring helped maintain or improve the activity of the peptides. In fact, the double mutant I4K/L6I and triple mutant I4K/S5F/L6I exhibited increased potency against indicator strains compared to wild-type nisin. On the other hand, mutations to ring B were not well tolerated, at times because the mutations prevented the enzymatic cyclization of Cys11 onto Dhb8. Disruption of the MeLan ring closure resulted in a dramatic loss of activity in these mutants.[51]

Mutations in the flexible hinge region between rings C and D have also generated analogues with improved antimicrobial activity. The M21V mutant was found to have the greatest change in activity, showing increased levels of potency against many strains of bacteria including MRSA, *L. monocytogenes*, *C. difficile*, and vancomycin-resistant enterococci (VRE).[52, 53]

The promising findings from these recent SAR studies on nisin suggest that there is great potential in tailoring bacteriocins into more active and stable peptide drug candidates. In addition to nisin, similar research is ongoing with regard to other lantibiotics. Techniques such as solid phase peptide synthesis

(SPPS) and *in vitro* mutasynthesis (use of biosynthetic enzymes to modify chemically synthesized prepeptides) have been used to generate analogues of lacticin 3147, lacticin 481, and haloduracin.[25, 35, 54-56] With multiple strategies being used to study the SAR of different lantibiotics, the developments in this field will help expand the applications of these bacteriocins in food preservation and therapeutics.

1.5. Subtilosin A

1.5.1. Biosynthesis

Subtilosin A is a 35 amino acid residue peptide produced by *Bacillus subtilis* that is active against *L. monocytogenes* and numerous other bacteria.[57, 58] Through extensive mass spectrometry and solution nuclear magnetic resonance (NMR) studies, it was established that subtilosin features a cyclized backbone and three sulfur to α-carbon (S-Cα) thioether bridges (**Figure 7**).[32, 37]

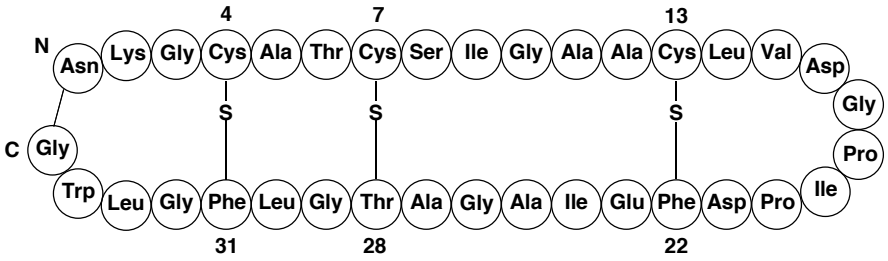

Figure 7. Diagram representing the structure of subtilosin.

Although the biosynthetic gene cluster of subtilosin has been sequenced, the enzymatic mechanisms involved in the production of this bacteriocin have yet to

be elucidated. The operon for subtilosin biosynthesis contains nine genes, including the *sboA* gene, which encodes for the subtilosin precursor peptide, and seven *alb* (or 'antilisterial bacteriocin') genes (**Figure 8**).[59, 60]

Figure 8. The biosynthetic gene cluster of subtilosin: *sboA* (yellow) encodes for the precursor peptide; *albA* (red) produces an enzyme thought to form the sulfur to α-carbon thioether bridges; *albB* (green) affords immunity; *albC*, *albD* (pink) enable subtilosin to be secreted from the cell; *albE*, *albF* (blue) are potentially involved in cleaving the leader and cyclizing the propeptide; and *sboX* (white) and *albG* (grey) have unknown functions.

The SboA peptide consists of an N-terminal 8-residue leader and a C-terminal 35-residue propeptide. Compared to the leader peptides of nisin and many other bacteriocins, the SboA leader is significantly shorter, prompting speculation about its exact role in the biosynthesis and secretion of mature subtilosin.[30] As of yet, it is uncertain when the leader peptide is cleaved off during subtilosin production and, thus, whether the leader serves as a recognition sequence for all of the enzymes that carry out the post-translational modifications.

The *sboX* gene overlaps with *sboA*: when the reading frame alignment for *sboA* is shifted over by a single nucleotide, a second start codon can be found that could represent the beginning of another gene transcript. The resulting *sboX* gene potentially encodes for the precursor of a class II bacteriocin, as its leader sequence shows homology to those of the class II bacteriocins. However, the predicted gene product of *sboX* has never been observed and disruption of the

gene itself does not affect subtilosin production. As such, *sboX* has no known function with regards to subtilosin biosynthesis.[60]

Amongst the *alb* genes, *albA*, *albE,* and *albF* are thought to be responsible for the post-translational modification of SboA.[60] AlbA shows sequence homology to other enzymes in the radical *S*-adenosylmethionine (SAM) superfamily of proteins. A common feature of this superfamily is the presence of cysteine triads arranged in a C-X_3-C-X_2-C motif that typically coordinates a [4Fe-4S] iron-sulfur cluster.[61] AlbA possesses two of these cysteine motifs, one in its N-terminal domain and the other in its C-terminal domain, and is therefore thought to contain two [4Fe-4S] centers.[60] Each [4Fe-4S] center will reductively cleave a molecule of SAM to generate a radical species that can be subsequently used by the enzyme to catalyze specific reactions (**Figure 9**).[62]

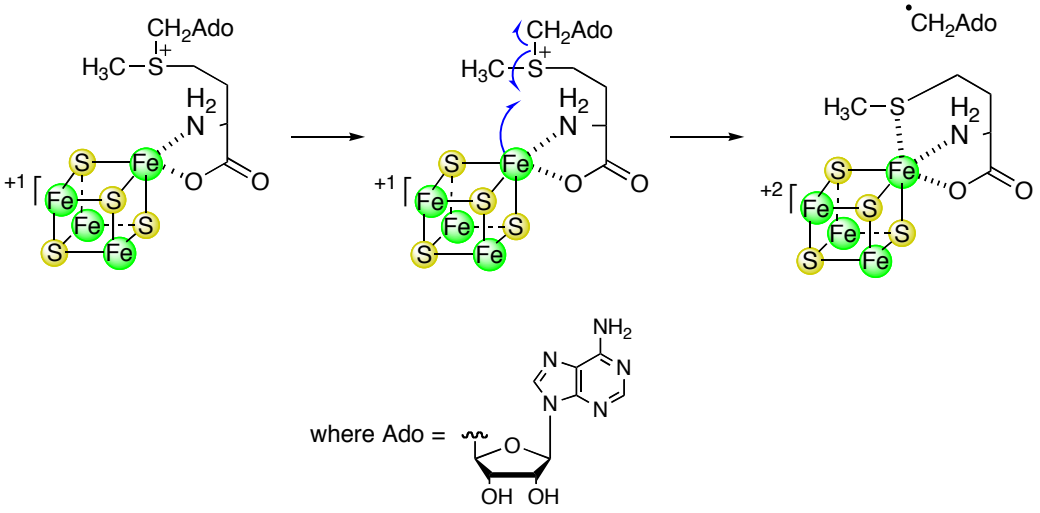

Figure 9. A possible mechanism for the reductive cleavage of SAM: SAM coordinates to the iron-sulfur cluster via its α-amino and carboxylate groups and, upon electron transfer from the [4Fe-4S] center, splits into methionine and a 5′-deoxyadenosine radical.

In AlbA, we propose that this radical species (5′-deoxyadenosine) is used to abstract a hydrogen atom from a cysteine thiol in the subtilosin propeptide (**Figure 10**). The resulting thiyl radical could remove the α-hydrogen from a downstream residue held in close proximity within the enzyme's active site. Oxidation of the regenerated thiol by an electron-deficient [4Fe-4S] center, followed by loss of a proton, would produce a diradical that could close to form a new S-Cα bond. In this manner, the three intramolecular S-Cα thioether linkages in subtilosin could be formed.

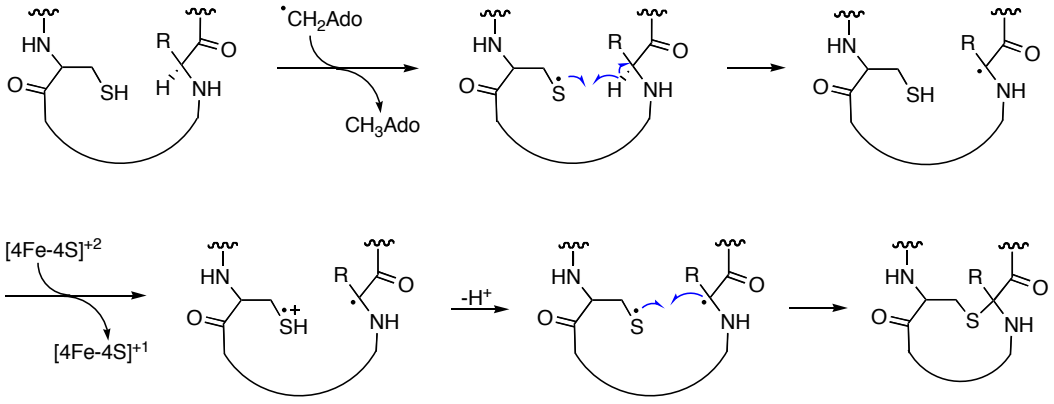

Figure 10. A proposed mechanism for the formation of sulfur to α-carbon thioether linkages by AlbA. "R" represents the side chain of the residue.

Although each of the crosslinking residues has an L-configuration prior to modification, there is currently no method available for predicting the stereochemistry of the resulting S-Cα bond. Because the reaction is thought to proceed via a diradical intermediate, rapid bond rotation in the substrate could occur leading to a radical inversion prior to the formation of the S-Cα bond.[63] Factors that could affect this stereochemical outcome include the conformation of

the enzyme active site, as well as the size and conformation of the amino acid side chain of the residue undergoing modification. Interestingly, the 3D structure of subtilosin (**Figure 11**) has been elucidated using solution NMR studies.[32, 37] The stereochemistry of its modified residues was established by comparing structure calculations of all eight possible stereoisomers to determine which isomer fit the NMR data the best and generated a family of structures with the lowest energy.[32] From the 3D structure, subtilosin is proposed to have L-stereochemistry at Phe22 (α-R), D-stereochemistry at Thr28 (α-S) and D-stereochemistry at Phe31 (α-S) (LDD isomer).[32]

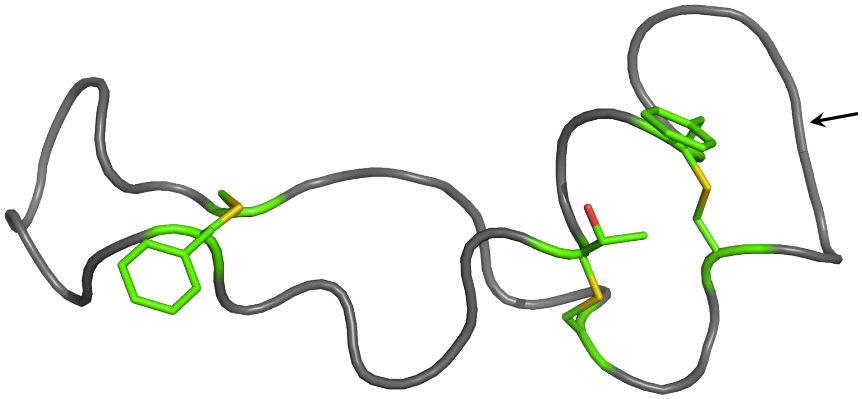

Figure 11. A cartoon representation of the 3D solution structure of subtilosin A. Yellow highlights the sulfur atoms and red highlights the oxygen atom in the side chains of the crosslinked residues. The peptide bond between the N- and C-termini are indicated by the arrow. This figure was generated using the PDB file 1PXQ.

Aside from the formation of thioether bridges, cleavage of the N-terminal leader and cyclization of the backbone are required to produce mature subtilosin. In this respect, AlbE and AlbF are thought to form a heterodimer that performs

these functions. Indeed, the N-terminal half of AlbF shows sequence homology to known zinc metalloproteases, suggesting that it may be responsible for cleaving the N-terminal leader of SboA.[31, 60]

Much investigation is still required to elucidate and confirm the enzymatic mechanisms of AlbA, AlbE and AlbF. Thus far, mutational analysis of the *sbo-alb* operon has been used to establish the possible functions of these genes. Mutations in *albA* and *albF* abolished the production of subtilosin altogether, while mutations in *albE* lead to a significant reduction in the antilisterial activity of the producer organism.[60] In order to fully understand the biosynthesis of subtilosin, however, AlbA, AlbE and AlbF will need to be heterologously expressed and purified for use in *in vitro* assays. Feeding synthetic SboA substrates to these enzymes will help answer several questions, including whether AlbA acts on SboA prior to, or following, AlbE/AlbF, and whether the presence of the leader peptide is necessary for the cyclization and thioether bridge formation to occur.

The four other genes in the biosynthetic cluster for subtilosin were also analyzed using sequence comparisons and mutational studies. It was determined that *albB* encodes for an immunity protein and *albC*/*albD* produce the components of an ABC-transporter.[60] Sequence homology suggests that AlbC serves as an ATP-binding domain while AlbD forms the membrane-spanning domain of the transporter. Mutations in either *albC* or *albD* increase the sensitivity of the producer organism to subtilosin, indicating that the ABC-transporter may function in both bacteriocin secretion and immunity. The last gene in the operon, *albG*, is also thought to encode for a membrane protein.

Although disruption of this gene leads to a significant decrease in the production of active subtilosin, the function of AlbG remains unknown.[60] Future studies on the *sbo-alb* operon, as well as the Alb proteins, will afford greater insight into subtilosin biosynthesis, export and immunity.

1.5.2. Structure-activity relationship studies

Subtilosin is thought to bind to the cytoplasmic membranes of Gram-positive bacteria in order to exert its antimicrobial activity. Studies have been performed using fluorescence spectroscopy, differential scanning calorimetry, and solid-state NMR spectroscopy to probe the mode of action of subtilosin when it interacts with model lipid bilayers and small unilamellar vesicles (SUVs).[64, 65] It was found that the peptide can partially insert into phospholipid bilayers and mildly disrupt the hydrophobic core of the membrane. As well, subtilosin can induce dye leakage from SUVs, but only at concentrations far above its minimum inhibitory concentration (MIC) values for sensitive bacteria.[64] These findings suggest that subtilosin binds to a specific receptor on the cell surface of its target strains.[30] Further investigation will be required to identify this receptor and determine how it facilitates the mechanism of action of this bacteriocin.

Due to the limited understanding of its biosynthesis and the significant synthetic challenges posed by its sulfur to α-carbon thioether bridges, *in vitro* mutasynthesis and SPPS approaches have yet to be employed in the SAR studies of subtilosin. Instead, chemical modification, enzymatic degradation, and directed

mutagenesis have been used to generate subtilosin analogues for biological evaluation.

In its native form, subtilosin is acid stable and highly resistant to proteolytic degradation.[57, 58] Only upon reductive cleavage of the sulfur to α-carbon bridges is the peptide rendered susceptible to enzymatic digestion.[32, 57] As well, after subtilosin was desulfurized using a nickel boride reaction, the peptide was found to be inactive, suggesting that the thioether linkages are essential for maintaining the physical stability and antimicrobial activity of the bacteriocin.[32]

Mutational SAR studies on subtilosin gave rise to intriguing results. Directed mutagenesis was used to generate a T6I mutant, which was found to exhibit a 2- to 10-fold enhancement in activity against *L. monocytogenes*, *Enterococcus faecalis*, *Streptococcus pyogenes*, and a range of bacilli.[66] Interestingly, the replacement of Thr6 for Ile also conferred hemolytic activity on the mutant.[66] This improved potency and new ability to disrupt the cytoplasmic membranes of mammalian red blood cells may have resulted from an increase in the peptide's overall hydrophobicity, or a more specific alteration to its mechanism of action. Since the sixth residue of subtilosin immediately precedes a thioether-forming cysteine, modifications at this position could affect the specific binding of the bacteriocin to its target receptors. Similar to the findings from the bioengineering of nisin, future studies involving the mutational scanning of each residue in subtilosin may allow researchers to isolate peptides with optimized antimicrobial and pharmacological properties.

1.6. Pediocin PA-1

1.6.1. Biosynthesis

As mentioned earlier, pediocin PA-1 is another antilisterial bacteriocin that is 44 residues in length. It does not contain any unusual amino acids, but features two disulfide bridges in its structure. Pediocin has been isolated from numerous strains of bacteria, including *P. acidilactici*, and is thus known by multiple names, such as pediocin PA-1 and pediocin AcH.[67]

The biosynthetic gene cluster of pediocin is relatively simple compared to those of nisin and subtilosin, and contains only four genes (**Figure 12**).[68] The structural gene *pedA* encodes for the pediocin precursor, which has an N-terminal 18-residue leader preceding the 44-residue propeptide (**Figure 13**). The leader peptide is thought to play several roles in the biosynthesis of the bacteriocin.[69] It may serving as a signaling sequence to track the peptide to the cytoplasmic membrane, as well as a recognition sequence for the ABC-transporters that cleave the leader off during export of the mature bacteriocin. The leader may also play a key role in maintaining the precursor in a folded, inactive state prior to export from the cell.

After ribosomal synthesis and disulfide bond formation, PedA undergoes further processing by PedD, an ABC-transporter that cleaves off the leader peptide before secreting the mature pediocin from the cell.[70] PedB serves as an immunity protein, protecting the producer organism from the bactericidal effects of its own bacteriocin. Although PedC is classified as an accessory protein that is

thought to be necessary for pediocin secretion, its function has yet to be fully established.[67]

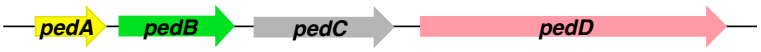

Figure 12. The biosynthetic gene cluster of pediocin PA-1: *pedA* (yellow) encodes for the precursor peptide; *pedB* (green) affords immunity; *pedD* (pink) is responsible for the N-terminal processing and secretion of the bacteriocin; and *pedC* (grey) has an unknown function.

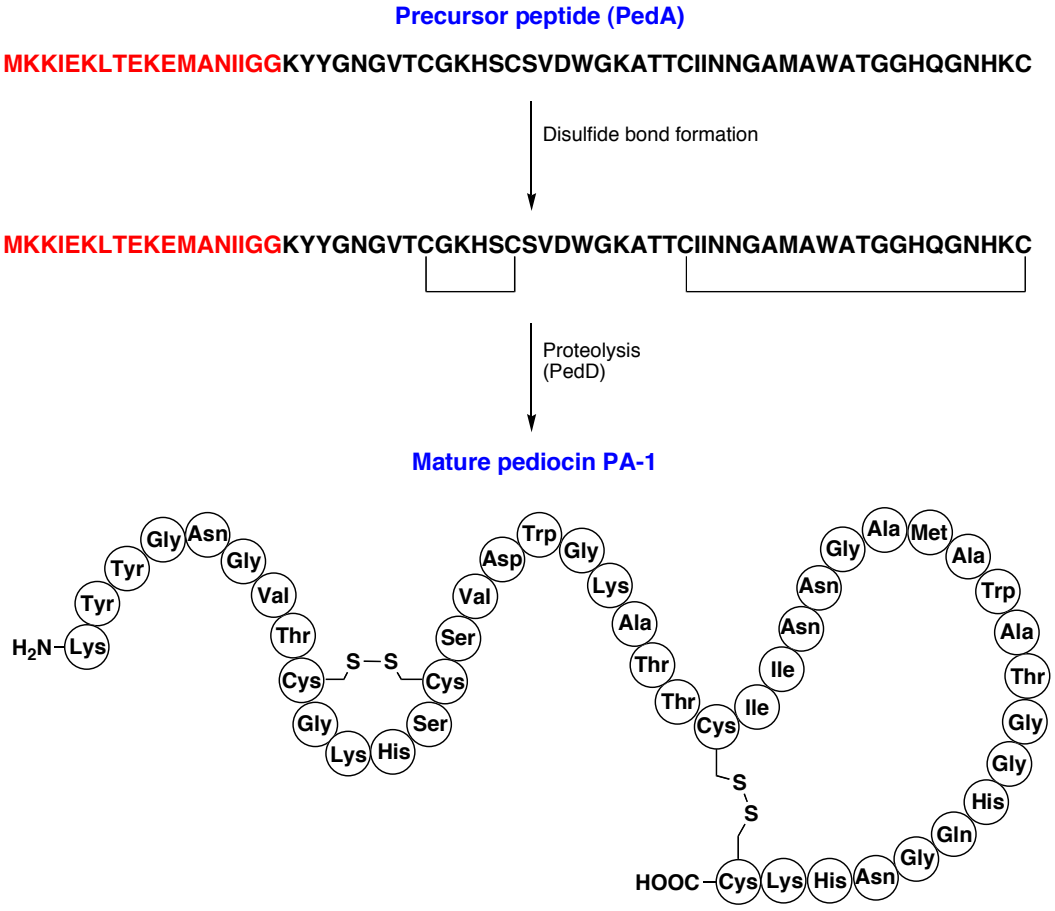

Figure 13. A schematic representing the biosynthesis of pediocin PA-1. After translation of the precursor peptide PedA (leader = red, propeptide = black), two disulfide bonds are formed within the propeptide segment. Subsequent proteolysis of the leader by PedD generates mature pediocin PA-1.

1.6.2. Structure-activity relationship studies

The amino acid sequence in the N-terminal region of pediocin is highly conserved amongst all of the pediocin-like bacteriocins and includes the disulfide bridge between Cys9 and Cys14 as well as a characteristic Y-G-N-G-V stretch. The first 16 residues of the peptide form a cationic and hydrophilic three-stranded β-sheet. Due to its charged nature, the N-terminal segment of pediocin is thought to help target the molecule to the anionic surface of bacterial cell membranes.[67]

A number of SAR studies have established that the C-terminal domain of the pediocin-like bacteriocins governs the target specificity and spectrum of activity of the peptides.[2, 71] One of the most interesting experiments involved the creation of hybrid bacteriocins, where genetic recombination was used to fuse together the N- and C-terminal domains of different pediocin-like peptides. Each hybrid showed the same spectrum of activity as the parent bacteriocin from which its C-terminal domain was derived.[71] These findings suggest that the antimicrobial activity of pediocin could be tailored for specific strains of bacteria by modifying the sequence of its C-terminal domain.

Once the bacteriocin binds to the cytoplasmic membrane, the amphipathic and α-helical C-terminal domain of pediocin will insert into the lipid bilayer and interact with a specific receptor, namely enzyme II permease (EII_t^{man}) of the mannose phosphotransferase system (man-PTS).[72] The man-PTS of bacteria imports and phosphorylates mannose and glucose, with EII_t^{man} serving as the membrane transporter. EII_t^{man} consists of three domains: a cytoplasmic domain (IIAB) and two membrane-bound domains (IIC and IID). The C-terminal portion

of pediocin recognizes and binds to the IIC and IID subunits of EII_t^{man}, before aggregating together to form pores that cause cytoplasmic leakage and, ultimately, cell death.[2, 67]

The functional role of the disulfide bonds in pediocin PA-1 was also investigated. Replacement of the N-terminal cystine with hydrophobic residues such as allyl glycine and phenylalanine completely abolished the activity of the peptide.[73] This indicates that the Cys9-Cys14 disulfide bridge in pediocin may play an essential role in maintaining the conformation of the N-terminal domain and in targeting the peptide to the surface of bacterial cell membranes. The use of hydrophobic interactions to mimic disulfide linkages in pediocin-like bacteriocins will be discussed in greater depth in Chapter 4.

Another investigation used directed mutagenesis to replace the C-terminal cystine of pediocin with serine residues. This C24S, C44S double mutant exhibited significantly decreased potency and temperature stability, as well as a narrower spectrum of activity compared to wild-type pediocin.[74] These results imply that this second disulfide bridge, which is absent in many of the other pediocin-like bacteriocins, makes the peptide more potent, heat stable and versatile as a food preservative. Further engineering of pediocin PA-1 to replace the readily oxidized Met31 with Ala, Ile or Leu has generated promising analogues with increased stability.[75] The knowledge accrued from the SAR studies on pediocin provide an avenue for optimizing its potential in food and agricultural applications.

1.7. Overview of projects

From a scientific perspective, much is still unknown about sulfur containing bacteriocins. The biosynthesis, mechanism of action and evolutionary importance of many of these peptides have yet to be fully understood. The projects described in this thesis will focus on the characterization and structural elucidation of sulfur-containing bacteriocins that exhibit antimicrobial activity against clinically significant pathogens.

Chapter 2 will describe the structural characterization of thuricin CD, a two-component bacteriocin that is highly active against *C. difficile*. The presence of three post-translational modifications in each of the two peptides was established through detailed mass spectrometry analyses. Multi-dimensional, heteronuclear NMR experiments were then used to determine the nature of these post-translational modifications. The 3D solution structures of the two peptides will be presented, confirming the chemical connectivity of the atoms in each molecule as well as indicating the stereochemistry at the α-carbon of each modified residue.

Chapter 3 will detail the structural elucidation of thurincin H, a single-component bacteriocin with activity against *L. monocytogenes*. Amino acid sequencing of the peptide using mass spectrometry techniques determined the positions of four post-translational modifications in the peptide. Heteronuclear NMR studies were also performed to generate the 3D structure of thurincin H, complete with the proposed stereochemistry of the four intramolecular bridges.

The sequence similarity of thurincin H to other bacteriocins reported in the literature will be discussed.

Chapter 4 will make use of solution NMR structures to justify the findings from the SAR studies of leucocin A, a pediocin-like antilisterial peptide. A Cys → Ser double mutant of leucocin was produced using molecular cloning and heterologous expression. Heteronuclear NMR experiments were performed on this biologically inactive mutant. The 3D solution structure of the double serine mutant will be compared to the structure of wild type leucocin to determine whether removal of the disulfide bridge leads to a significant conformational change that would explain the loss of activity.

The 3D structures of bacteriocins, as determined by solution NMR studies, provide a foundation for investigating the mechanisms of action of these peptides. Gaining a better understanding of how bacteriocins are employed by bacteria to target each other may, in turn, shed light on new methods to overcome the drug resistance observed in many virulent pathogens.

Chapter 2. Thuricin CD

2.1. Background

Much of the following chapter has been adapted from our publications on the isolation and structural characterization of thuricin CD.[61, 76]

2.1.1. Isolation and initial characterization of thuricin CD

Thuricin CD was discovered by our collaborators, Ross and Hill at University College Cork, during a screen of 30,000 bacterial isolates obtained from human fecal samples. The screening was performed using *C. difficile* ATCC 43593 as the indicator strain, in hopes of finding an organism that would exhibit antimicrobial activity against the pathogen without affecting other beneficial flora that normally inhabit the gut.

Out of all the specimens tested, only one colony was observed to inhibit the growth of *C. difficile*. Our collaborators used genotypic characterization to identify this organism as a *Bacillus thuringiensis* strain, which they designated DPC 6431. Upon culturing of this strain in brain-heart infusion (BHI) media, the bacteria were found to secrete an antimicrobial factor into the supernatant during the late log phase and stationary phase of its growth. This factor, which was named thuricin CD (to denote its activity against *C. difficile*), is sensitive to digestion with Proteinase K, establishing it as a proteinaceous substance. Stability testing on the cell-free supernatant (CFS) indicated that thuricin CD maintains its activity at temperatures up to 85 °C and at a pH range of 2–9.

The CFS was also used in a well diffusion assay (WDA) to determine the inhibition spectrum of *B. thuringiensis* DPC 6431. In this assay, CFS is added to wells that have been bored out of solidified agar seeded with an indicator strain.[77] If the bacteria are sensitive to the CFS, a zone of growth inhibition surrounding each well will appear after overnight incubation. The results of the assay showed that the CFS from *B. thuringiensis* DPC 6431 is active against several *Bacillus* species, *L. monocytogenes* and a range of *C. difficile* strains, including the hypervirulent strain PCR ribotype 027. Antimicrobial activity was also observed against other clostridia, such as *C. indolis*, *C. lituseburense*, and *C. tyrobutyricum*. Interestingly, out of all the lactic acid bacteria (LAB) that were screened, only *Lactobacillus fermentum* showed any significant level of sensitivity, suggesting that thuricin CD does not target strains generally considered beneficial to human gut health.[78] On the other hand, none of the Gram-negative organisms tested were inhibited by the CFS.

Further purification of thuricin CD from the CFS using a series of hydrophobic interaction columns led to the discovery that the antimicrobial factor consists of two distinct molecules (for more details on the purification, see section 2.2.1.). In particular, reversed phase high-performance liquid chromatography (RP-HPLC) enabled the separation of two well-resolved peaks, designated Trn-α and Trn-β, that both exhibited activity against *C. difficile*. Analysis of the two peaks using matrix assisted laser desorption ionization time of flight mass spectrometry (MALDI-TOF MS) found that the exact mass for the molecular ion $[M+H]^+$ of Trn-α is 2763 Da, while that of Trn-β is 2861 Da.

Our collaborators went on to measure the concentration of Trn-α or Trn-β required to inhibit a *C. difficile* population by 50% (i.e. the minimum inhibitory concentration-50 or MIC_{50}) by measuring the optical density at 600 nm (OD_{600}) of liquid cultures in 96-well microtiter plates. They determined that Trn-β (MIC_{50} = 0.5 μM) is 10-fold more potent than Trn-α (MIC_{50} = 5 μM) when the peptides are assayed individually. However, when the two factors are tested together, it gives rise to significantly stronger levels of inhibition. First, it was found that a 1:2 ratio of Trn-α to Trn-β gave the best inhibition. Titrating the two peptides against each other showed that the optimum MIC_{50} values for Trn-α and Trn-β in combination are 0.025 μM and 0.05 μM, respectively.

Purification to homogeneity and subsequent activity testing has revealed that thuricin CD is a two-component bacteriocin, where the individual components have inherent antimicrobial activity but operate synergistically when combined together at nanomolar concentrations. The optimum ratio of 1:2 Trn-α to Trn-β molecules from the MIC_{50} measurements suggests a well-defined mechanism of action for the synergistic activity of these two peptides.

2.1.2. Significance of thuricin CD activity

The finding that thuricin CD is highly active against *C. difficile* argues for the clinical significance of this bacteriocin. Certain strains of *C. difficile* are prone to developing resistance against multiple antibiotics, and have surfaced in recent years as dangerous human pathogens. Patients who have recently been treated with antibiotics, such as clindamycin, broad-spectrum cephalosporins and

fluoroquinolones, are at increased risk of developing a *C. difficile* infection (CDI).[79] A CDI occurs when the bacteria are able to colonize large portions of the gut, leading to diarrhea, fever, abdominal pain, and inflammation of the intestinal membrane. In severe cases, toxic megacolon can result, where the colon becomes extremely dilated or distended, and may easily rupture, leading to septic shock.

As mentioned previously, the activity profile of thuricin CD is particularly interesting because it can inhibit the growth of *C. difficile* ribotype 027. This hypervirulent strain is associated with more severe cases of CDI and more *C. difficile* associated deaths than any other strain.[80] Different isolates of ribotype 027 have been found in hospitals around the world, and each of these isolates exhibits a unique profile of drug resistance that, in total, includes nearly every antibiotic in clinical use.[79] Ribotype 027 has been responsible for several outbreaks of CDI in Europe and North America and its incidence is still on the rise in Canada and the United States.[79, 81] A recent survey of health-care associated CDI in Canada found that in 2005, Quebec had a higher incidence of infection (12.8 cases per 1000 patient admissions) than the rest of the country (4.0 cases per 1000 admissions), as well as four times the mortality rate (14.9% vs. 3.5% for the rest of Canada).[82] Interestingly, another investigation determined that, from 2001 to 2004, ribotype 027 constituted 75.2% of the *C. difficile* isolates in Montreal, Quebec, but only 7.9% of isolates in Calgary, Alberta, suggesting that the high mortality rates in Quebec may be a reflection of ribotype 027 prevalence.[80, 83]

Currently, the antibiotic metronidazole serves as the first line of treatment for CDI. However, an observational study showed that metronidazole had only a 50% success rate. Another 22% of patients continued to exhibit symptoms even after ten days of treatment, while 28% had a recurrence within 90 days of treatment.[84] Vancomycin is the second line alternative against CDI, but is frequently avoided due to the risk of selecting for VRE and other vancomycin-resistant bacteria. In cases of severe damage to the large intestine, physicians may perform a colectomy (surgical resectioning of the colon) to help improve a patient's chances of survival.[79] For *C. difficile* strains that prove refractory to antibiotic treatment, fecal bacteriotherapy, where stool is transplanted from a healthy donor to an ill patient, has also been used to successfully combat CDI.[85]

Due to the significant challenges of drug resistance and maintenance of healthy gut flora in CDI patients, thuricin CD may serve as an attractive candidate for targeting *C. difficile* without affecting *Bifidobacterium*, *Lactobacillus*, and other LAB populations in the gut flora. Its potential utility in this regard has inspired further research with the ultimate goal of understanding its biosynthesis, structure, and mechanism of action.

2.1.3. Biosynthetic gene cluster of thuricin CD

After the initial characterization of thuricin CD, our collaborators went on to sequence the putative biosynthetic gene cluster for this two-component bacteriocin. They found that the cluster contains seven genes (**Figure 14**).

Figure 14. The biosynthetic gene cluster of thuricin CD: *trnF*, *trnG* (pink) are likely responsible for the secretion of Trn-α and Trn-β from the cell; *trnβ*, *trnα* (yellow) encode for the precursor peptides for thuricin CD; *trnC*, *trnD* (red) produce two enzymes thought to perform post-translational modifications on the precursors; and *trnE* (grey) has an unknown function.

The *trnα* and *trnβ* genes encode for the precursor peptides of the two components of thuricin CD. Comparison of the gene sequences with the results of the N-terminal Edman sequencing of the peptides established the length of the leader peptides in the precursors. The Trn-α precursor has a 17-residue leader followed by a 30-residue propeptide while the Trn-β precursor has a 19-residue leader followed by a 30-residue propeptide. Interestingly, it was found that the calculated $[M+H]^+$ masses for the Trn-α and Trn-β propeptides are 2769 Da and 2867 Da, respectively. Both of these theoretical masses are 6 Da heavier than the experimental values observed by MALDI-TOF MS, suggesting that the propeptides are post-translationally modified and that each peptide loses 6 Da during its conversion into a mature bacteriocin.

Two proteins that may be responsible for modifying the precursor peptides are TrnC and TrnD. These two enzymes show sequence homology to the radical SAM superfamily of proteins, and contain within their N-terminal domains the C-X_3-C-X_2-C sequence that typically coordinates to a [4Fe-4S] cluster. Notably, TrnC and TrnD share 19% and 17% identity with the AlbA enzyme from the biosynthetic gene cluster of subtilosin A.

Sequence comparisons also indicate that TrnF and TrnG likely form the domains of an ABC transporter. It is thought that TrnF serves as an ATP-binding subunit while TrnG constitutes the integral membrane portion of the transporter. Currently, it is unknown whether TrnF and TrnG also cleave off the N-terminal leader of the precursor peptides before secreting mature Trn-α and Trn-β.

The remaining gene in the operon, *trnE*, encodes for an intracellular protein that shows sequence homology to a superfamily of C-terminal processing peptidases. As of yet, it has no known function in the biosynthesis of thuricin CD.

2.1.4. Project objectives

There were three main objectives for this project. First, we wanted to confirm the amino acid sequences of Trn-α and Trn-β, and ascertain which of the residues are post-translationally modified. Second, we wanted to determine the nature of these post-translational modifications and establish the chemical structure of these peptides. Third, we wanted to elucidate the 3D structures of Trn-α and Trn-β. These goals were achieved using mass spectrometry analysis, as well as isotopic labeling of the peptides followed by solution NMR studies.

2.2. Results and discussion

2.2.1. Purification of Trn-α and Trn-β

Trn-α and Trn-β were isolated in a three-step process from an overnight culture of *B. thuringiensis* DPC 6431 grown in BHI media. The supernatant of this culture was loaded onto a hydrophobic interaction resin (Amberlite XAD-16), and 30% ethanol (EtOH) was used to wash away crude contaminants before

eluting with 70% isopropanol (IPA) and 0.1% trifluoroacetic acid (TFA). The presence of Trn-α and Trn-β was identified by activity testing. The active component was then applied to a Phenomenex C-18 solid phase extraction (SPE) cartridge, which was then washed with EtOH prior to elution with acidified IPA. These first two steps were performed to clean up and concentrate the peptides before final purification by RP-HPLC, which separated Trn-α and Trn-β into two well-resolved peaks. To improve the yield, the cell pellet obtained from the overnight culture was resuspended in 70% IPA/ 0.1% TFA to extract any Trn-α and Trn-β that may have adhered to the surface of the bacteria. This IPA extract was then subjected to C-18 SPE and RP-HPLC purification as well. On average, 1 L of bacterial culture would yield 2 mg of Trn-α and 4 mg of Trn-β. The identities of both peptides were confirmed by MALDI-TOF MS (**Figure 15**) and WDA activity testing (**Figure 16**).

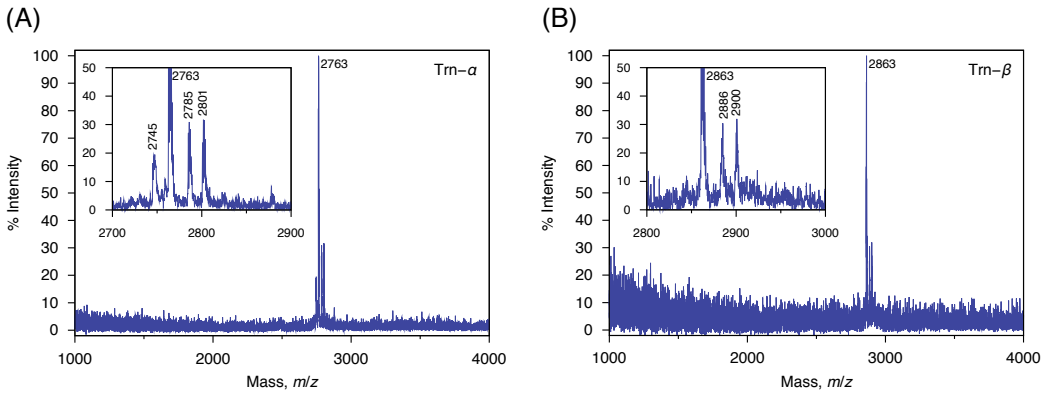

Figure 15. MALDI-TOF spectrum of (A) Trn-α and (B) Trn-β. Inset shows expansion of significant peaks, including $[M+H]^+$, $[M+Na]^+$ and $[M+K]^+$. The *m/z* = 2745 peak represents a loss of water from Trn-α.

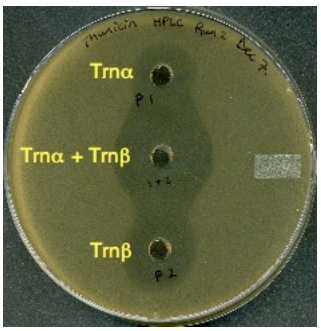

Figure 16. Activity testing of Trn-α and Trn-β against an indicator strain. In this WDA, testing solutions were pipetted into wells bored out of agar that was inoculated with *Bacillus firmus* LMG 7125. The top and bottom wells show that 50 μL of HPLC fraction containing Trn-α and Trn-β, respectively, inhibit bacterial growth. The middle well indicates that when 25 μL of the Trn-α fraction is mixed with 25 μL of the Trn-β fraction, a larger zone of inhibition is observed.

2.2.2. Characterization by mass spectrometry

2.2.2.a. MS/MS sequencing

Tandem mass spectrometry (MS/MS) sequencing of Trn-α and Trn-β was performed by Dr. Randy Whittal and Jing Zheng (Mass Spectrometry Facility, Department of Chemistry, University of Alberta). Infusion MS/MS indicated that the sequence of each peptide matched with its corresponding genetic sequence, except at positions 21, 25 and 28. At these three positions, the MS/MS data suggest that the residues in the mature peptides have lost two mass units compared to the expected masses of the natural amino acids (**Figure 17**).

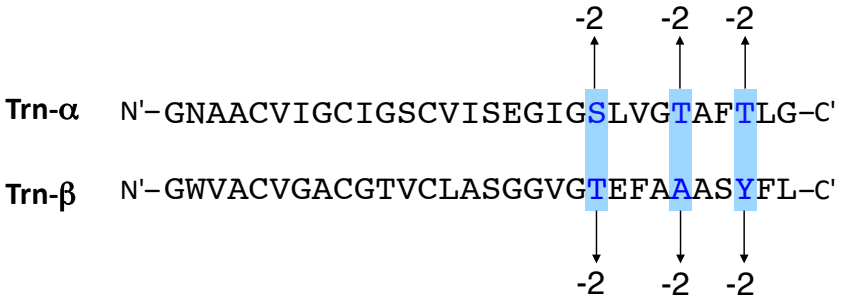

Figure 17. The sequences of Trn-α and Trn-β, as determined by infusion MS/MS. The residues that are two mass units lighter than expected are highlighted in blue (figure adapted from Rea *et al.*[61]).

2.2.2.b. FTICR

To confirm the exact mass and to propose a molecular formula for Trn-α and Trn-β, each peptide was subjected to high resolution Fourier transform ion cyclotron resonance (FTICR) MS (performed by Dr. Randy Whittal). In addition to analyzing the mass of the molecular ion, MALDI FTICR MS/MS was also used to determine the masses of the b_{20}, b_{24}, and b_{27} ions, which are the ionized N-terminal peptide fragments that immediately precede each modified residue (**Table 2** and **Table 3**).

Table 2: Exact masses and proposed formulae for Trn-α and its fragments[a]

Peptide Fragment	Proposed Formula $[M+H]^+$	Calculated Mass $[M+H]^+$	Observed Mass $[M+H]^+$	Error (ppm)
1-20 (b_{20} ion)	$C_{74}H_{126}N_{21}O_{25}S_3$	1804.8390	1804.8391	0.0
1-24 (b_{24} ion)	$C_{90}H_{152}N_{25}O_{30}S_3$	2159.0294	2159.0326	-1.5
1-27 (b_{27} ion)	$C_{106}H_{171}N_{28}O_{34}S_3$	2476.1669	2476.1638	1.2
1-30 (molecular ion)	$C_{118}H_{192}N_{31}O_{39}S_3$	2763.3150	2763.3218	-2.4

[a]The predicted $[M+H]^+$ molecular formula from genetic sequencing of Trn-α is $C_{118}H_{198}N_{31}O_{39}S_3$.

Table 3: Exact masses and proposed formulae for Trn-β and its fragments[a]

Peptide Fragment	Proposed Formula $(M+H)^+$	Calculated Mass $(M+H)^+$	Observed Mass $(M+H)^+$	Error (ppm)
1-20 (b_{20} ion)	$C_{74}H_{118}N_{21}O_{22}S_3$	1748.7917	1748.7910	0.4
1-24 (b_{24} ion)	$C_{95}H_{144}N_{25}O_{29}S_3$	2194.9718	2194.9698	0.9
1-27 (b_{27} ion)	$C_{104}H_{157}N_{28}O_{33}S_3$	2422.0625	2422.0614	0.4
1-30 (molecular ion)	$C_{128}H_{186}N_{31}O_{38}S_3$	2861.2732	2861.2698	1.2

[a]The predicted $[M+H]^+$ molecular formula from genetic sequencing of Trn-β is $C_{128}H_{192}N_{31}O_{38}S_3$.

The FTICR results show that the 6 Da discrepancy between the expected mass from genetic sequencing and the observed mass from the mature peptide is due to a loss of six hydrogen atoms. Specifically, it appears that post-translational modification removes two hydrogen atoms from residues 21, 25 and 28 of Trn-α and Trn-β. To elucidate the structure of these modifications, NMR studies were undertaken to characterize each peptide.

2.2.3. Production of [^{13}C, ^{15}N]Trn-α and [^{13}C, ^{15}N]Trn-β for NMR

In order to make complete chemical shift assignments for the carbon, nitrogen and proton nuclei in each peptide, Trn-α and Trn-β had to first be fully labeled with ^{13}C- and ^{15}N-isotopes. Because *B. thuringiensis* DPC 6431 does not grow in defined minimal media, a doubly labeled rich media ([^{13}C, ^{15}N]Celtone-CN) had to be used for the production of [^{13}C, ^{15}N]Trn-α and [^{13}C, ^{15}N]Trn-β. The labeled peptides were isolated using the same steps employed for unlabeled Trn-α and Trn-β, except for one addition. [^{13}C, ^{15}N]Trn-α and [^{13}C, ^{15}N]Trn-β were both reinjected for a second round of RP-HPLC to ensure >95% purity, for the purpose

of avoiding interfering peaks in the NMR spectra that would result from sample contamination. From 1 L of [^{13}C, ^{15}N]Celtone-CN, an average of 0.5 mg of [^{13}C, ^{15}N]Trn-α and 1 mg of [^{13}C, ^{15}N]Trn-β could be obtained. The identity of each peptide was confirmed by MALDI-TOF MS, with the $[M+H]^+$ peaks of [^{13}C, ^{15}N]Trn-α and [^{13}C, ^{15}N]Trn-β appearing at 2911 Da and 3018 Da, respectively (**Figure 18**). The sodium ($[M+Na]^+$) and potassium ($[M+K]^+$) adducts of each peptide were also observed in the spectra, as well as a couple of smaller degradation products (2887 Da and 2877 Da) in the [^{13}C, ^{15}N]Trn-α spectrum. Due to the hydrophobicity of the peptides, [^{13}C, ^{15}N]Trn-α and [^{13}C, ^{15}N]Trn-β were each dissolved in CD_3OH for NMR studies. Fully deuterated methanol (CD_3OD) was not selected as the solvent, as this would lead to deuterium exchange of the amide protons from the backbone, rendering the signals unobservable by NMR.

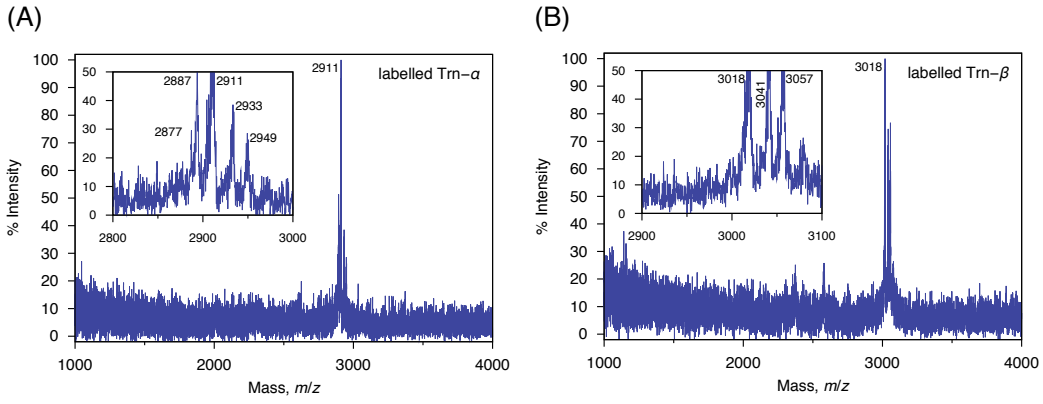

Figure 18. MALDI-TOF spectrum of (A) [^{13}C, ^{15}N]Trn-α and (B) [^{13}C, ^{15}N]Trn-β.

2.2.4. Secondary structure prediction via CD and ^{15}N HSQC

To establish whether Trn-α and Trn-β held any defined secondary structure in solution, circular dichroism (CD) and ^{15}N heteronuclear single quantum coherence (^{15}N HSQC) spectra were acquired. CD spectra were collected by David Zinz and Dr. Wayne Moffat (Analytical and Instrumentation Laboratory, Department of Chemistry, University of Alberta). In the presence of 80% trifluoroethanol (TFE) and 10% methanol (MeOH), both of which are membrane-mimicking solvents, CD indicated that the two peptides were somewhat helical (**Figure 19**). Trn-β exhibited approximately 19% helicity while Trn-α featured a slightly more pronounced helicity at 25%. In the ^{15}N HSQC spectra of Trn-α and Trn-β, the backbone amide crosspeaks were well dispersed, with 29 out of 30 amides giving rise to unique chemical shifts (**Figure 20**). This spectral dispersion provides further support for the presence of secondary structural elements in Trn-α and Trn-β.

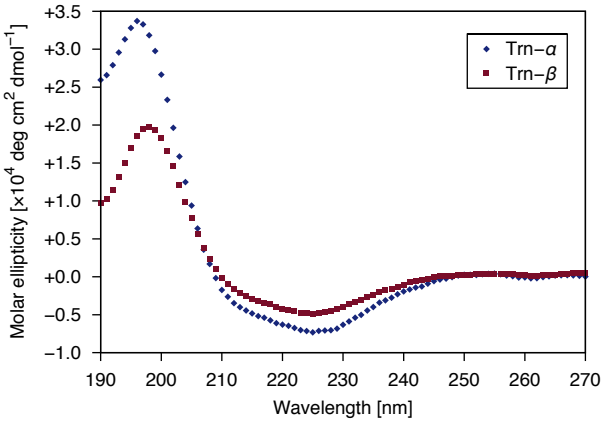

Figure 19. CD spectra of Trn-α and Trn-β in 80% TFE/ 10% MeOH/ 10% H_2O.

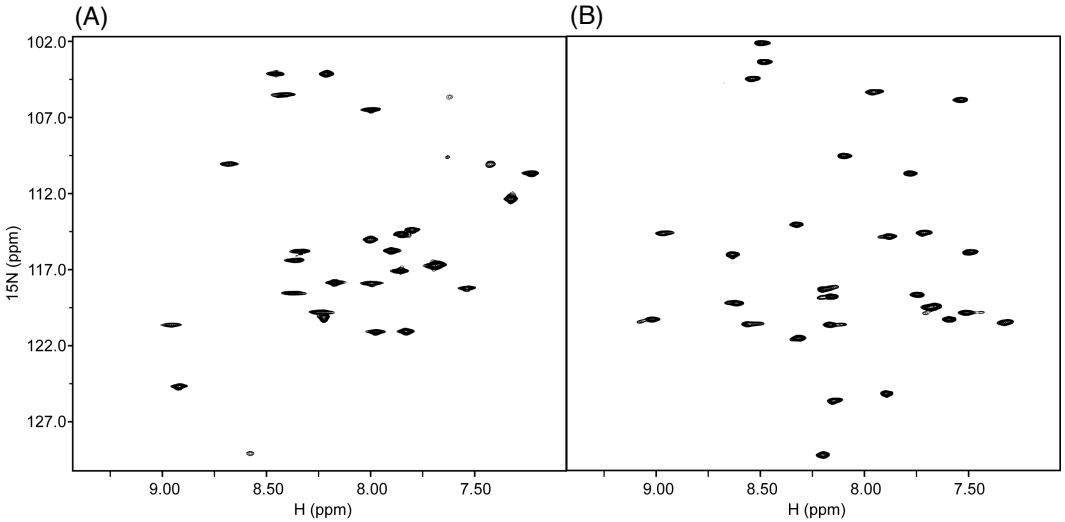

Figure 20. ^{15}N HSQC of (A) Trn-α and (B) Trn-β.

2.2.5. Structural elucidation of post-translational modifications

2.2.5.a. Chemical shift assignments

Chemical shift assignments for Trn-α and Trn-β were made using a suite of multidimensional NMR experiments. Analysis of these heteronuclear experiments established the identity of the backbone and side chain resonances for each residue (see Appendix A for a full list of the Trn-α and Trn-β chemical shift assignments). Interestingly, it was found that the chemical shifts for the α-carbons of residues 21, 25 and 28 in each peptide are 15 to 20 ppm downfield of average values observed in unmodified residues (**Table 4** and **Table 5**).[86] Furthermore, total correlation spectroscopy (TOCSY) experiments indicate that these α-carbons have no attached α-protons, and are thus fully substituted. This evidence suggests that an electronegative atom, such as sulfur, may be bonded to the α-carbons of these post-translationally modified residues.

Table 4: ^{13}C and ^{1}H chemical shift assignments of the Trn-α modified residues[a]

	Trn-α Ser21	Natural Ser[b]	Trn-α Thr25	Natural Thr[b]	Trn-α Thr28	Natural Thr[b]
Cα	73.7	58.3	75.2	61.8	78.5	61.8
Cβ	67.6	63.8	76.9	69.8	76.9	69.8
Hα	**none**	4.47	**none**	4.35	**none**	4.35
Hβ	3.99, 3.73	3.89, 3.87	4.05	4.24	4.11	4.24

[a]All chemical shifts are reported in units of ppm.
[b]The expected chemical shifts of unmodified residues in a random coil peptide (from Wishart *et al.*[86]) have been listed for comparison.

Table 5: ^{13}C and ^{1}H chemical shift assignments of the Trn-β modified residues[a]

	Trn-β Thr21	Natural Thr[b]	Trn-β Ala25	Natural Ala[b]	Trn-β Tyr28	Natural Tyr[b]
Cα	76.1	61.8	70.2	52.5	76.1	57.9
Cβ	77.1	69.8	28.1	19.1	45.0	38.8
Hα	**none**	4.35	**none**	4.32	**none**	4.35
Hβ	4.43	4.24	1.83	1.39	3.16, 2.91	3.03, 2.98

[a]All chemical shifts are reported in units of ppm.
[b]The expected chemical shifts of unmodified residues in a random coil peptide (from Wishart *et al.*[86]) have been listed for comparison.

2.2.5.b. Comparison with the chemical shifts of subtilosin A

Prior to NMR characterization of thuricin CD, the only known examples of sulfur to α-carbon bridging in a peptide were the thioether linkages found in subtilosin A.[32, 37] Since the side chain sulfur of Cys7 forms a thioether bond with the α-carbon of Thr28 in subtilosin A, the chemical shifts of this Thr were compared with the assigned resonances for the modified Thr in Trn-α and Trn-β (**Table 6**). Although some variation is observed between the chemical shifts, all of the α-carbon values are in the 70-80 ppm range and are significantly downfield from the expected average value of 61.8 ppm.[86]

Table 6: Chemical shifts of modified Thr from Trn-α, Trn-β, and subtilosin A[a]

	Trn-α Thr25	Trn-α Thr28	Trn-β Thr21	Subtilosin A Thr28
Cα	75.2	78.5	76.1	72.8
Cβ	76.9	76.9	77.1	70.9
Hα	**none**	**none**	**none**	**none**
Hβ	4.05	4.11	4.43	4.23

[a]All chemical shifts are reported in units of ppm.

2.2.5.c. NOE analysis of modified residues

Since Trn-α and Trn-β each have three Cys residues in its N-terminal half that can link to the three modified residues in its C-terminal half, it was important to determine specifically which Cys residue forms a bridge with a given modified residue. Nuclear Overhauser effect spectroscopy (NOESY) data, which shows through-space interactions between nuclei, was analyzed to establish whether certain residues are held in close proximity to each other within the peptides. Long-range ^{1}H-^{1}H NOEs were observed between the amide (HN) and side chain protons of the cysteines and the modified residues (**Figure 21**).

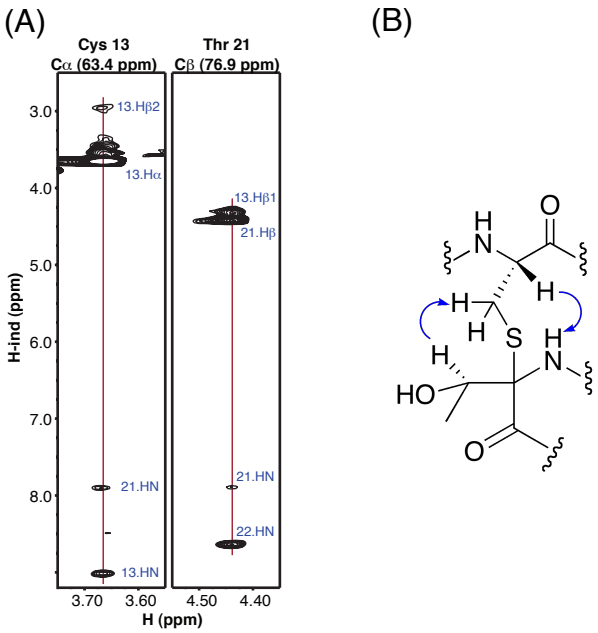

Figure 21. (A) Two strips of ^{1}H-^{1}H data taken from a ^{13}C HSQC-NOESY experiment of Trn-β. The observed NOE correlations include Cys13 Hα ↔ Thr21 HN and Thr21 Hβ ↔ Cys13 Hβ1 (figure reproduced with permission from Rea *et al.*[61]). (B) Diagram indicating the NOE correlations (blue arrows) observed between protons.

Overall, the pattern of NOE correlations in both peptides suggests that the thioether linkages occur between Cys5 and residue 28, Cys9 and residue 25, and Cys13 and residue 28 (see Appendix A for a complete list of relevant NOE correlations). The proposed connectivity of the amino acids in Trn-α and Trn-β is shown in **Figure 22**.

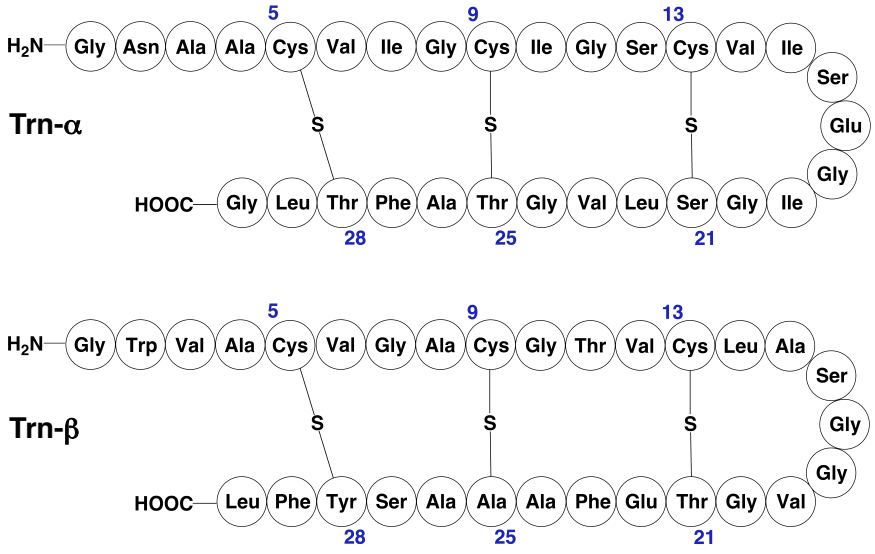

Figure 22: Diagram representing the proposed connectivity of residues in Trn-α and Trn-β.

2.2.5.d. Justification of mass spectrometry findings

Although the proposed sulfur to α-carbon thioether linkages account for the loss of six hydrogen atoms from each peptide, the NMR findings do not entirely match with the results from MS/MS sequencing. As mentioned earlier, infusion MS/MS and MALDI FTICR MS/MS found that each modified residue had lost 2 H, whereas NMR analysis suggests that 1 H is lost from the thiol of each Cys and from the α-position of each modified residue. This discrepancy may arise from the cleavage of the thioether linkages during ionization and fragmentation of the peptides in the mass spectrometer. Specifically, an amide proton could be lost from the modified residue, causing the thioether bridge to break apart and generate an N-acyl imine and a free cysteine (**Figure 23**). Tautomerization of the acyl imine to a more stable form gives rise to an oxidized residue that, under MS analysis, appears to have lost 2 H.

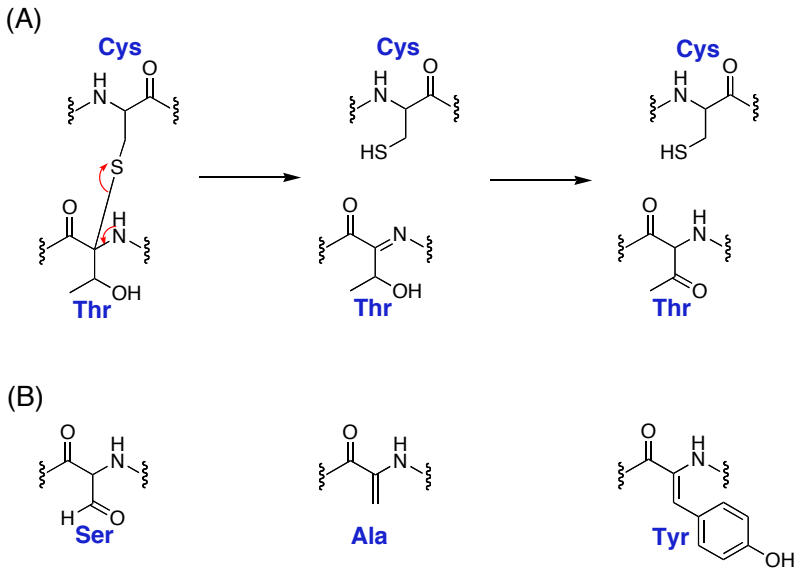

Figure 23: (A) A proposed mechanism for the cleavage of a sulfur to α-carbon linkage during MS/MS fragmentation to generate free Cys and an oxidized Thr, and (B) the structures of oxidized Ser (formylglycine), dehydroalanine, and dehydrotyrosine that may also result from similar thioether bond cleavage (figure reproduced with permission from Rea *et al.*[61]).

Through chemical shift assignment and NOE analysis, the connectivity of all the atoms in Trn-α and Trn-β were established. However, since the sulfur to α-carbon thioether bridges are thought to be formed by TrnC and TrnD via a radical mechanism, it is unknown whether the modified residues maintain an L-configuration or invert to the D-configuration. To determine the stereochemistry of these bridges, the NOESY data collected from each peptide was used to calculate the 3D solution structures of Trn-α and Trn-β.

2.2.6. 3D NMR solution structures of Trn-α and Trn-β

All structures were generated using the program CYANA 2.1, which performs calculations based on distance restraints and torsion angle dynamics.[87]

Because there are two possible stereochemical configurations at each of the three bridges in Trn-α and Trn-β, eight stereoisomers must be calculated and compared as possible candidates for the structure of each peptide. Before structure calculations can be carried out, though, the modified residues need to be defined within the residue library of CYANA.

2.2.6.a. Design of a modified residue library for CYANA*

CYANA defines the basic structures of the 20 common amino acids in its residue library and refers to this library during the structure calculation of a peptide with a given sequence. In addition to the atoms that constitute an amino acid, CYANA also considers the peptide bond immediately preceding and immediately following the residue, and assigns a number to each atom for nomenclature purposes (**Figure 24**). The first step to creating a modified residue was to delete the Hα and re-number all atoms following the Hα in sequence.

* Modification of the CYANA library was performed with advice and assistance from Dr. Pascal Mercier, Dr. Leah Martin-Visscher, and Dr. Jeremy Sit.

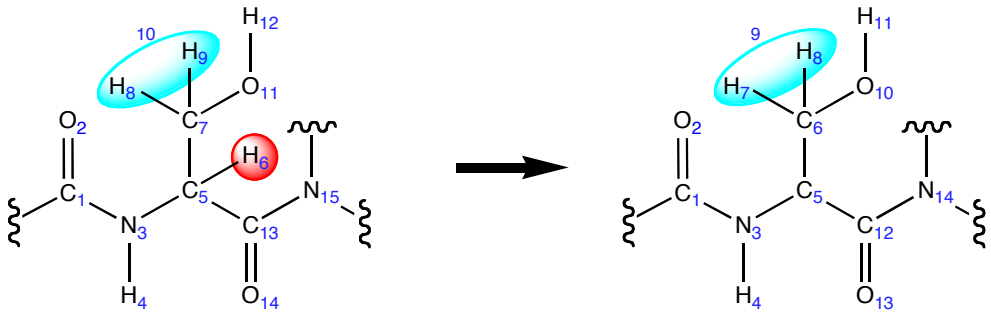

Figure 24. Nomenclature used by CYANA to define the atoms in a serine residue, and alteration of that nomenclature to reflect the loss of the Hα in the modified serine. The blue shading represents a pseudoatom group (that considers Hβ1 and Hβ2 together), and the red shading indicates the proton that was deleted to form the modified residue.

The next step in this process was to examine how CYANA describes the positions of each atom in the residue library, and alter these descriptions accordingly. The program defines the relative positions of the atoms in 3D space using dihedral angles and Cartesian coordinates (**Figure 25** and **Figure 26**).

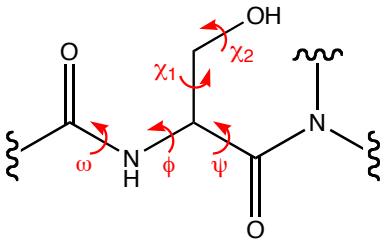

Figure 25. Diagram showing the dihedral angles that orient the backbone and side chain atoms of a serine residue.

```
RESIDUE   SER      5   15    3   14
  1 OMEGA     0    0    0.0000    2    1    3    4    0
  2 PHI       0    0    0.0000    1    3    5   13    0
  3 CHI1      0    0    0.0000    3    5    7   11   12
  4 CHI2      0    0    0.0000    5    7   11   12   12
  5 PSI       0    0    0.0000    3    5   13   15    0
  1 C     C_BYL    0    0.0000    0.0000    0.0000    0.0000    2    3    0    0    0
  2 O     O_BYL    0    0.0000   -0.6702    0.0000   -1.0325    1    0    0    0    0
  3 N     N_AMI    0    0.0000    1.3292    0.0000    0.0000    1    4    5    0    0
  4 H     H_AMI    0    0.0000    1.8069    0.0014    0.8560    3    0    0    0    0
  5 CA    C_ALI    0    0.0000    2.0936    0.0018   -1.2418    3    6    7   13    0
  6 HA    H_ALI    0    0.0000    1.4845    0.4623   -2.0053    5    0    0    0    0
  7 CB    C_ALI    0    0.0000    3.3790    0.8141   -1.0730    5    8    9   11    0
  8 HB2   H_ALI    0    0.0000    4.1957    0.1471   -0.8427    7    0    0    0   10
  9 HB3   H_ALI    0    0.0000    3.5921    1.3405   -1.9922    7    0    0    0   10
 10 QB    PSEUD    0    0.0000    3.8934    0.7433   -1.4169    0    0    0    0    0
 11 OG    O_HYD    0    0.0000    3.2513    1.7588   -0.0245    7   12    0    0    0
 12 HG    H_OXY    0    0.0000    2.7779    2.5303   -0.3443   11    0    0    0    0
 13 C     C_BYL    0    0.0000    2.4313   -1.4219   -1.6739    5   14   15    0    0
 14 O     O_BYL    0    0.0000    3.3640   -2.0335   -1.1556   13    0    0    0    0
 15 N     N_AMI    0    0.0000    1.6647   -1.9418   -2.6269   13    0    0    0    0
```

Legend

- Number and name of dihedral angles
- The four atoms that define each dihedral angle
- The last atom affected by a rotation of the dihedral angle (0, if backbone)
- Number, name and type of atom
- The x-, y-, and z-coordinates of the atoms
- Neighboring atoms to which a given atom is connected
- The number of the corresponding pseudoatom (if applicable)
- Description of the residue:
  - 5 – number of rotatable dihedral angles
  - 15 – number of atoms listed for this residue
  - 3 – atom number that represents the start of the residue
  - 14 – atom number that represents the end of the residue

Figure 26. A description of serine in the residue library of CYANA.

To create a description for modified serine with L-stereochemistry (MSER), the entire line describing Hα ("6 HA") was deleted, and all subsequent atoms were re-numbered. The atom numbers that described the dihedral angles and the connectivity were also changed to reflect this re-numbering (**Figure 27**). To generate a description for modified serine with D-stereochemistry (DSER), the

atoms of MSER were simply reflected about the x-axis by changing the sign of all the x-coordinates (**Figure 28**).

```
RESIDUE  MSER      5   14    3   13
   1 OMEGA    0    0    0.0000    2    1    3    4    0
   2 PHI      0    0    0.0000    1    3    5   12    0
   3 CHI1     0    0    0.0000    3    5    6   10   11
   4 CHI2     0    0    0.0000    5    6   10   11   11
   5 PSI      0    0    0.0000    3    5   12   14    0
   1 C    C_BYL    0    0.0000    0.0000    0.0000    0.0000    2    3    0    0    0
   2 O    O_BYL    0    0.0000   -0.6702    0.0000   -1.0325    1    0    0    0    0
   3 N    N_AMI    0    0.0000    1.3292    0.0000    0.0000    1    4    5    0    0
   4 H    H_AMI    0    0.0000    1.8069    0.0014    0.8560    3    0    0    0    0
   5 CA   C_ALI    0    0.0000    2.0936    0.0018   -1.2418    3    6   12    0    0
   6 CB   C_ALI    0    0.0000    3.3790    0.8141   -1.0730    5    7    8   10    0
   7 HB2  H_ALI    0    0.0000    4.1957    0.1471   -0.8427    6    0    0    0    9
   8 HB3  H_ALI    0    0.0000    3.5921    1.3405   -1.9922    6    0    0    0    9
   9 QB   PSEUD    0    0.0000    3.8934    0.7433   -1.4169    0    0    0    0    0
  10 OG   O_HYD    0    0.0000    3.2513    1.7588   -0.0245    6   11    0    0    0
  11 HG   H_OXY    0    0.0000    2.7779    2.5303   -0.3443   10    0    0    0    0
  12 C    C_BYL    0    0.0000    2.4313   -1.4219   -1.6739    5   13   14    0    0
  13 O    O_BYL    0    0.0000    3.3640   -2.0335   -1.1556   12    0    0    0    0
  14 N    N_AMI    0    0.0000    1.6647   -1.9418   -2.6269   12    0    0    0    0
```

Figure 27. A description of modified serine with L-stereochemistry (MSER) that was added to the residue library of CYANA. Green highlights indicate the changes that were made from the original Ser description.

```
RESIDUE  DSER      5   14    3   13
   1 OMEGA    0    0    0.0000    2    1    3    4    0
   2 PHI      0    0    0.0000    1    3    5   12    0
   3 CHI1     0    0    0.0000    3    5    6   10   11
   4 CHI2     0    0    0.0000    5    6   10   11   11
   5 PSI      0    0    0.0000    3    5   12   14    0
   1 C    C_BYL    0    0.0000    0.0000    0.0000    0.0000    2    3    0    0    0
   2 O    O_BYL    0    0.0000    0.6702    0.0000   -1.0325    1    0    0    0    0
   3 N    N_AMI    0    0.0000   -1.3292    0.0000    0.0000    1    4    5    0    0
   4 H    H_AMI    0    0.0000   -1.8069    0.0014    0.8560    3    0    0    0    0
   5 CA   C_ALI    0    0.0000   -2.0936    0.0018   -1.2418    3    6   12    0    0
   6 CB   C_ALI    0    0.0000   -3.3790    0.8141   -1.0730    5    7    8   10    0
   7 HB2  H_ALI    0    0.0000   -4.1957    0.1471   -0.8427    6    0    0    0    9
   8 HB3  H_ALI    0    0.0000   -3.5921    1.3405   -1.9922    6    0    0    0    9
   9 QB   PSEUD    0    0.0000   -3.8934    0.7433   -1.4169    0    0    0    0    0
  10 OG   O_HYD    0    0.0000   -3.2513    1.7588   -0.0245    6   11    0    0    0
  11 HG   H_OXY    0    0.0000   -2.7779    2.5303   -0.3443   10    0    0    0    0
  12 C    C_BYL    0    0.0000   -2.4313   -1.4219   -1.6739    5   13   14    0    0
  13 O    O_BYL    0    0.0000   -3.3640   -2.0335   -1.1556   12    0    0    0    0
  14 N    N_AMI    0    0.0000   -1.6647   -1.9418   -2.6269   12    0    0    0    0
```

Figure 28. A description of modified serine with D-stereochemistry (DSER) that was added to the residue library of CYANA. Blue highlights indicate the only changes that were made from the MSER description (changing the sign of the x-coordinates).

The descriptions of modified L- and D-alanine, modified L- and D-tyrosine and modified L-threonine were generated in the same fashion. For modified D-threonine, additional adjustments were made to several of the atom coordinates after reflection about the x-axis in order to maintain an *R* configuration at Cβ. Using straightforward vector algebra, the atom positions in the modified D-threonine enantiomer were determined by swapping the positions of its Hβ and Oγ-Hγ groups. The complete descriptions of all modified residues added to the CYANA library are listed in Appendix A.

2.2.6.b. Constraints used to create sulfur to α-carbon linkages

In order to create the sulfur to α-carbon linkages in CYANA, constraints files were designed to instruct the program to form the desired bonds during structure calculations. As a point of reference, the sulfur to α-carbon bond lengths in subtilosin A were measured from its NMR structure (found in the Protein Data Bank, PDB ID: 1PXQ). The average bond length (1.8 Å) was then used to develop an upper limit (2.0 Å) and a lower limit (1.6 Å) for the S-Cα bond length, and these values were incorporated into the constraints files (**Figure 29A**). Instructions for connecting the Sγ of the Cys residues to the Cα of the modified residues were also written into a sequence file that defines which residues are connected to each other in the peptide (**Figure 29B**).

(A)

Upper limit constraints file:

```
5    CYSS SG   28   MTYR CA   2.0   5.00E+00
9    CYSS SG   25   MALA CA   2.0   5.00E+00
13   CYSS SG   21   DTHR CA   2.0   5.00E+00
```

Lower limit constraints file:

```
5    CYSS SG   28   MTYR CA   1.6   5.00E+00
9    CYSS SG   25   MALA CA   1.6   5.00E+00
13   CYSS SG   21   DTHR CA   1.6   5.00E+00
```

(B)

Sequence file instructions:

```
link SG 5 CA 28
link SG 9 CA 25
link SG 13 CA 21
```

Figure 29. Creation of sulfur to α-carbon linkages in CYANA: (A) the upper and lower limit constraints files of a Trn-β isomer [blue columns define the residue numbers, names and specific atoms involved in the S-Cα linkage, green column defines the bond length constraint in Å, and yellow column gives the weighting function of the constraint]; (B) the instructions written into the sequence file to form the thioether bridge between residues 5 and 28, 9 and 25, and 13 and 21.

2.2.6.c. Structure calculations and comparison of stereoisomers

With the modified residue library and S-Cα linkage instructions in hand, structure calculations were performed for the eight possible stereoisomers of Trn-α and Trn-β. Eight rounds of calculations were carried out for each isomer, resulting in a family of 20 structures representative of the solution structure for that isomer. To provide a fair basis of comparison, structure calculations for the isomers of each peptide used automatically assigned distance constraints from the same NOE peak lists, as well as the same angle constraints derived from the HNHA experiment and the TALOS program.[88] The statistics from the generated structures were analyzed to determine which of the isomers best fits the NMR data.

In choosing the representative solution structure for Trn-α and Trn-β, four criteria were considered: greatest number of assigned NOEs included in the

structure, low root mean square deviation (rmsd), low average target function value, and absence of constraint violations or Ramachandran plot irregularities.[89] Upon evaluating these criteria, it was interesting to find that the single stereoisomer that best fit the NOE data for Trn-α had the same pattern of bridging stereochemistry as the best-fitting stereoisomer for Trn-β. In Trn-α, this stereoisomer had L-stereochemistry at Ser21 (α-*R*), L-stereochemistry at Thr25 (α-*R*) and D-stereochemistry at Thr28 (α-*S*) (LLD isomer). Similarly, the representative stereoisomer for Trn-β was also the LLD isomer, with L-stereochemistry at Thr21 (α-*R*), L-stereochemistry at Ala25 (α-*R*) and D-stereochemistry at Tyr28 (α-*S*) (**Figure 30**).

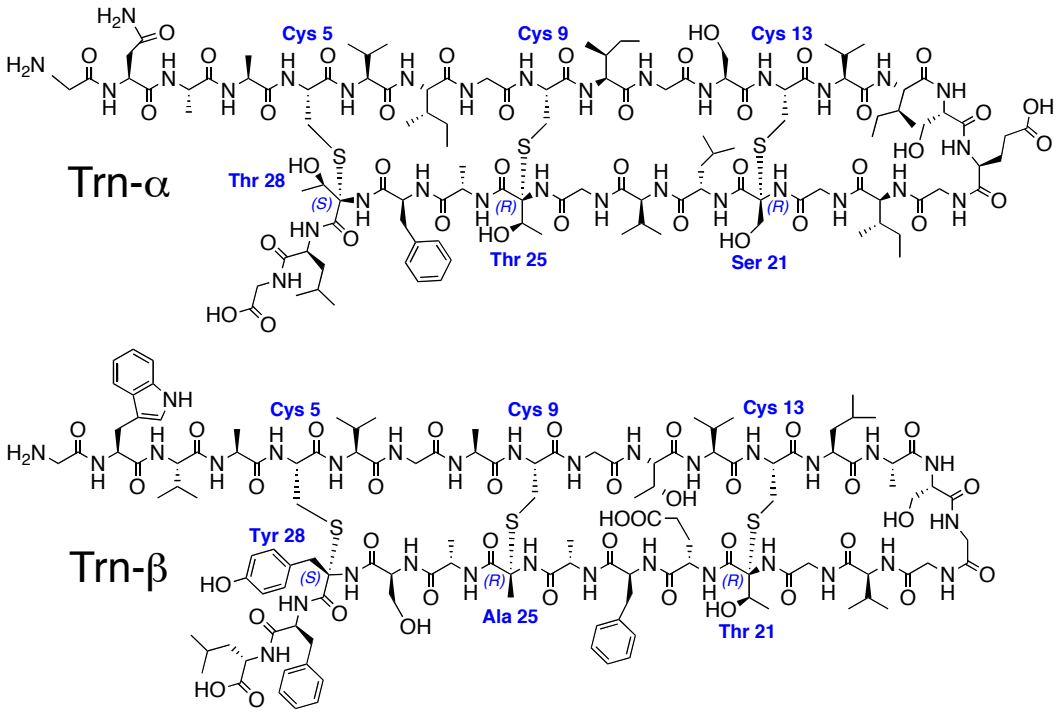

Figure 30. The chemical structures of Trn-α and Trn-β (figure reproduced with permission from Sit *et al.*[76]).

In the case of Trn-α, the LLD isomer was one of two stereoisomers that made use of the greatest number of NOE cross-peak assignments (381) in its structure (**Table 7**). Only the DLD isomer used the same number of assignments whereas the remaining six isomers used up to two fewer assignments. In other words, for these six isomers up to two assignments generated violations that could not be fit, and were automatically discarded from the calculations by CYANA. Depending on the isomer, the assignments in question were NOEs between a γCH_2 proton of Ile7 and the HN proton of Ala4, the HN of Gly20 and the HN of Leu22, or the Hα of Val23 and the Hα of Gly24. In CYANA's automated structure calculations, exclusion of these NOEs from six of the stereoisomers led to the generation of unnatural bends in the otherwise helical loops that form the two arms of the peptide (see below for a description of the 3D structure). To choose between the LLD and DLD isomers, it was noted that LLD has a lower rmsd, indicating that there is less error between the 20 averaged structures generated for LLD than for DLD (**Table 7**). As well, the LLD isomer has a lower average target function value, which serves as a measure of accuracy between the NOE restraint data entered into CYANA and the structures that are ultimately generated by the program. Finally, the overall structure of the LLD isomer gave better-formed α-helical loops than the structure of the DLD isomer.

Table 7: Comparison of statistics generated by the 8 stereoisomers of Trn-α

Isomers	Assigned NOEs[a]	rmsd (Å)	Average target function value	Ramachandran plot statistics[b]
LLL	380	1.64 ± 0.42	0.03	92.8% / 7.2%
DLL	380	1.77 ± 0.49	0.03	89.7% / 10.3%
DDL	379	1.63 ± 0.59	0.05	93.8% / 6.3%
DDD	380	1.72 ± 0.48	0.05	88.8% / 11.3%
LDL	380	1.55 ± 0.30	0.04	88.8% / 11.3%
LDD	379	1.55 ± 0.42	0.05	90.6% / 9.4%
LLD	381	2.02 ± 0.76	0.05	90.3% / 9.7%
DLD	381	2.18 ± 0.54	0.06	91.9% / 8.1%

[a]Represents total number of off-diagonal NOE assignments used by CYANA to perform the structure calculation.

[b]Values represent percentage of dihedral angles plotted as ϕ versus ψ that fall into the most favoured regions / additionally allowed regions for polypeptide backbone angles.

In the case of Trn-β, the structures of the LLD and LDD isomers used 313 NOE cross-peak assignments (**Table 8**). Comparison of these structures with those of the other six isomers revealed a consistent pattern. If the stereochemistry of Thr21 were set to D instead of L, the generated structures would discard two NOEs observed between the Hβ of Thr21 and the HN of Glu22. In fact, the structure calculations for the DLL and DLD isomers generated a coupling constant violation and a distance constraint violation, respectively. If the stereochemistry of Tyr28 were set to L instead of D, a long range NOE between the HN of Tyr28 and one of the Hβ of Cys5 would be discarded from the structure calculations. Since these NOEs involve crucial contacts to the post-translationally modified residues, they provide strong evidence to support Thr21 having L-stereochemistry and Tyr28 having D-stereochemistry. To choose between the

LLD and LDD isomers, then, it was again noted that the LLD isomer has a lower rmsd and a lower average target function value than does the LDD isomer.

Table 8: Comparison of statistics generated by the 8 stereoisomers of Trn-β

Isomers	Assigned NOEs[a]	rmsd (Å)	Average target function value	Ramachandran plot statistics[b]
LLL	312	1.80 ± 0.67	0.05	89.0% / 10.7% / 0.3%
DLL[c]	310	2.06 ± 0.49	0.13	92.0% / 8.0%
DDL	310	1.74 ± 0.53	0.09	95.7% / 4.3%
DDD	311	1.85 ± 0.45	0.18	92.7% / 7.0% / 0.3%
LDL	312	1.97 ± 0.64	0.11	91.3% / 8.7%
LDD	313	2.02 ± 0.68	0.15	93.7% / 6.3%
LLD	313	1.73 ± 0.50	0.06	92.3% / 7.7%
DLD[d]	307	2.10 ± 0.58	0.07	85.7% / 14.3%

[a]Represents total number of off-diagonal NOE assignments used by CYANA to perform the structure calculation.
[b]Values represent percentage of dihedral angles plotted as ϕ versus ψ that fall into the most favoured regions / additionally allowed regions / generously allowed regions for polypeptide backbone angles.
[c]One violated coupling constant constraint (for Cys5 HN-HA)
[d]One violated distance constraint (Val12 HB ↔ Cys13 HN)

2.2.6.d. Trn-α and Trn-β solution structures

Overall, the 3D structures of Trn-α and Trn-β each consist of a helical backbone that is folded in half and held together by the three sulfur to α-carbon thioether bridges (**Figure 31**). The structural statistics of Trn-α LLD and Trn-β LLD are summarized in **Table 9**.

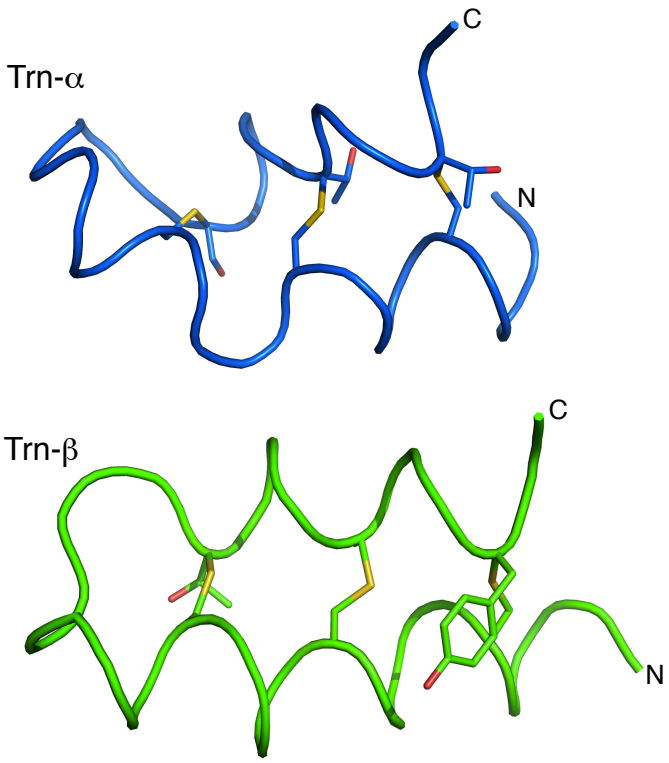

Figure 31. Cartoon representation of the three-dimensional solution structures of Trn-α (LLD isomer) and Trn-β (LLD isomer). The N- and C-termini have been labeled in both structures. The sulfur and oxygen atoms of the bridging residues are indicated in yellow and red, respectively (figure reproduced with permission from Sit *et al*.[76]).

Table 9: Structural statistics for Trn-α LLD and Trn-β LLD

	Trn-α LLD	Trn-β LLD
Distance and angle restraints		
total cross peak assignments	381	313
short ($\|i-j\| \leq 1$)	346	298
medium ($1 < \|i-j\| < 5$)	26	5
long ($\|i-j\| \geq 5$)	9	10
no. of ϕ angles	12	19
average target function value	0.05	0.06
rmsd (Å) for residues 1-29		
backbone	2.02 ± 0.76	1.73 ± 0.50
heavy atoms	2.50 ± 0.94	2.22 ± 0.49
rmsd (Å) for residues 5-13 & 21-28		
backbone	1.62 ± 0.71	1.14 ± 0.29
heavy atoms	2.20 ± 0.96	1.66 ± 0.29

The backbone rmsds for Trn-α (2.02 Å) and Trn-β (1.73 Å) are comparable to the backbone rmsd for subtilosin A (2.0 Å), the only other 3D structure of a peptide containing S-Cα linkages that has been reported to date.[32, 37] Since most of the long-range NOEs in Trn-α and Trn-β arise from the residues that form the thioether bridges, the portions of the two peptides that are encompassed by the bridges (residues 5-13 and 21-28) are better defined and thus have lower backbone rmsds (1.62 Å for Trn-α and 1.14 Å for Trn-β). Indeed, if the backbones of the 20 lowest energy conformers for each peptide are overlaid, it can be seen that the two helical coils (residues 5-13 and 21-28) superimpose reasonably well (**Figure 32**). In contrast, the region that connects the two coils (residues 14-20) as well as the N- and C-termini have poor overlap between the 20 conformers, indicating a high degree of flexibility and freedom of movement in those segments of the peptides.

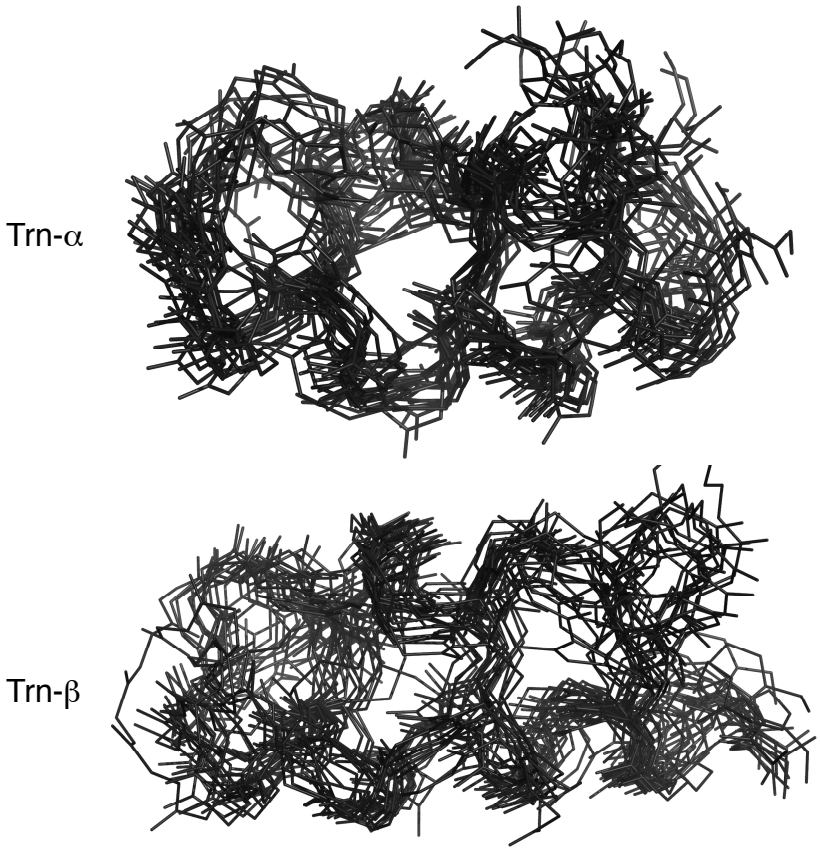

Figure 32. Backbone overlay of the 20 lowest energy conformers of Trn-α LLD and Trn-β LLD (figure reproduced with permission from Sit *et al*.[76]).

2.2.6.e. Structural features of Trn-α and Trn-β

Several interesting observations were made from examining the structures of Trn-α and Trn-β in detail. Similar to subtilosin A, most of the side chains of Trn-α and Trn-β are pointing outwards, away from the center of the molecules (**Figure 33**).[32, 37] In addition, a high prevalence of glycine residues in each peptide is thought to afford increased flexibility, enabling the backbones to form two helical coils that are packed together in close proximity.

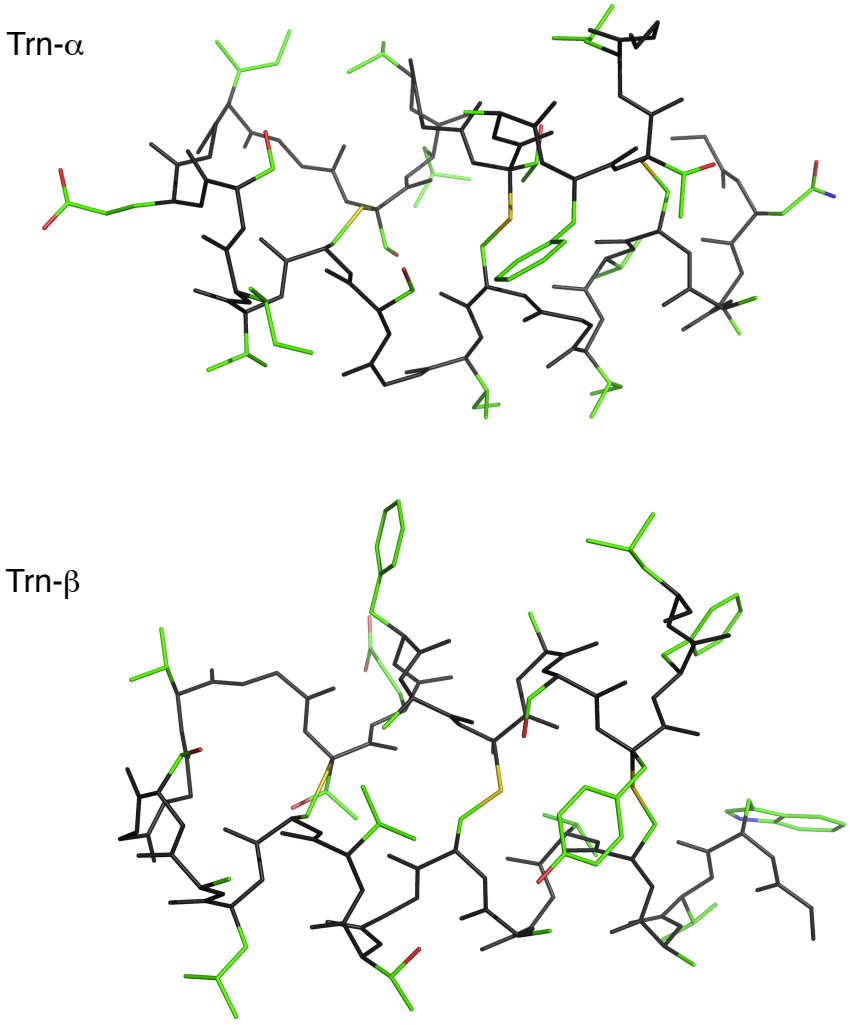

Figure 33. Stick representation of Trn-α LLD and Trn-β LLD, illustrating most of the side chains pointing outward. The backbone is colored grey and all of the side chains are highlighted according to element [carbon = green, oxygen = red, nitrogen = blue, and sulfur = yellow] (figure reproduced with permission from Sit *et al*.[76]).

The distribution of the side chains also governs the surface properties of each peptide. In Trn-α, most of its hydrophilic residues are either bound in the thioether bridges or concentrated toward the flexible loop region (**Figure 34A**). Trn-β, on the other hand, has its hydrophilic residues distributed over different parts of the molecule (**Figure 34B**). In both cases, however, the vast majority of

the peptide surface is hydrophobic as a result of having a large number of hydrophobic side chains that extend outward. These solution structures help explain the inherent insolubility of Trn-α and Trn-β, both of which require at least 50% organic solvent to dissolve.

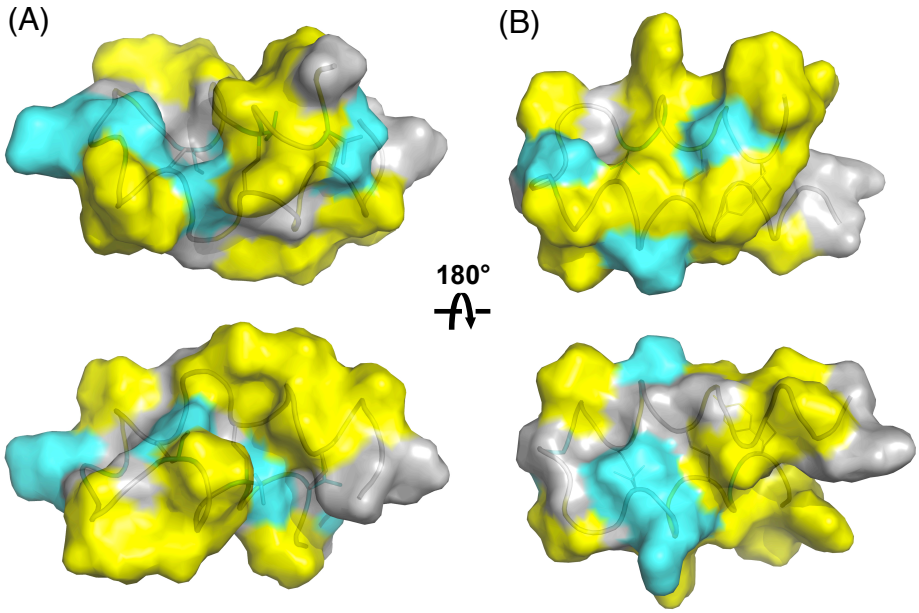

Figure 34. Surface hydrophobicity of (A) Trn-α LLD and (B) Trn-β LLD, with hydrophobic residues highlighted in yellow and hydrophilic residues highlighted in cyan. The backbone coil and sulfur to α-carbon bridges are drawn in to indicate the orientation of the peptides (figure reproduced with permission from Sit *et al.*[76]).

The electrostatic surface potential of both peptides is largely governed by the presence of a glutamic acid residue in each sequence, as well as by the N- and C-termini. Overall, the peptides are anionic at neutral pH, with positively and negatively charged regions distributed evenly over the surfaces of the peptides.

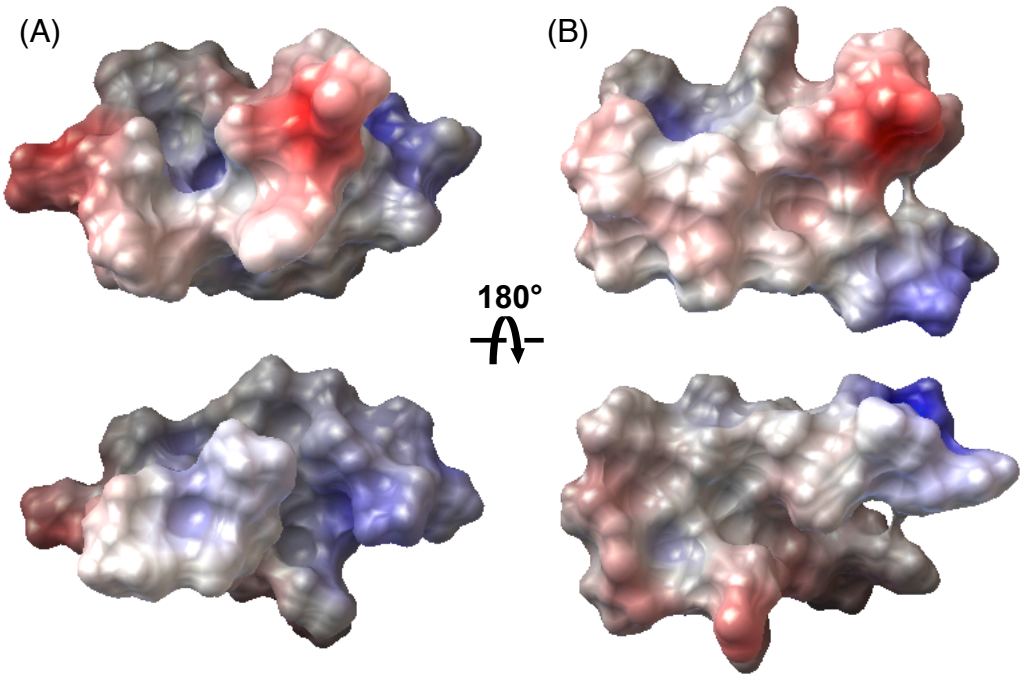

Figure 35. Electrostatic surface potential of (A) Trn-α LLD and (B) Trn-β LLD. Blue indicates positive charge and red indicates negative charge. In all cases, the N- and C-termini are oriented toward the right hand side of the image (figure reproduced with permission from Sit *et al*.[76]).

2.3. Conclusion and future directions

Elucidating the 3D structures of Trn-α and Trn-β may have implications for several areas of study. Due to similarities in their solution structures and the presence of the sulfur to α-carbon thioether bridges, it could be said that the two components of thuricin CD belong to a new, emerging class of bacteriocins alongside subtilosin A.[32] Liu *et al.* have characterized another example of this class: a sporulation killing factor (SKF) from *Bacillus subtilis* that features a thioether bridge to the α-carbon of a methionine residue.[90] There have also been reports of other peptides with similar amino acid sequences as Trn-α and Trn-β, suggesting that numerous peptides with sulfur to α-carbon crosslinks exist and

that our approach could be used to elucidate the three-dimensional structures of these highly related bacteriocins (see Chapter 3 for further discussion).[91-96] More importantly, the solution structures of Trn-α and Trn-β may provide a starting point for the study of thuricin CD's mechanism of action. Although it has been proposed that subtilosin A and related peptides target and disrupt bacterial cell membranes, no specific receptor has been identified for these molecules.[64-66, 97] In this regard, NMR binding studies to determine the specific target of thuricin CD and the mechanism of synergistic activity between Trn-α and Trn-β may prove to be highly interesting.

Chapter 3. Thurincin H

3.1. Background

Much of the following chapter has been adapted from our publication on the structural characterization of thurincin H.[63]

3.1.1. Isolation and initial characterization of thurincin H

Thurincin H was first isolated by our collaborators (Worobo and co-workers, Cornell University) from *Bacillus thuringiensis* SF361, a strain that was found in sunflower honey.[91, 98] This antimicrobial peptide was purified from the supernatant of the bacterial culture via ammonium sulfate precipitation and subsequent hydrophobic interaction chromatography. Electrospray ionization (ESI)-MS established that the $[M+H]^+$ of thurincin H has an average molecular weight of 3139.5 Da. N-terminal sequencing of the peptide using Edman degradation gave the first 18 residues as DWTXWSXLVXAAXSVELL, where X represents an unidentified amino acid.[91]

The spectrum of antimicrobial activity for thurincin H was also determined by screening its producer strain against a range of Gram-positive and Gram-negative bacteria. It was found to inhibit nearly all of the *Bacillus* species tested, including *B. subtilis*, *B. cereus*, and other *B. thuringiensis* strains. As well, it was shown to be highly active against *L. monocytogenes* and other *Listeria* species, such as *L. ivanovii* and *L. innocua*. Among the LAB, only *Carnobacterium piscicola* CU216 was sensitive. On the other hand, no activity was observed against any of the Gram-negative bacteria screened in the assay.

3.1.2. Biological significance of thurincin H

The fact that the thurincin H producer was isolated from honey suggests that it may play a role in defining the spectrum of antimicrobial activity of this medium. Since different types of honey exhibit varying ranges of antimicrobial activity, it has been postulated that bacterial honey isolates could originate from flowers, plants, hives, and even the stomachs of the bees themselves.[91, 99] This latter possibility would imply that the bees are actively cultivating these bacteria in a symbiotic relationship to help protect the food source for the hive.

Irrespective of its original source, *B. thuringiensis* SF361 may be commercially useful because of the bacteriocin it produces. Thurincin H can target *L. monocytogenes* without affecting LAB strains that constitute part of the beneficial flora in the gut. *L. monocytogenes* is the causative agent of the foodborne disease listeriosis, which targets pregnant women (and their unborn fetuses), newborn infants, the elderly, and the immunocompromised.[100] Clinical manifestations of listeriosis include septicemia, meningitis, and miscarriage.[100] As listerial contamination of deli meats and cheeses cannot be detected by visual inspection, there is significant interest in developing antilisterial agents, such as thurincin H, into viable food preservatives that would prevent this contamination altogether. In order to do so, further studies on thurincin H would be needed to characterize its structure and biosynthesis before evaluating its safety, efficacy, and feasibility for large-scale production.

3.1.3. Biosynthetic gene cluster of thurincin H

Worobo and co-workers also sequenced the biosynthetic gene cluster of thurincin H (**Figure 36**).[91] Interestingly, they found three copies of the structural gene (*thnA1*, *thnA2*, and *thnA3*) arranged in tandem within the cluster. All three of these genes are thought to be under the control of the same promoter, such that transcriptional activation at this site will likely result in the production of three times the amount of bacteriocin compared to if only one copy of the gene were present. Each *thnA* gene encodes for a 40-amino acid prepeptide that consists of a nine-residue leader and a 31-residue propeptide. Calculating the expected average molecular weight of the $[M+H]^+$ for this propeptide gives a mass of 3147.6 Da, which is eight daltons heavier than the observed mass (3139.5 Da) of thurincin H. Similar to the observations made with thuricin CD, this mass discrepancy indicates the presence of post-translational modifications in the mature bacteriocin.

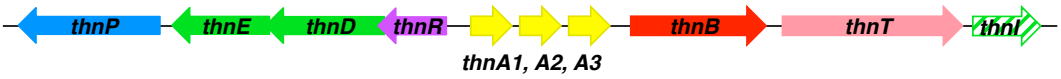

Figure 36. The biosynthetic gene cluster of thurincin H: *thnP* (blue) encodes for a protease that may cleave off the leader peptide; *thnE* and *thnD* (green) are thought to afford the producer strain resistance to thurincin H; *thnR* (purple) serves as a transcriptional regulator; *thnA1*, *A2*, and *A3* (yellow) encode for the bacteriocin precursor; *thnB* (red) produces an enzyme thought to post-translationally modify the precursor; *thnT* (pink) is likely responsible for the secretion of thurincin H from the cell; and *thnI* (green striped) has an unknown function, but is proposed to be involved in bacteriocin immunity.

Functions for the other genes in the cluster were proposed based on sequence homology analysis. *thnB* encodes for an enzyme that shows similarities

to AlbA, the Fe-S oxidoreductase that is proposed to form the S-Cα thioether bridges in subtilosin A.[60] This suggests that ThnB may catalyze a similar reaction to generate thioether linkages in thurincin H as well. Further processing of the bacteriocin precursor may be carried out by ThnP, which appears to be a serine protease that might cleave off the leader peptide, and by ThnT, an ABC transporter that likely exports the mature peptide from the cell.[91]

The remaining genes in the biosynthetic cluster are thought to be involved in immunity and regulation of thurincin H production. ThnD, an ATP-binding protein, and ThnE, a transmembrane protein, form the two domains of an ABC-transporter that may serve to expel bacteriocin molecules bound to the cytoplasmic membrane, similar to the function of NisFEG in nisin-producing bacteria.[3, 6] Although its role has yet to be confirmed, ThnI is proposed to be involved in immunity since its small size (95 aa) is comparable to that of other immunity proteins, such as NisI (245 aa), AlbB (53 aa) and PedB (112 aa).[6, 60, 68] ThnR is a putative transcriptional regulator, and may thus control the production of thurincin H.[91]

3.1.4. Project objectives

The objectives of this project were to confirm the amino acid sequence of thurincin H, determine the nature of its post-translational modifications, and elucidate its 3D structure. In a similar fashion to the studies conducted on thuricin CD, these goals were achieved using mass spectrometry and solution NMR techniques.

3.2. Results and discussion

3.2.1. Purification of thurincin H

Production of thurincin H was achieved by growing *B. thuringiensis* SF361 in tryptic soy broth (TSB) overnight. The supernatant of this culture was run through an Amberlite XAD-16 column and a Phenomenex C-18 SPE cartridge, before final purification by RP-HPLC. The cell pellet from the overnight culture was also resuspended in 70% IPA/ 0.1% TFA to extract any thurincin H adhered to the surface of the bacteria. Subsequent purification of this IPA extract employed C-18 SPE and RP-HPLC as well. On average, 1 L of bacterial culture yielded 12 mg of thurincin H. MALDI-TOF MS and spot-on-lawn activity testing were used to confirm the identity of the peptide (**Figure 37**).

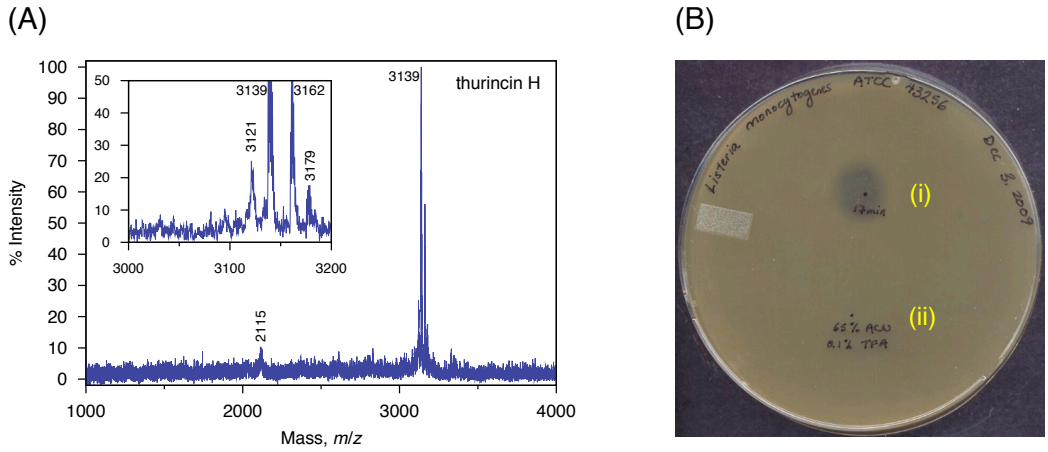

Figure 37. Characterization of thurincin H by MALDI-TOF MS and activity testing. (A) MALDI-TOF spectrum of thurincin H, where inset shows the $[M+H]^+$, $[M+Na]^+$ and $[M+K]^+$ peaks. 3121 Da represents a loss of H_2O from the parent ion, and 2115 Da represents a minor contaminant. (B) Spot-on-lawn activity test of thurincin H. Soft agar containing *L. monocytogenes* ATCC 43256 was overlaid onto a TSB plate. A 10 µL aliquot of an HPLC fraction containing the purified bacteriocin was spotted on top of the soft agar (i), along with 65% acetonitrile / 0.1% TFA as the negative control (ii). Results are observed after overnight incubation.

3.2.2. Characterization by FTICR MS and MS/MS sequencing

MALDI FTICR MS, which was performed by Dr. Randy Whittal, confirmed that thurincin H has an exact monoisotopic mass of 3137.36 Da. It also established that the molecular formula of the peptide ($C_{134}H_{204}N_{34}O_{45}S_4$) has eight fewer hydrogen atoms than the molecular formula predicted from genetic sequencing. Infusion nanoESI MS/MS and MALDI MS/MS (performed by Jing Zheng, Bela Reiz and Dr. Randy Whittal) were used to obtain complete coverage of the sequence for thurincin H (see Appendix B for a list of all peptide fragments). The bacteriocin was found to match the sequence of its structural gene in all but four positions. Specifically, Asn19, Thr22, Thr25 and Ser28 appear to be two mass units lighter than expected, indicating that these residues are post-translationally modified during maturation of the propeptide (**Figure 38**).[63]

Figure 38. The sequence of thurincin H, as determined by infusion nanoESI MS/MS and MALDI MS/MS. The residues that are two mass units lighter than expected are highlighted in blue (figure reproduced with permission from Sit *et al.*[63]).

3.2.3. Production of [^{13}C, ^{15}N]thurincin H

Labeling of thurincin H was undertaken to generate a peptide sample suitable for multidimensional NMR studies. Unfortunately, a test inoculation of *B. thuringiensis* SF361 into unlabeled Celtone revealed that the bacteria cannot grow and produce the bacteriocin in this media; instead, it sporulates and precipitates to

the bottom of the culture flask. To overcome this obstacle, different proportions of TSB were mixed with [^{13}C, ^{15}N]Celtone-CN on a small scale (10 mL) to test bacterial growth conditions and thurincin H production. It was found that 20% (v/v) unlabeled TSB and 80% (v/v) [^{13}C, ^{15}N]Celtone-CN gave the best compromise between the level of labeling achieved in thurincin H and a high yield of production. The partially labeled peptide was isolated using the same steps employed for unlabeled thurincin H. From 1 L of 20% TSB and 80% [^{13}C, ^{15}N]Celtone-CN, an average of 8 mg of partially [^{13}C, ^{15}N]-labeled thurincin H could be obtained. MALDI-TOF MS gave a predominant peak at 3213 Da, which appears within a wide spread of isotopic peaks (**Figure 39**). This peak has gained only 76 mass units, compared to the 168 mass units expected for fully [^{13}C, ^{15}N]-labeled thurincin H (theoretical $[M+H]^+$ = 3306 Da), suggesting that the peptide sample is on average 45% labeled. Assuming an even distribution of ^{13}C and ^{15}N incorporation over the entire molecule, it was hypothesized that each carbon and nitrogen would be statistically and sufficiently labeled for NMR purposes. Hence, the purified sample of partially [^{13}C, ^{15}N]-labeled thurincin H was dissolved in CD_3OH and used to collect spectroscopic data, without further attempts to optimize the levels of isotopic labeling.

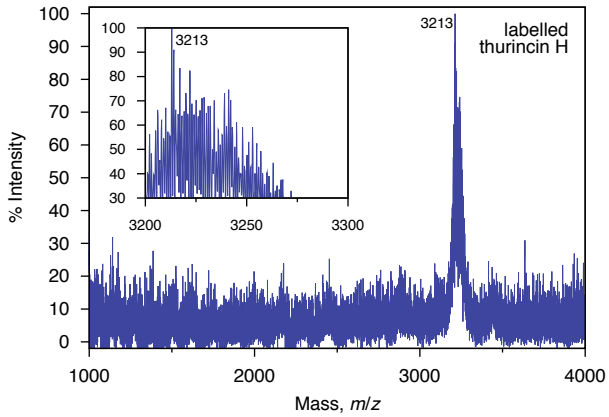

Figure 39. MALDI-TOF spectrum of partially [^{13}C, ^{15}N]-labeled thurincin H. Inset shows expansion of the predominant peak at 3213 Da.

3.2.4. Secondary structure prediction via CD and ^{15}N HSQC

To determine whether thurincin H holds any defined secondary structure in solution, CD and ^{15}N HSQC spectra were acquired. When dissolved in 100% MeOH, the CD spectrum (which was collected by David Zinz and Craig Turk) gave an unusual trace that differs from the typical spectra observed for alpha helices, beta sheets or random coil peptides (**Figure 40**). With a strong negative band at 206 nm and a positive band at 229 nm, the thurincin H spectrum appears to show some similarities to the CD spectra of polyproline helices, such as collagen.[101, 102] Another factor that may contribute to the unique shape of the CD trace is the presence of β-turns, which are frequently characterized by negative bands at 205 nm.[102] As well, depending on its conformation within a peptide, tryptophan residues are known to alter the molar ellipticities observed at 227 nm, suggesting that Trp2 and Trp5 of thurincin H may also have affected the CD spectrum.[102, 103] Although the type of secondary structure held by thurincin H is

unclear, CD spectroscopy has established that the peptide is not a random coil in solution.

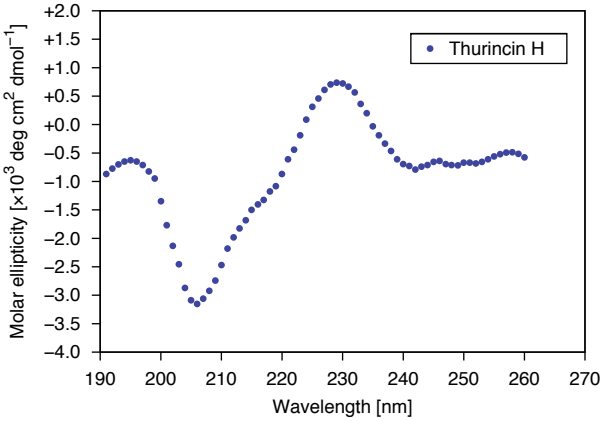

Figure 40. CD spectrum of thurincin H in 100% MeOH.

In the ^{15}N HSQC spectra of thurincin H, the backbone amide crosspeaks were well dispersed, with 28 out of 31 amides giving rise to unique chemical shifts (**Figure 41**). This spectral dispersion provides further evidence that the bacteriocin holds a defined structure in solution.

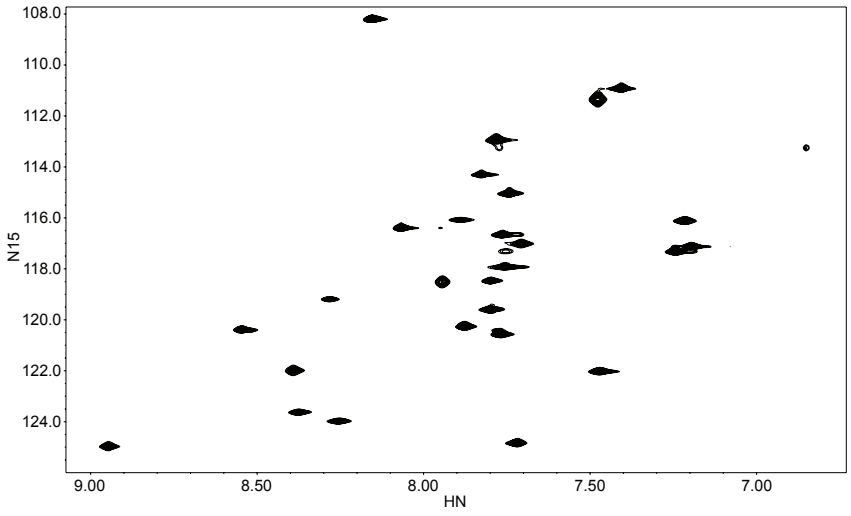

Figure 41. ^{15}N HSQC spectrum of thurincin H (figure adapted from Sit *et al*.[63]).

3.2.5. Structural elucidation of post-translational modifications

3.2.5.a. Chemical shift assignments

A series of two- and three-dimensional NMR experiments was run on thurincin H to assign chemical shifts for the majority of its atoms (see Appendix B for a full list of chemical shift assignments). Notably, the chemical shifts for the α-carbons of Asn19, Thr22, Thr25 and Ser28 are 10 to 15 ppm downfield of average values expected for unmodified Asn, Thr and Ser residues in random coil peptides (**Table 10**).[86] These downfield values are similar to the chemical shifts of the modified α-carbons in thuricin CD and subtilosin A (see Chapter 2).[32, 76] Examination of TOCSY and ^{13}C-HSQC data indicated that there are no attached protons at the α-carbons of the modified residues, consistent with the presence of sulfur to α-carbon linkages at positions 19, 22, 25 and 28 in thurincin H.

Table 10: Chemical shifts of the modified residues in thurincin H[a]

	Asn19[b]	Thr22	Thr25	Ser28
Cα	67.1	72.4	72.4	72.7
Cβ	41.2	71.5	70.9	65.3
Hα	**none**	**none**	**none**	**none**
Hβ	3.23, 3.13	4.80	4.88	4.34, 3.93

[a]All chemical shifts are reported in units of ppm.
[b]To compare, the expected chemical shifts for unmodified Asn are 53.1 ppm (Cα), 38.9 ppm (Cβ), 4.74 ppm (Hα), 2.83 ppm (Hβ1), and 2.75 ppm (Hβ2).[86]

3.2.5.b. NOE analysis of modified residues

The connectivity of the four cysteines to the four modified residues was determined by analysis of the NOE data collected for thurincin H. Long-range ^{1}H-^{1}H NOEs were observed between the β-protons of Cys4 and the amide proton

(HN) of Ser28, the β-protons of Cys7 and the HN of Thr25, and the β-protons of Cys13 and the HN of Asn19. Likewise, NOEs were seen between the α-proton of Cys10 and the HN of Thr22, and one of the β-protons of Cys10 and the HN of Thr22 (for a complete list of relevant NOE correlations, see Appendix B). Altogether, this NOE data implies that sulfur to α-carbon thioether linkages connect Cys4 to Ser28, Cys7 to Thr25, Cys10 to Thr22, and Cys13 to Asn19 (**Figure 42**).[63]

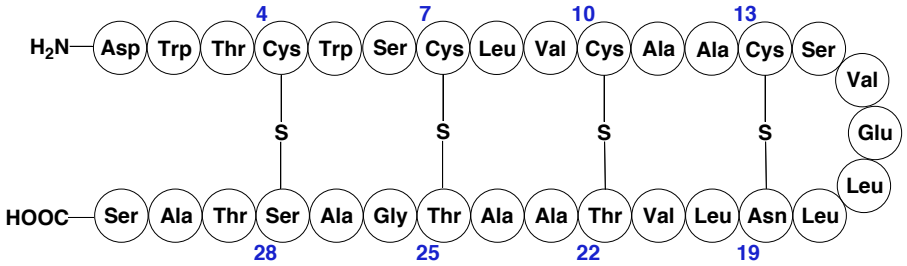

Figure 42. Diagram representing the connectivity of residues in thurincin H.

3.2.6. NMR solution structure of thurincin H

3.2.6.a. Structure calculations and comparison of stereoisomers

Following the same procedure detailed in section **2.2.6.a.**, descriptions of modified asparagine with L-stereochemistry (MASN) or D-stereochemistry (DASN) were designed and added to the CYANA residue library. Corresponding constraints files were also used to create the S-Cα linkages in thurincin H (see Appendix B for the complete residue descriptions and constraints files). Since there are four bridges, each of which can hold one of two possible stereochemical conformations at the α-carbon, 16 distinct stereoisomers must be considered when

determining the 3D structure of thurincin H.[63] Eight rounds of structure calculations were performed for all 16 stereoisomers using the same NOE peak lists and angle constraints derived from the HNHA experiment and the TALOS program.[88] The results were compared to determine which structure best fits the NMR data.

Interestingly, the stereoisomer that gave the best match to the NOE data featured D-stereochemistry at Asn19 (α-S), Thr22 (α-S), Thr25 (α-S), and Ser28 (α-S) (**Figure 43**).[63] Having the same stereochemistry at all four bridges (i.e. a DDDD isomer) is a feature unique to thurincin H, as the structures for thuricin CD (discussed in Chapter 2) and subtilosin A indicate that these peptides hold an LLD and LDD configuration, respectively.[32, 37, 76]

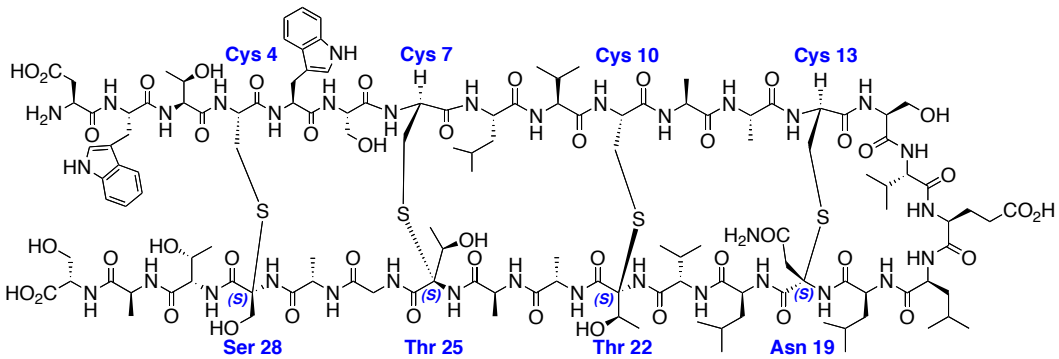

Figure 43. The chemical structure of thurincin H (figure reproduced with permission from Sit *et al.*[63]).

The DDDD isomer was chosen as the representative structure of thurincin H over the other stereoisomers for several reasons. First, the DDDD isomer was the only structure that did not generate any constraint violations in CYANA. All of the other stereoisomers gave rise to structures with at least one distance, van

der Waals, angle or coupling constant violation (**Table 11**). Secondly, CYANA incorporated the greatest number of assigned NOEs into the structure calculations for the DDDD isomer, using anywhere from three to thirty-five more NOEs than for the other stereoisomers (**Table 12**). The DDDD isomer also has, by far, the lowest average target function value of the sixteen stereoisomers, indicating that its structure most accurately reflects the NOE restraint data that formed the original basis of the structure calculations.[63]

Table 11: Constraint violations generated by each stereoisomer of thurincin H[63]

Table entry	Isomers	Distance violations	van der Waals violations	Angle violations	Coupling constant violations
1	LLLL	2	10	2	3
2	DLLL	2	7	1	2
3	DDLL	0	0	0	1
4	DDDL	0	0	0	1
5	DDDD	0	0	0	0
6	LDLL	2	5	1	5
7	LDDL	1	5	1	1
8	LDDD	1	5	1	0
9	LLDL	3	8	2	10
10	LLDD	4	9	3	4
11	LLLD	3	9	0	6
12	LDLD	1	5	1	3
13	DDLD	0	0	0	3
14	DLLD	5	5	1	12
15	DLDD	1	5	1	1
16	DLDL	2	0	0	4

Table 12: Comparison of statistics generated by stereoisomers of thurincin H[63]

	Isomers	Assigned NOEs[a]	rmsd (Å)	ATFV[b]	Ramachandran plot statistics[c]
1	LLLL	492	0.66 ± 0.25	10.56	76.5% / 22.9% / 0.6%
2	DLLL	490	0.95 ± 0.37	5.71	76.8% / 22.9% / 0.3%
3	DDLL	485	0.95 ± 0.41	0.45	68.8% / 30.9% / 0.3%
4	DDDL	489	1.09 ± 0.26	0.15	83.2% / 15.0% / 1.8%
5	DDDD	502	0.74 ± 0.17	0.03	86.8% / 13.2%
6	LDLL	484	1.07 ± 0.24	5.50	73.5% / 25.6% / 0.9%
7	LDDL	494	1.91 ± 0.55	5.18	77.1% / 22.6% / 0.3%
8	LDDD	499	0.77 ± 0.21	4.97	80.6% / 19.4%
9	LLDL	485	1.58 ± 0.56	7.93	43.2% / 53.8% / 2.9%
10	LLDD	490	0.79 ± 0.27	11.36	60.9% / 38.8 % / 0.3%
11	LLLD	483	0.79 ± 0.27	4.81	71.2% / 19.4% / 8.8% / 0.6%
12	LDLD	494	0.80 ± 0.30	5.55	58.2% / 38.8% / 2.9%
13	DDLD	492	1.06 ± 0.24	0.39	70.3% / 29.7%
14	DLLD	479	1.20 ± 0.47	2.83	43.2% / 50.6% / 6.2%
15	DLDD	483	1.06 ± 0.22	5.54	65.9% / 33.8% / 0.0% / 0.3%
16	DLDL	467	1.79 ± 0.80	1.11	52.1% / 40.6% / 5.6% / 1.8%

[a]Represents total number of off-diagonal NOE assignments used by CYANA to perform the structure calculation.
[b]ATFV = Average target function value
[c]Values represent percentage of dihedral angles plotted as ϕ versus ψ that fall into the most favoured regions / additionally allowed regions / generously allowed regions / disallowed regions for polypeptide backbone angles.

The 3D structure of thurincin H (**Figure 44**) features a helical backbone that is folded over and held in position by its four S-Cα thioether bridges, similar to the structures of the thuricin CD peptides Trn-α and Trn-β. The backbones of the 20 lowest energy conformers for the DDDD isomer superimpose quite well, resulting in a reasonably low backbone rmsd of 0.74±0.17Å (**Figure 45**). The structural statistics of the DDDD isomer are summarized in **Table 13**.[63]

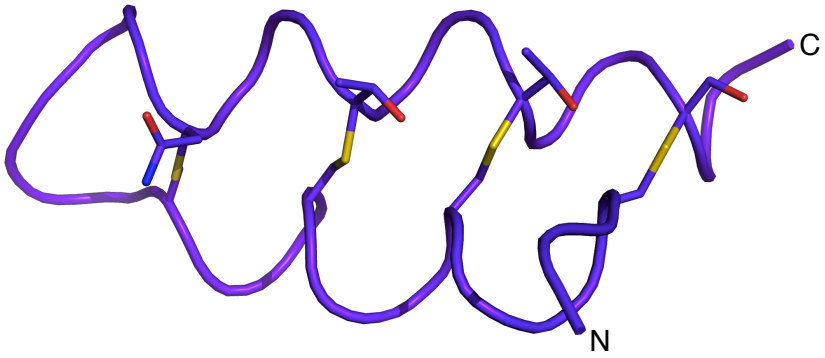

Figure 44. Cartoon representation of the 3D solution structure of thurincin H (DDDD isomer). The N- and C-termini are indicated in the structure (figure reproduced with permission from Sit *et al*.[63]).

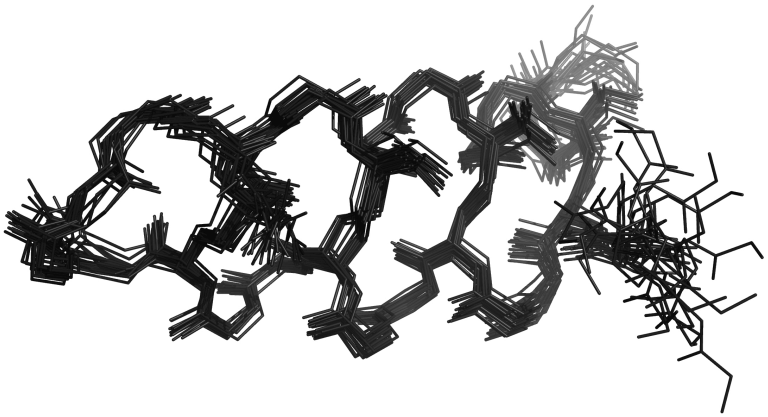

Figure 45. Backbone overlay of the 20 lowest energy conformers of thurincin H (DDDD isomer) (figure reproduced with permission from Sit *et al*.[63]).

Table 13: Structural statistics for thurincin H (DDDD)[63]

Structural statistics	Thurincin H
Distance and angle restraints	
total cross peak assignments	502
short ($\|i–j\| \leq 1$)	378
medium ($1 < \|i–j\| < 5$)	59
long ($\|i–j\| \geq 5$)	65
number of ϕ angles	22
Average target function value	0.03
rmsd (Å) for residues 1-30	
backbone	0.74 ± 0.17
heavy atoms	1.44 ± 0.22

3.2.6.b. Structural features of thurincin H

The 3D solution structure of thurincin H has several notable features. Similar to thuricin CD and subtilosin A, most of the side chains of thurincin H point in an outward direction, allowing the helical coils of the backbone to pack together more tightly along the central axis of the molecule (**Figure 46**).[32, 37, 76]

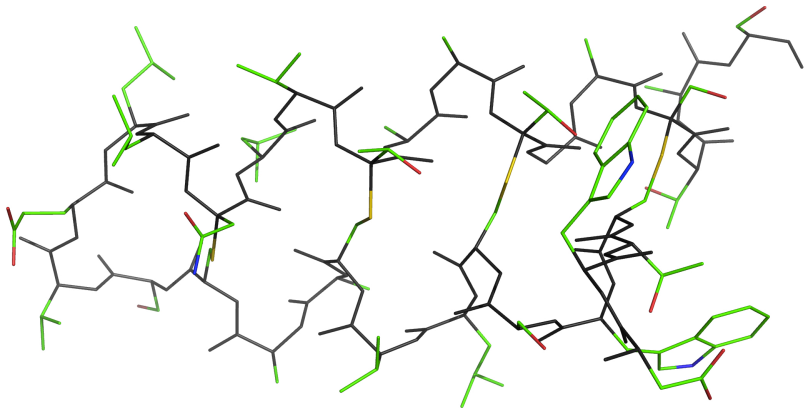

Figure 46. Stick representation of thurincin H, illustrating most of the side chains pointing outward. The backbone is colored grey and all of the side chains are highlighted according to element [carbon = green, oxygen = red, nitrogen = blue, and sulfur = yellow] (figures reproduced with permission from Sit *et al*.[63]).

Another unusual observation from the NMR characterization of thurincin H was that the Thr29 methyl group protons have a chemical shift of 0.14 ppm, which deviates significantly from the average expected value of 1.2 ppm for threonine Hγ protons.[86] Closer examination of the 20 lowest energy conformers reveals that the methyl group of Thr29 spends a predominating amount of time being held within 5 Å of the face of the Trp5 indole ring (**Figure 47**). This suggests that the Hγ protons experience significant diamagnetic anisotropy from the electron cloud of the indole ring, providing a rationale for the resultant upfield

chemical shift. This structural feature involving Thr29 and Trp5 represents yet another interaction between two residues widely separated in sequence, reinforcing the tightly packed nature of the peptide's structure.[63]

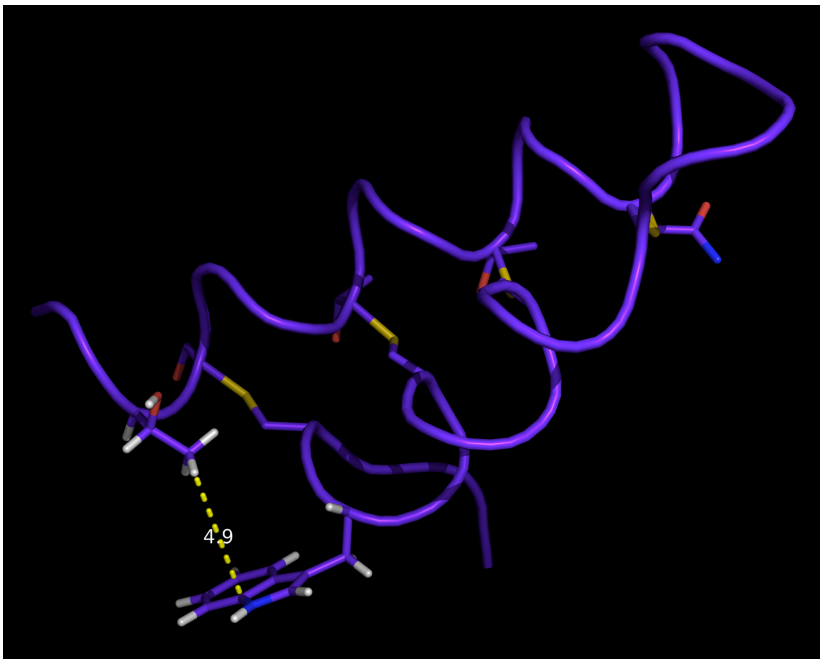

Figure 47. Cartoon representation of thurincin H, showing the interaction of Thr29 with Trp5. A distance of 4.9 Å was measured between one of the Hγ of Thr29 and $C\varepsilon_2$ of Trp5 (figure reproduced with permission from Sit *et al*.[63]).

The electrostatic surface potential of thurincin H is characterized by a net anionic charge (**Figure 48A**). The regions of negative charge localize to the C-terminal carboxylate and aspartic acid on one end of the molecule, as well as to the glutamic acid extending outwards from the other end of the molecule. Aside from the charged residues, the other hydrophilic residues cluster together on one face of thurincin H, while the hydrophobic residues form prominent patches over the remaining surface of the peptide (**Figure 48B**). If thurincin H operates by

disrupting bacterial cell membranes, similar to the mechanism of action proposed for subtilosin A, then its amphipathic nature would suggest that it can form pores in the membranes of its target strains.[32, 63, 64]

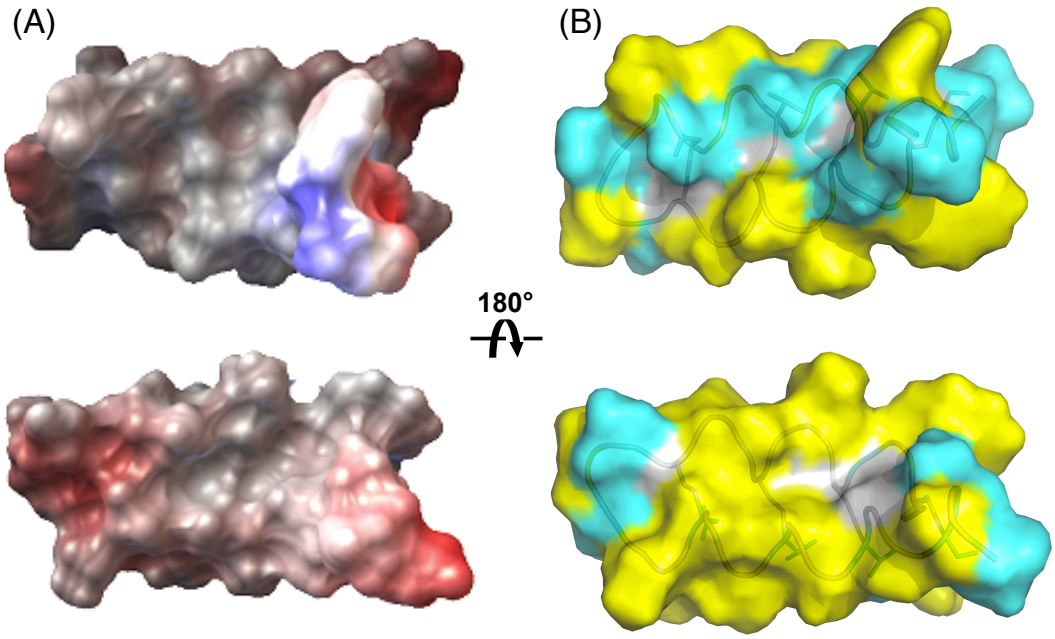

Figure 48. (A) Electrostatic surface potential of thurincin H, where blue indicates positive charge and red indicates negative charge. (B) Surface hydrophobicity of thurincin H, where yellow represents hydrophobic residues and cyan represents hydrophilic residues (figure reproduced with permission from Sit *et al*.[63]).

3.3. Conclusion and future directions

The structural elucidation of thurincin H is significant not only because it describes the first example of a peptide with four S-Cα bridges, but also because it may represent the structure of multiple peptides reported in the literature. From our MALDI MS and FTICR analyses, we found the exact monoisotopic mass of thurincin H to be 3137.36 Da.[63] By comparison, the monoisotopic masses reported for thuricin S and cerein MRX1 are 3137.61 Da and 3137.93 Da,

respectively.[92, 93] Edman or MS/MS sequencing indicated that both of these peptides have similar, if not identical, N-terminal sequences to thurincin H.[92, 93] Gray *et al.* reported the average molecular weight of thuricin 17 to be 3162 Da. However, a smaller peak at 3139 Da, which is 23 Da or one sodium ion lighter than 3162 Da, can be observed in the MALDI-QTOF spectrum of the peptide.[104] If 3139 Da represents the average molecular weight of the parent $[M+H]^+$ ion, then its monoisotopic mass would be calculated as 3137 Da. Coincidentally, the open reading frame prediction for the thuricin 17 gene gives a predicted peptide sequence identical to that of thurincin H.[105] Likewise, bacthuricin F4 has a homologous N-terminal (DWTXWSXL) sequence, physical and biological properties that are highly similar to thuricin 17, and a molecular mass of 3160.05 Da, which also happens to be 23 Da heavier than 3137 Da.[96, 106] Although further FTICR-MS/MS analysis would be needed to confirm their amino acid sequences, it is highly probable that thuricin S, cerein MRX1, thuricin 17 and bacthuricin F4 all have the same structure as thurincin H. As such, it is interesting to find that several distinct strains of *Bacillus thuringiensis* produce the same peptide, underscoring the biological and ecological importance of this molecule. Future studies on thurincin H will focus on elucidating its mechanism of action through structure-activity relationship studies and on identifying its cellular target through NMR binding studies.

Chapter 4. Double serine mutant of leucocin A

4.1. Background

4.1.1. Structure and biological activity of leucocin A

Leucocin A is a bacteriocin produced by *Leuconostoc gelidum* UAL 187, an LAB strain that was isolated from vacuum packaged meat.[107] The peptide is 37 residues long, and features a disulfide bond between Cys9 and Cys14 (**Figure 49**). It shares a highly conserved N-terminal YGNGV sequence with other non-post-translationally modified bacteriocins, such as pediocin PA-1, mesentericin Y105, carnobacteriocin B2, sakacin A (also known as curvacin A) and sakacin P.[108] As such, it is classified as a pediocin-like bacteriocin. In terms of biological activity, leucocin A can inhibit *L. monocytogenes*, *E. faecalis*, and a variety of LAB.[107]

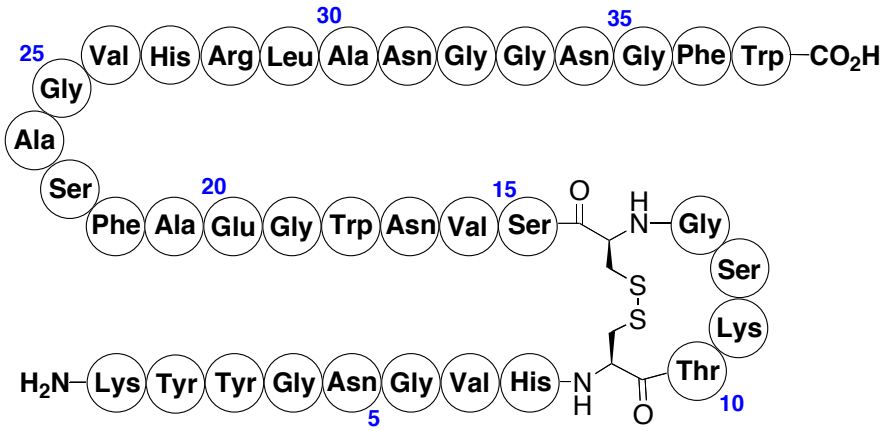

Figure 49. Diagram representing the structure of leucocin A. The chemical structure of the disulfide bridge between Cys9 and Cys14 has been drawn out in full (figure adapted from Sit and Vederas[25]).

4.1.2. Biosynthetic gene cluster of leucocin A

The putative biosynthetic gene cluster of leucocin A consists of five genes found in two separate operons that are located on opposite strands of DNA (**Figure 50**).[109, 110] The structural gene, *lcaA*, encodes for a precursor peptide that consists of a 24-residue N-terminal leader and a 37-residue propeptide. After ribosomal translation, the disulfide bond in the propeptide portion is thought to form prior to further processing of the precursor (i.e. proteolysis of the N-terminal leader and export from the cell). Within the same operon, *lcaB* serves as an immunity gene to protect the producer strain from the activity of its own bacteriocin.[109] The remaining three genes in the biosynthetic cluster are located further upstream and on the opposite strand of *lcaA-lcaB*. Based on sequence homology, LcaC is thought to be an ABC-transporter that cleaves off the N-terminal leader peptide before exporting the mature leucocin A molecule. LcaD is a mostly hydrophilic protein with an N-terminal hydrophobic segment that anchors it to the intracellular leaflet of the cell membrane. It is proposed to act as an accessory to LcaC, facilitating the secretion of the bacteriocin. The hydrophilic LcaE shows homology to a protein encoded by the mesentericin Y105 gene cluster, but has no known function and does not appear to be essential for leucocin A production.[110]

Figure 50. The biosynthetic gene cluster of leucocin A: *lcaA* (yellow) encodes for the precursor peptide; *lcaB* (green) affords immunity; *lcaC* (pink) is responsible for the N-terminal processing and secretion of the bacteriocin; *lcaD* (orange) produces an accessory protein that facilitates leucocin export; and *lcaE* (grey) has an unknown function.

4.1.3. NMR structure of leucocin A

The structure of leucocin A has been previously studied in our group using solution NMR techniques. It was found that the peptide exists as a random coil in water or aqueous dimethylsulfoxide (DMSO), but assumes a defined conformation when dissolved in TFE or dodecylphosphocholine (DPC) micelles.[108] The 3D solution structure of leucocin A in TFE (**Figure 51**) features an N-terminal three-stranded β-sheet (residues 2-16) and a C-terminal amphipathic α-helix (residues 17-31).[108, 111] In DPC micelles, the peptide exhibits the same structural features, but the orientation of the β-sheet with respect to the α-helix varies slightly compared to the structure in TFE.[108]

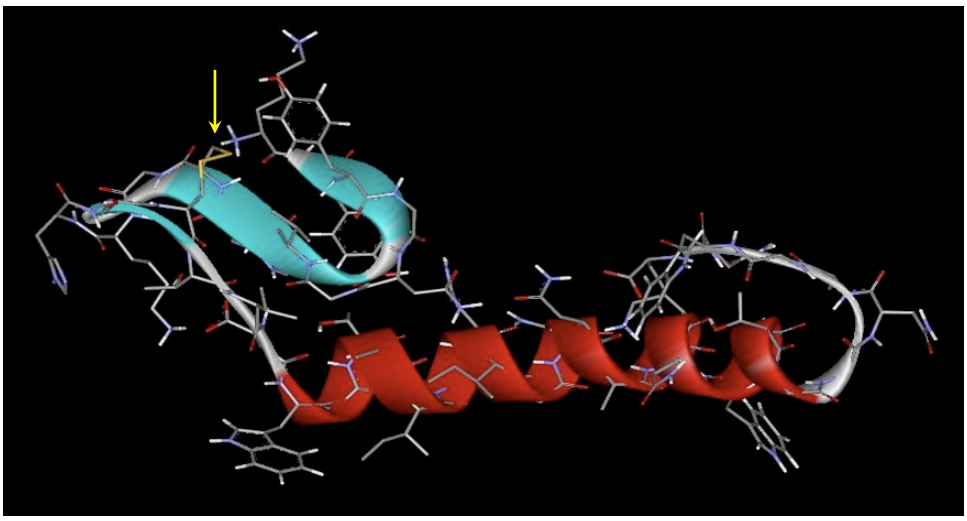

Figure 51. The 3D NMR structure of leucocin A in TFE, with its N-terminal β-sheet shown in blue and its C-terminal α-helix coloured in red. The yellow arrow highlights the position of the disulfide bridge (figure reproduced with permission from Sit and Vederas[25]).

The solution NMR structure of leucocin A represents the first 3D structure reported for a pediocin-like bacteriocin. The structures of three other closely related peptides have since been elucidated: carnobacteriocin B2 (and precarnobacteriocin B2),[111, 112] sakacin P (and a mutant of sakacin P),[113] and curvacin A.[114] Comparison of these NMR structures has led to several interesting observations. Although all of these peptides have highly conserved N-terminal sequences, the N-terminal domains show the greatest variation in conformation and appear to be somewhat unstructured in solution.[111, 113, 114] On the other hand, the C-terminal portions of the peptides form the same α-helical motif, despite significant differences in their sequences. As discussed in chapter 1 (section 1.6.2.), this C-terminal helix is thought to recognize and bind to specific man-PTS transmembrane proteins expressed on the surface of sensitive bacteria, and therefore governs the spectrum of activity for a given bacteriocin.[2, 71, 72] It has

been proposed that after inserting into the cell membrane and interacting with its protein receptor, the amphipathic helices from several bacteriocin molecules will aggregate together to form pores, leading to cytosolic leakage and eventual cell death.[2, 25, 72, 115] Despite extensive NMR, biochemical and genetic studies, however, a general function for the structurally varied N-terminal domains of the pediocin-like bacteriocins has yet to be established.

4.1.4. Structure-activity relationship studies of leucocin A

SAR studies on leucocin A were conducted to determine whether its disulfide bridge is essential for biological activity. Using chemical synthesis, a series of analogues with substitutions at residues 9 and 14 were generated.[73, 116] It was found that replacement of the disulfide loop with a carbocyclic ring (carba leucocin A, **Figure 52A**) led to a 10-fold decrease in activity.[116] However, since the MIC_{50} of carba-leucocin A is still in the nanomolar range (370 nmol/L against *C. maltaromaticum* UAL26), this suggests that the carbocyclic ring might preserve the overall folding of the N-terminus and that the sulfur atoms in the disulfide bridge of natural leucocin A are not directly recognized in intermolecular interactions (e.g. during receptor binding or pore formation).[25, 116] Replacement of the cystine with unlinked amino acids (**Figure 52B**) at positions 9 and 14 produced analogues with varied antimicrobial potencies. Interestingly, phenylalanyl-leucocin A (also known as (C9F, C14F)-leucocin A), diallyl-leucocin A, and norvaline-leucocin A all retained activity comparable to that of the natural peptide against *C. maltaromaticum* UAL26, *C. divergens* LV13, and *L. monocytogenes* EGDe.[73] To explain these findings, it was postulated that

hydrophobic interactions between the side chains of these residues might hold the loop between residues 9 and 14 together, helping to maintain the active conformation of the bacteriocin.[73, 116] By contrast, the serine analogue, (C9S, C14S)-leucocin A, was found to be inactive, implying that hydrogen bonding between the hydrophilic side chains is insufficient to substitute for the role of the disulfide bridge, or that the serine residues alter the native secondary structure of the N-terminus altogether.[116]

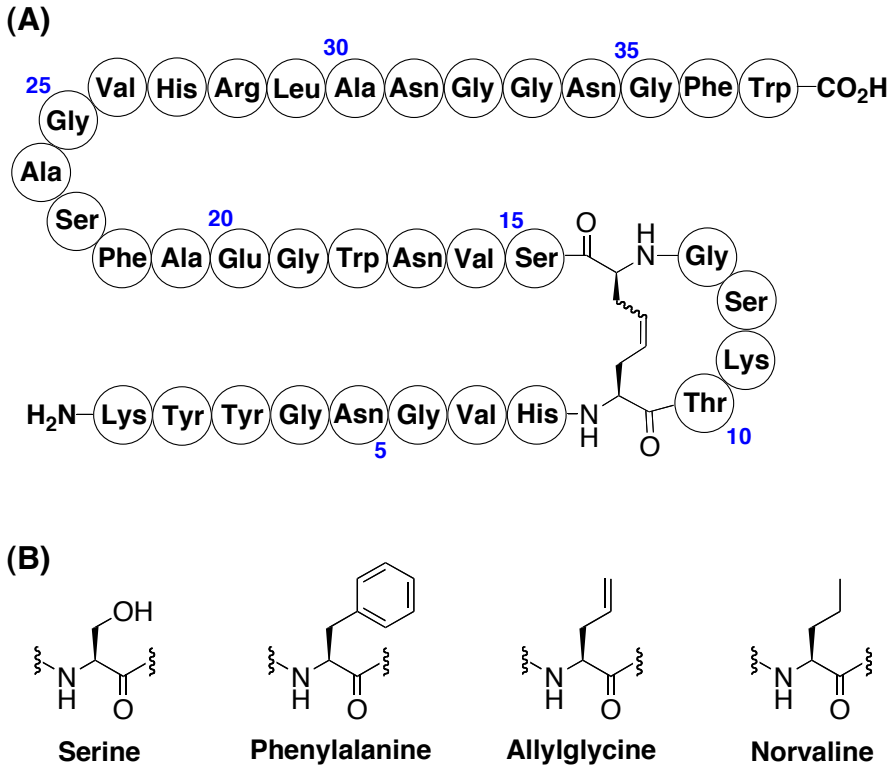

Figure 52. (A) Diagram representing the structure of carba-leucocin A, which was synthesized and biologically tested as a mixture of the *cis*- and *trans*-isomers.[116] (B) Structures of serine, phenylalanine, allylglycine, and norvaline used to replace Cys9 and Cys14 to generate (C9S, C14S)-leucocin A, (C9F, C14F)-leucocin A, diallyl-leucocin A, and norvaline-leucocin A, respectively.

4.1.5. Project objectives

Although it has been hypothesized that active leucocin A analogues maintain the same 3D geometry as the natural bacteriocin, as of yet there is no experimental evidence to support this proposal. The objectives for this project are to elucidate the 3D solution structures of active and inactive leucocin A analogues to determine how mutations at positions 9 and 14 affect the conformation of the peptide. To achieve these goals, (C9L, C14L)-leucocin A, (C9F, C14F)-leucocin A and (C9S, C14S)-leucocin A were heterologously expressed in *E. coli* as a method of producing [^{13}C, ^{15}N]-labeled peptides. The isotopically labeled analogues were then subjected to solution NMR studies to generate 3D structures. The following sections will discuss the production and structural elucidation of (C9S, C14S)-leucocin A. Experimental work on the other two mutants, (C9L, C14L)-leucocin A and (C9F, C14F)-leucocin A, is currently being performed by Christopher Lohans and Chantel Campbell, respectively.

4.2. Results and discussion

4.2.1. Heterologous expression of (C9S, C14S)-leucocin A

To facilitate purification of the protein, (C9S, C14S)-leucocin A was overexpressed as a maltose-binding protein (MBP) fusion. With assistance from Dr. Marco van Belkum, a gene that encodes for (C9S, C14S)-leucocin A was constructed and fused to the 3′-end of the MBP gene (*malE*) in the pMAL^{TM}-c2X expression vector. In brief, since *malE* contains unique cut sites for the *Sac*I and *Bam*H1 restriction endonucleases, a DNA sequence encoding (C9S, C14S)-

leucocin A fused to the MBP C-terminus was designed with a *Sac*I and *Bam*H1 recognition sequence at its 5′- and 3′-ends, respectively (**Figure 53**). Immediately following the C-terminal residues of MBP is a cleavage sequence (Ile-Glu-Gly-Arg) that is recognized by the factor Xa (FXa) protease. The (C9S, C14S)-leucocin A sequence is followed by a stop codon (TAA) and the *Bam*H1 recognition sequence. To create this DNA sequence, two long, overlapping primers (MVB193 and MVB194) were subjected to five cycles of PCR to build the full-length template. Two shorter primers (MVB191 and MVB192) were then added to the reaction mixture before performing another 15 cycles of PCR to amplify the gene. **Table 14** lists the primers used to construct and amplify the gene of interest.

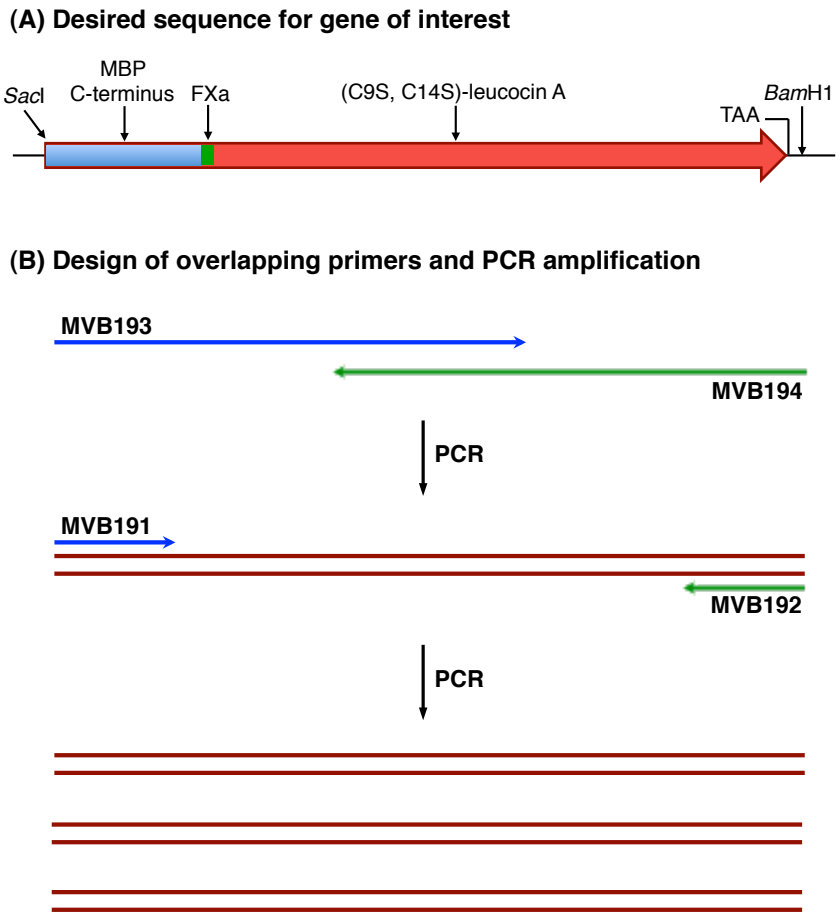

Figure 53. (A) A diagram representing the desired sequence for the gene of interest, which includes the *Sac*I recognition sequence, the C-terminal end of MBP, the FXa cleavage sequence, the sequence for (C9S, C14S)-leucocin A (LeuA mutant), a stop codon (TAA), and the *Bam*H1 recognition sequence. (B) A schematic representing the use of two long, overlapping primers (MVB193 and MVB194) to construct the full-length template of the gene of interest via PCR, followed by amplification with two short primers (MVB191 and MVB192).

Table 14: Primers used for constructing the (C9S, C14S)-leucocin A gene insert

Primer	Sequence[a]	Purpose
MVB193	5′-AATATGAGCTCGAACAACAACAACAATA ACAATAACAACAACCTCGGGATCGAGGGAAGG AAATACTACGGTAACGGCGTTCACTCTACCAA ATCTGGTTCTTCCG-3′	Forward long primer
MVB194	5′-TATATGGATCCTTACCAGAAACCGTTGCC ACCGTTCGCCAGACGGTGCACGCCAGCAGAGA ACGCTTCACCCCAGTTAACGGAAGAACCAGAT TTGGTAGAGTGAA-3′	Reverse long primer
MVB191	5′-AATATGAGCTCGAACAACAACAA-3′	Forward short primer
MVB192	5′-TATATGGATCCTTACCAGAAAC-3′	Reverse short primer

[a]The *Sac*I (GAGCTC) and *Bam*H1 (GGATCC) restriction sites are underlined, the FXa cleavage site is coloured green, and the DNA encoding the C-terminal end of MBP is coloured in blue. (C9S, C14S)-leucocin A is coloured in red, with the serine mutations highlighted in yellow. The stop codon is highlighted in grey.

The pMAL™-c2X vector and the PCR product containing the (C9S, C14S)-leucocin A gene were then digested with *Sac*I and *Bam*H1 to create complementary sticky ends in the DNA (**Figure 54**). Subsequent ligation of the digest products generated the MalE–(C9S, C14S)-LeuA construct, which was transformed into *E.coli* JM109 cells by electroporation. The resulting clones were sequenced, confirming that the desired gene had been incorporated and that no mutations by PCR had been introduced.

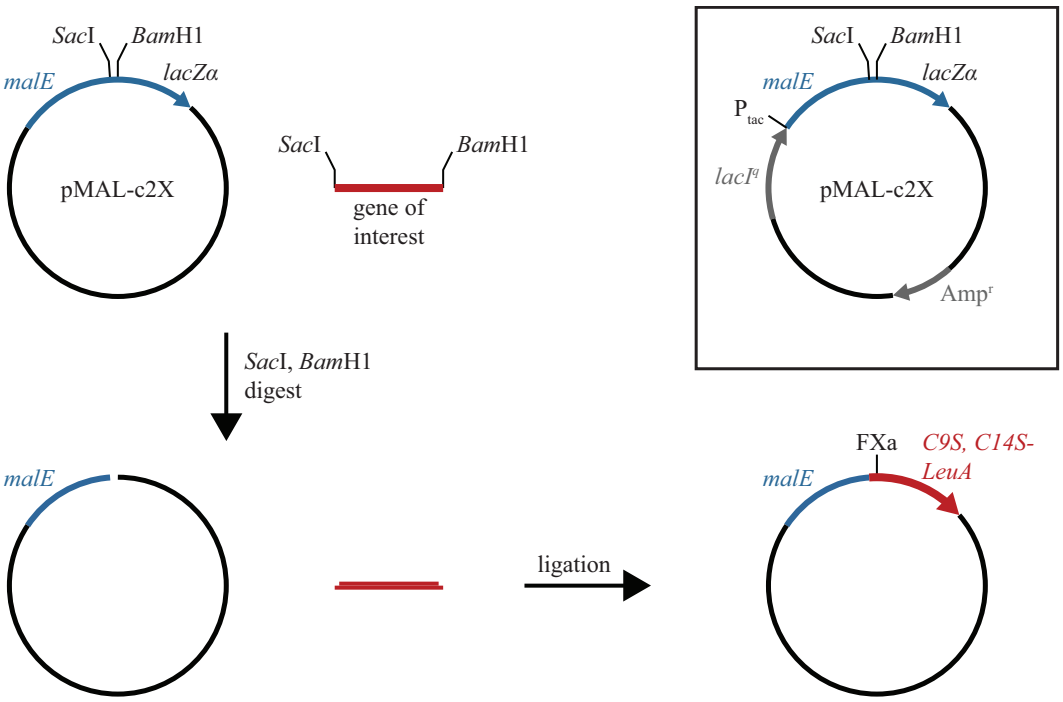

Figure 54. A schematic of the procedure to build the MalE–(C9S, C14S)-LeuA construct: the pMAL^{TM}-c2X vector and the (C9S, C14S)-leucocin A gene insert (labeled as "gene of interest") are digested with the *Sac*I and *Bam*H1 endonucleases; the resultant digest products are then ligated together to form the construct. Inset shows details of the original pMAL^{TM}-c2X vector, which contains an ampicillin resistance gene (Amp^{r}) as well as a Lac repressor gene (*lacI*^{q}) that induces expression from the P_{tac} promoter in the presence of isopropyl-β-D-1-thiogalactopyranoside (IPTG). The malE gene is initially fused to *lacZα*, which encodes for the α-fragment of β-galactosidase.

4.2.2. Purification of unlabeled and [^{13}C, ^{15}N]-labeled (C9S, C14S)-leucocin A

Overexpression of the MBP fusion protein was achieved by growing the transformed *E. coli* JM109 cells in Luria-Bertani (LB) broth until an OD_{600} (optical density measured at 600 nm) of 0.5 was reached, before supplementing the media with IPTG to a final concentration of 0.3 mM. Induction of gene expression by IPTG was monitored by sodium dodecyl sulfate polyacrylamide gel electrophoresis (SDS-PAGE) (**Figure 55**). After incubating for 3 h post-induction,

the cells were lysed using a cell disruptor, and the fusion protein was purified by amylose affinity chromatography. The isolated protein was subsequently dialyzed against water and lyophilized.

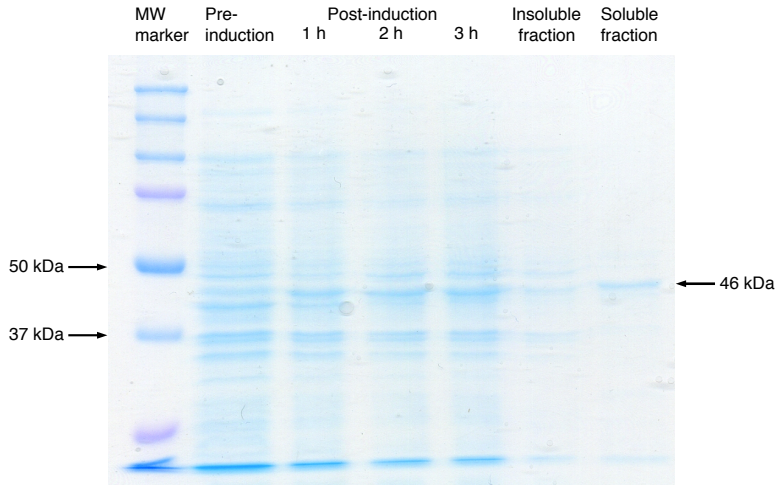

Figure 55. SDS-PAGE gel showing expression of protein in transformed JM109 cells before and up to 3 h after induction (i.e. addition of IPTG to the culture). The pre- and post-induction samples were obtained by mixing cells with SDS sample buffer (Tris-HCl, glycerol, SDS, bromophenol blue, pH 6.8). After 3 h post-induction, a sample of cells was sonicated and centrifuged to obtain the soluble fraction of proteins (the supernatant) and the insoluble fraction (pellet), both of which were mixed with SDS sample buffer prior to loading on the gel. The darkest band observed in the soluble fraction has a molecular weight of ~ 46 kDa, the expected mass of the fusion protein.

A pilot study was then conducted to determine the length of time needed to digest the fusion protein with FXa. Samples of the digest at different time points were analyzed by SDS-PAGE to track the cleavage of the fusion protein and appearance of free MBP. Since smaller peptides (MW < 5000 Da) would not be retained by SDS-PAGE, the digest samples were also monitored by MALDI-TOF MS to estimate the production of (C9S, C14S)-leucocin A. Through SDS-

PAGE and MALDI-TOF MS analysis, 2 h was established as the optimum length of time for the reaction. If the digest was run for longer than 2 h, significant amounts of a degradation product (2520 Da) would appear in the MALDI spectrum in addition to the desired (C9S, C14S)-leucocin A (3900 Da) (data not shown). In fact, when the fusion protein was dissolved in only the FXa reaction buffer (Tris-HCl, NaCl, $CaCl_2$, pH 8.0) for a control experiment, it slowly degraded over 24 h (**Figure 56**). Due to concerns that the (C9S, C14S)-leucocin A portion of the fusion protein is unstable at pH 8.0, each batch of the FXa cleavage reactions was immediately injected into the HPLC following 2 h of digestion. RP-HPLC purification led to the isolation of 2.5 mg of (C9S, C14S)-leucocin A per 1 L of LB. The identity of the desired peptide was checked by MALDI-TOF MS (**Figure 57**).

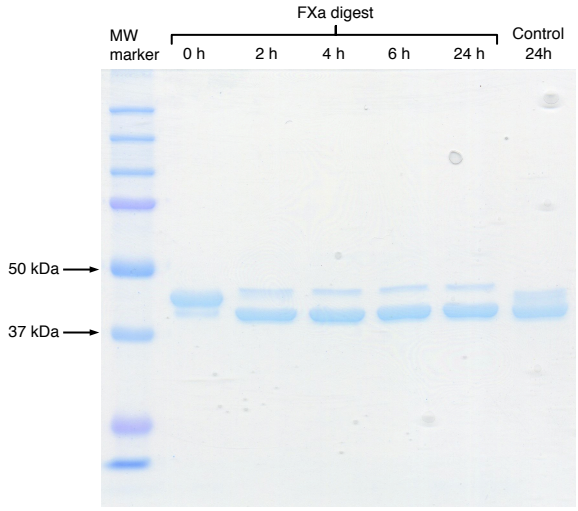

Figure 56. SDS-PAGE gel of a FXa digest of MBP–(C9S, C14S)-leucocin A during different time points, where a band at ~ 46 kDa (the fusion protein) fades and a band at ~ 42 kDa (the expected MW of MBP) appears. The control reaction suggests that the fusion protein is unstable when dissolved in FXa reaction buffer.

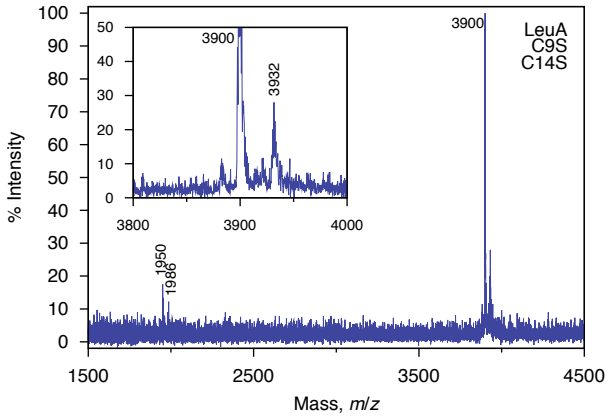

Figure 57. MALDI-TOF spectrum of (C9S, C14S)-leucocin A (3900 Da), where the inset shows an expansion of the predominant peak.

To produce [^{13}C, ^{15}N]-labeled (C9S, C14S)-leucocin A, the transformed *E. coli* JM109 cells would need to be grown in [^{13}C, ^{15}N]-labeled M9 minimal media. Prior to conducting the labeling experiment, a test growth of the JM109 cells in unlabeled M9 was first attempted. It was immediately observed that the cells grew extremely slowly (required 21-24 h to reach an OD_{600} of 0.5 as opposed to an average of 3.5 h in LB media to attain the same OD_{600}), and yielded only a tenth of the amount of fusion protein compared to expression in LB. To solve this problem, the MalE–(C9S, C14S)-LeuA expression vector was instead transformed into *E. coli* BL21(DE3) cells. Upon growth in M9 and subsequent IPTG induction, the BL21(DE3) cells grew well and expressed the fusion protein in amounts comparable to those obtained from JM109 grown in LB.

To complete the labeling, the transformed *E. coli* BL21(DE3) cells were grown in [^{13}C, ^{15}N] M9, induced with IPTG, and lysed. The expressed fusion protein was isolated by amylose affinity chromatography, dialyzed, and lyophilized prior to FXa cleavage and purification by RP-HPLC. MALDI-TOF

MS gave the expected mass of labeled peptide (4119 Da, **Figure 58**). For NMR studies, [^{13}C, ^{15}N]-(C9S, C14S)-leucocin A was dissolved in TFE-d_3/H_2O, 9:1 (v/v), to mirror the same conditions used to elucidate the 3D solution structure of wild-type leucocin A in TFE.[108]

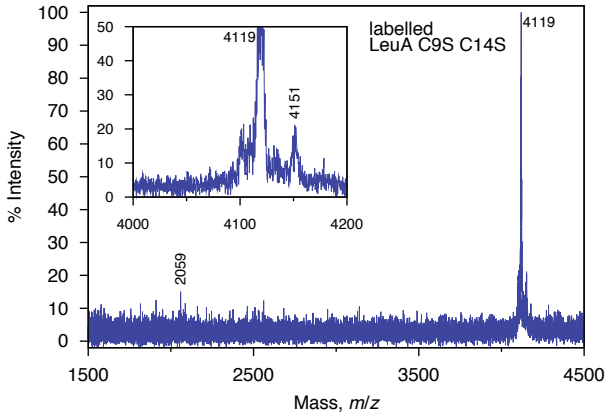

Figure 58. MALDI-TOF spectrum of [^{13}C, ^{15}N]-(C9S, C14S)-leucocin A (4119 Da), where the inset shows an expansion of the predominant peak.

4.2.3. Activity testing of (C9S, C14S)-leucocin A

Activity testing was performed on (C9S, C14S)-leucocin A, confirming that the double serine mutation renders the peptide inactive against strains that are sensitive to the wild-type bacteriocin (**Figure 59**).[107, 116] Spot-on-lawn assays against *C. maltaromaticum* UAL26, *C. divergens* LV13, *L. lactis* cremoris HP, and *L. monocytogenes* ATCC 43256 were performed using concentrations of 200 μM, 100 μM, 50 μM, 25 μM, 12.5 μM and 6.25 μM (C9S, C14S)-leucocin A. Wild-type leucocin A (200 μM) was used as the positive control and water was used as the negative control. A very faint zone of activity was observed for (C9S, C14S)-leucocin A against *C. maltaromaticum* UAL26 at 200 μM. At such a high concentration, however, the peptide is likely operating as a detergent on the cell

membranes of the bacteria. *L. lactis* cremoris HP, a strain that had not been previously tested for sensitivity to leucocin A, was found to be resistant to both (C9S, C14S)-leucocin A and the wild-type bacteriocin.

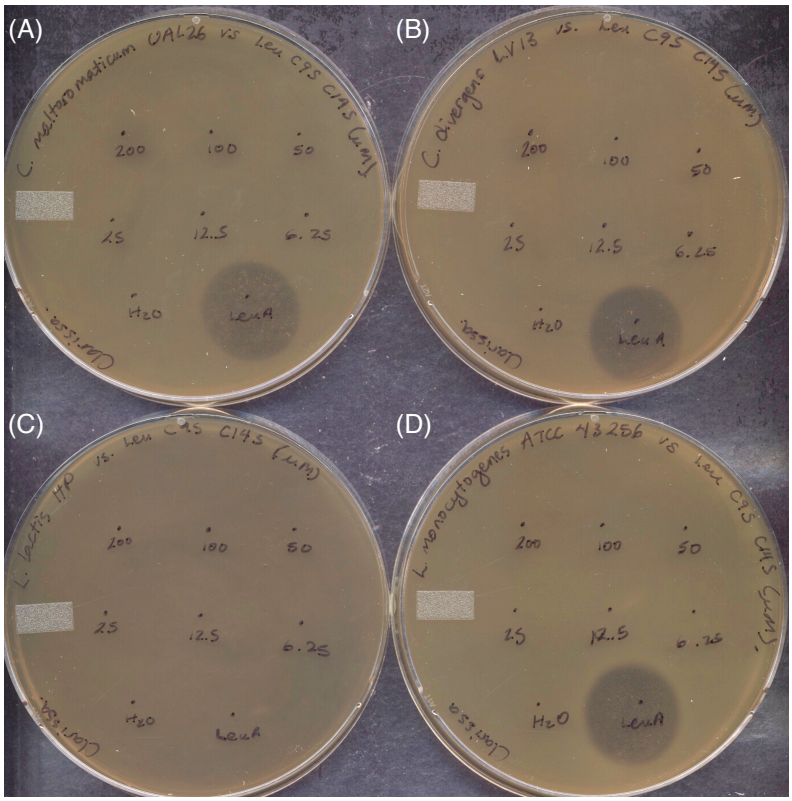

Figure 59. Activity testing (by spot-on-lawn assay) of (C9S, C14S)-leucocin A against (A) *C. maltaromaticum* UAL26, (B) *C. divergens* LV13, (C) *L. lactis* cremoris HP, and (D) *L. monocytogenes* ATCC 43256.

4.2.4. 3D NMR solution structure of (C9S, C14S)-leucocin A

4.2.4. Chemical shift assignments and structure calculations

A suite of multidimensional NMR experiments was run on [^{13}C, ^{15}N]-(C9S, C14S)-leucocin A to assign chemical shifts for most of the carbon, nitrogen and proton nuclei in the peptide (see Appendix C for a full list of chemical shift

assignments). The backbone amide crosspeaks in the ^{15}N HSQC of (C9S, C14S)-leucocin A were reasonably well dispersed, suggesting that the peptide holds a defined structure when dissolved in 90% TFE (**Figure 60**).

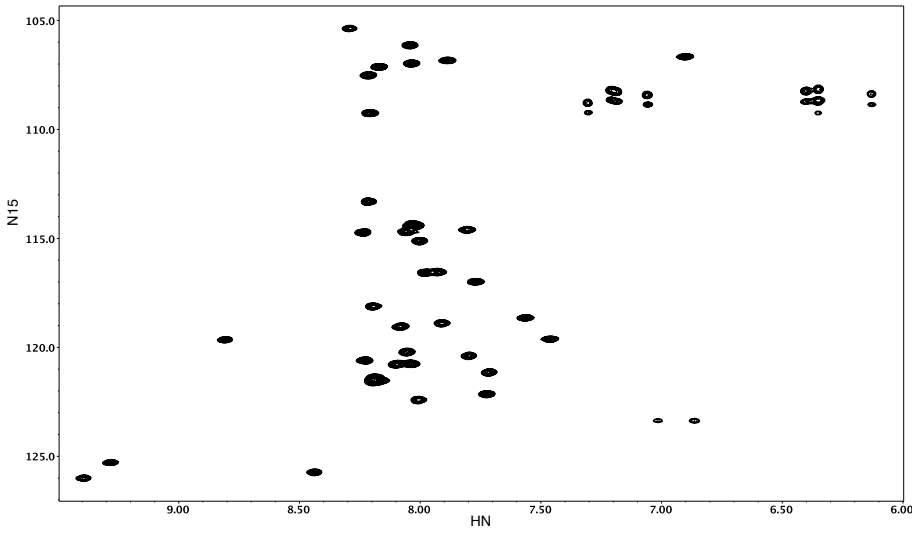

Figure 60. ^{15}N HSQC spectrum of (C9S, C14S)-leucocin A.

Structure calculations based on NOE data collected for the peptide, as well as on angle constraints derived from the HNHA experiment and the TALOS program,[88] were performed using CYANA 2.1.[87] A family of 20 structures, representative of the solution structure of (C9S, C14S)-leucocin A, formed an α-helix between residues 14 to 30 (**Figure 61**). The structural statistics for this ensemble are summarized in **Table 15**.

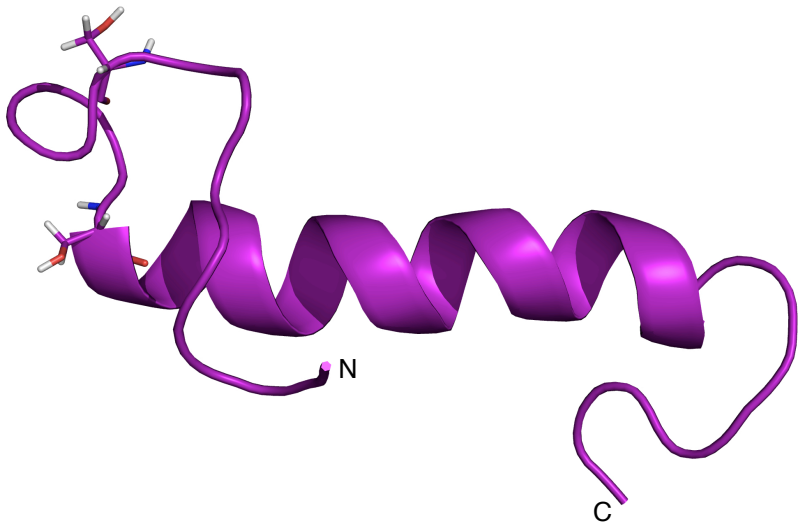

Figure 61. Cartoon representation of the 3D solution structure of (C9S, C14S)-leucocin A. The side chains and backbones of Ser9 and Ser14 are shown in stick form. The N- and C-termini are indicated in the structure.

Table 15: Structural statistics for (C9S, C14S)-leucocin A

Parameter	Value
Total NOE cross peak assignments	403
short range ($\|i–j\| \leq 1$)	328
medium range ($1 < \|i–j\| < 5$)	61
long range ($\|i–j\| \geq 5$)	14
Number of ϕ angles	27
Average target function value	0.17
rmsd (Å) for residues 1-36	
backbone	2.13 ± 0.72
heavy atoms	3.07 ± 0.78
rmsd (Å) for residues 14-30	
backbone	0.68 ± 0.27
heavy atoms	1.11 ± 0.21
Ramachandran plot for residues 1-36	
ϕ/ψ in most favoured regions	84.8%
ϕ/ψ in additionally allowed regions	15.2%
ϕ/ψ in generously allowed regions	0
ϕ/ψ in disallowed regions	0

The backbone rmsd value of 2.13 ± 0.72 Å for the first 36 residues of (C9S, C14S)-leucocin A is comparable to the rmsd values obtained for the structures of carnobacteriocin B2 and wild-type leucocin A.[108, 111] The backbones of the 20 structures for (C9S, C14S)-leucocin A overlap well in the helical region from Ser14 to Ala30, but the N- and C-terminal ends show much greater variation in conformation (**Figure 62**). Indeed, if the rmsd is calculated for only residues 14 to 30, the backbone rmsd value drops to 0.68 ± 0.27 Å.

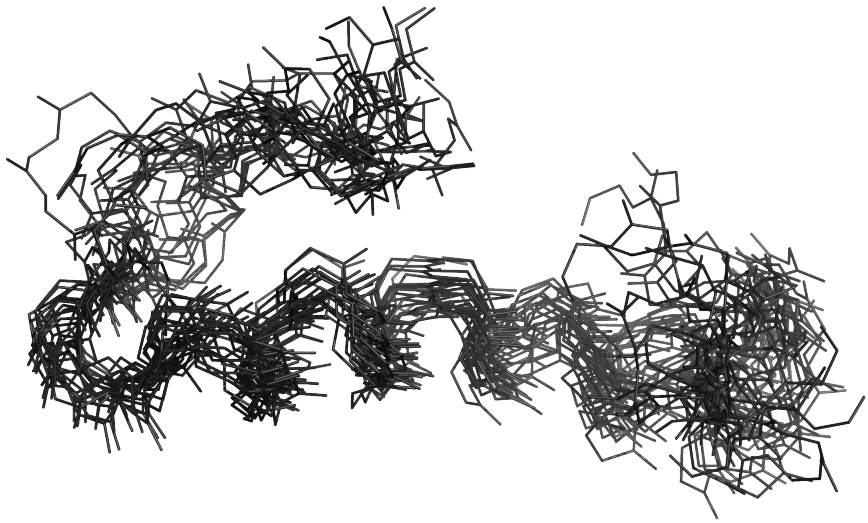

Figure 62. Backbone overlay of the 20 lowest energy conformers of (C9S, C14S)-leucocin A. The C-terminus is oriented toward the lower right corner of the image.

4.2.4.b. Structural features

The electrostatic surface potential of (C9S, C14S)-leucocin A shows that all of the positively charged residues are oriented to one side of the molecule while the negatively charged residues point out of the opposite face (**Figure 63A**).

The distribution of hydrophobic and hydrophilic residues follows a similar pattern, giving rise to a mostly amphipathic α-helix (**Figure 63B**). The N- and C-termini curl back over the helix such that its hydrophobic residues (e.g. Tyr2, Tyr3, Phe36) interact with the hydrophobic face of the helix.

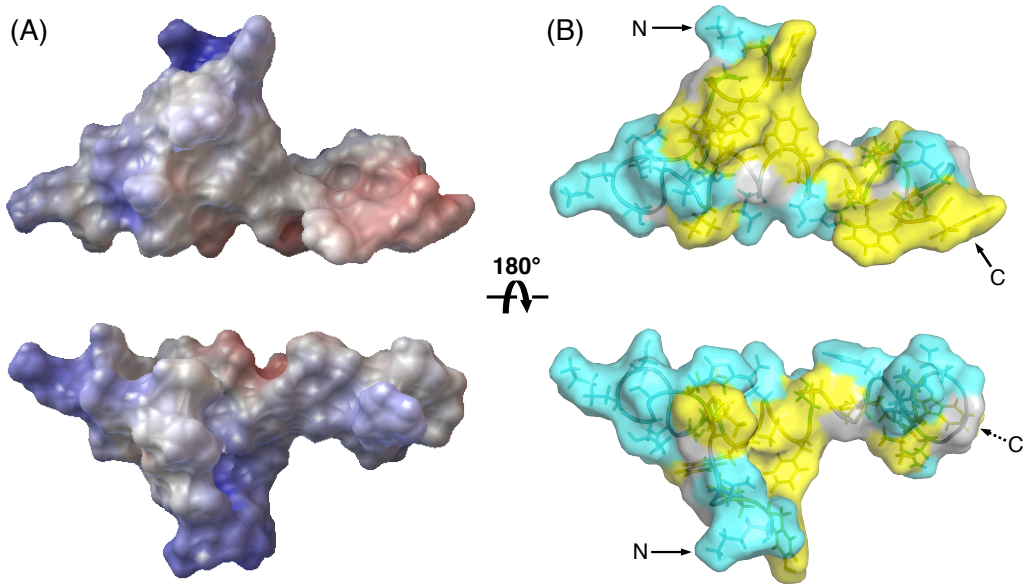

Figure 63. (A) Electrostatic surface potential of (C9S, C14S)-leucocin A, where blue indicates positive charge and red indicates negative charge. (B) Surface hydrophobicity of (C9S, C14S)-leucocin A, where yellow represents hydrophobic residues and cyan represents hydrophilic residues. The N- and C-termini are indicated on the surface hydrophobicity images (dashed arrow indicates that C-terminus is hidden underneath).

4.2.4.c. Structural comparison with wild-type leucocin A

Several structural elements differ between (C9S, C14S)-leucocin A and the wild-type leucocin A. Although (C9S, C14S)-leucocin A features an α-helix similar to that of the natural bacteriocin, the length of the helix in the mutant has extended by several residues. While the helix in leucocin A runs from

approximately residue 17 to residue 31, the helix in (C9S, C14S)-leucocin A starts earlier at residue 14.[108] This finding suggests that substitution of Cys14 with a hydrophilic residue may cause the formation of an extra loop in the α-helix involving residues 14 to 17. This may provide one rationale for the loss of antimicrobial activity in (C9S, C14S)-leucocin A. Extension of the α-helix could disrupt the recognition of the peptide by its protein receptor (the EII_t^{man} enzyme of the man-PTS system), preventing its insertion into the lipid bilayer of the bacterial membrane.

As well, the N-terminal residues of (C9S, C14S)-leucocin A appear to be far more disordered compared to the N-terminal end of wild-type leucocin A. The side chains of Ser9 and Ser14 do not interact with each other, such that no evidence of a β-sheet can be observed. Overall, the N-terminus of (C9S, C14S)-leucocin A seems largely unstructured, and this loss of conformation may serve as another structural basis to explain the mutant's lack of activity.

4.3. Conclusions and future directions

It has been previously suggested that the role of the N-terminal domain in pediocin-like bacteriocins is to track the peptide to the surface of bacterial cell membranes through electrostatic interactions.[2, 117, 118] Once at the membrane surface, the N-terminus and the hinge portion of the peptide (residues 16 and 17) are proposed to assist in the insertion of the C-terminal α-helix into the lipid bilayer.[119] However, the 3D solution structure of the inactive (C9S, C14S)-leucocin A peptide implies that the role of this N-terminal domain may be more

complex than previously thought. Mutation of the two cysteine residues to serines does not affect the overall charge of the peptide and is highly unlikely to interfere with the electrostatic interactions it forms with bacterial cell surfaces. In addition, the role of the N-terminal domain arguably extends beyond acting as a lever to insert the amphipathic helix into the membrane, as the helix already has a propensity to bind to the EII_t^{man} receptor. In order to explain the dramatic loss in activity in (C9S, C14S)-leucocin A, the N-terminus may be serving a more crucial function, such as forming intermolecular contacts with other leucocin A–EII_t^{man} complexes during pore formation in the bacterial cell membrane. Future work on this project will entail comparison of the 3D structure of (C9S, C14S)-leucocin A with the structures obtained for the biologically active analogues (C9L, C14L)-leucocin A (work performed by Christopher Lohans) and (C9F, C14F)-leucocin A (work performed by Chantel Campbell). Through these structural comparisons, we hope to improve our understanding of which structural features govern the activity of leucocin A and what role the features play in the bacteriocin's mechanism of action.

Chapter 5. Future perspectives

The 3D solution structures of four peptides have been presented in this thesis in hopes of gaining insight into the mechanisms of action and structure-activity relationships that characterize thuricin CD, thurincin H and leucocin A. The fact that all three of these bacteriocin systems are active against potentially lethal human pathogens, such as *C. difficile* and *L. monocytogenes*, underscores the importance of studying these peptides.

The 3D structures of Trn-α and Trn-β represent the first example of a two-component bacteriocin that features three intramolecular S-Cα bridges, while the structure of thurincin H represents the first example of a peptide that contains four S-Cα bridges. Characterization of these peptides has greatly expanded the class of S-Cα containing bacteriocins, which previously featured only subtilosin A.[32] There are, however, limitations associated with the representative structures of Trn-α, Trn-β and thurincin H. From in-depth NMR analysis and comparison of the possible stereoisomers, the isomer that best fits the NOE data gives the most reasonable proposal for the stereochemistry of the sulfur-linked α-carbons, but does not establish the stereochemistry with absolute certainty. As such, work is ongoing in our group to develop a method of crystalizing these peptides for analysis by X-ray crystallography.

The 3D structure of (C9S, C14S)-leucocin A provides a potential explanation for the loss of activity observed when Cys9 and Cys14 in the wild-type peptide are replaced with hydrophilic residues. In comparison with wild-type

leucocin A, the loss of the N-terminal β-sheet and the elongation of the C-terminal α-helix in the mutant suggest that the structure of the peptide is exquisitely sensitive to substitutions in its amino acid sequences. Work is currently underway to elucidate the 3D structures of two active leucocin mutants, (C9F, C14F)- and (C9L, C14L)-leucocin A, to see how the peptide structures compare to that of the wild-type.

Because the NMR studies of Trn-α, Trn-β, thurincin H and (C9S, C14S)-leucocin A have been performed in defined solvent systems (either CD_3OH or 90% TFE-d_3), the 3D solution structures of these peptides represent only one major conformation, reflecting the characteristic folding they assume in membrane-mimicking solvents. To gain more insight into the bacteriocins' mechanisms of action, an ideal future experiment would be to conduct NMR studies of the peptides in the presence of lipid membranes containing their specific receptors.

Ultimately, through structural studies of bacteriocins, we aim to elaborate on the fundamental understanding of how these peptides operate to kill bacteria. Application of this knowledge could, in turn, lead to the development of clinically effective peptide antibiotics for the treatment of specific bacterial infections.

Chapter 6. Experimental procedures

6.1. General methods

6.1.1. Culture conditions

All bacterial cultures were performed using sterilized materials and media. Materials and solutions were autoclaved (at 121 ºC for 15 mins) or filter sterilized (using a 0.22 μm syringe driven filter) prior to use. An Innova 4330 Refrigerated incubator shaker (New Brunswick Scientific, Edison, NJ) was used to incubate the cultures. To measure the optical density of cell cultures at a wavelength of 600 nm (OD_{600}), a Hewlett-Packard 8451A Diode Array Spectrophotometer (Hewlett-Packard, Palo Alto, CA) or a Thermo Spectronic BioMate3 Spectrophotometer (Thermo Scientific, Waltham, MA) was employed. Hard agar plates were prepared as follows: 1.5% granulated agar (w/v) (Difco) was added to the broth media, which was then autoclaved and poured into sterile petri dishes (~ 20 mL per plate) to solidify. Soft agar was prepared by adding 0.7% granulated agar (w/v) to the broth media, boiled to dissolve, aliquoted (10 mL per tube) into test tubes with screw cap lids, and autoclaved. Bacteria were maintained as frozen stock cultures at -80 °C, and stored in the growth media supplemented with 20% glycerol. Unless otherwise stated, percentage concentration implies v/v ratios.

6.1.2. Instrumentation used for protein purification

For procedures involving centrifugation, large volumes of liquid were centrifuged with either a Beckman J2-21 (Beckman Coulter, Inc., Brea, CA) or a Sorvall RC-5B Refrigerated SuperSpeed centrifuge. For small volumes (samples

with < 1.5 mL), solutions were centrifuged with an Eppendorf 5415D centrifuge (Eppendorf, Hamburg, Germany) at room temperature (RT), or a Galaxy 16DH centrifuge (VWR International, Inc., West Chester, PA) at 4 °C.

For cell lysis procedures, bacteria were either passed through a Constant Systems Cell Disrupter, model TS (Constant Systems, Ltd., Northants, UK), or sonicated with a Branson Sonifier 450 (Branson Ultrasonics Corporation, Danbury, CT).

During protein purification with Amberlite XAD-16 columns, an Econo Pump peristaltic pump (BioRad, Hercules, CA) was used. For amylose affinity chromatography, the amylose column was connected to a BioRad BioLogic LP system (with peristaltic pump, conductance detection and UV detection at 280 nm) and a BioRad 2128 Fraction Collector. SDS PAGE gels were run with a BioRad 3000Xi Electrophoresis Power Supply.

HPLC purification was performed on either Beckman System Gold machines (analytical or preparative), equipped with 32karat software, or on Varian Prostar Model 210 machines (analytical or preparative), equipped with Varian Star Workstation software (Varian, Inc., Palo Alto, CA).

6.1.3. Instrumentation used for genetic manipulations

DNA concentration was determined spectrophotometrically at 260 nm using the BioMate 3 Spectrophotometer (2% dilutions of DNA were prepared and a 100 μL quartz micro-cuvette was used for absorbance readings). Polymerase chain reactions (PCR) were performed using either an Eppendorf Mastercycler

Gradient (Eppendorf) or a Techgene PCR machine (Techne, Cambridge, UK). Electroporation was performed using a Gene Pulser Electroporator (BioRad).

6.1.4. Peptide characterization

6.1.4.a. MALDI-TOF MS

Samples were acidified and prepared for MALDI-TOF MS analysis using the two-layer method,[120] with 3,5-dimethoxy-4-hydroxycinnamic acid (sinapinic acid) as the matrix. A Perspective Biosystems Voyager Elite MALDI-TOF mass spectrometer (AB Sciex, Foster City, CA), operating in reflectron mode with delayed extraction, was used to record the spectra. Samples were run in positive ion mode, with an acceleration of 20 kV in the presence of a nitrogen laser (λ = 337 nm).

6.1.4.b. Circular dichroism

CD measurements were performed on an Olis DSM 17CD spectrophotometer (Olis, Bogart, GA) in a thermally controlled quartz cell (pathlength = 0.02 cm, temperature set at 20 °C) by David Zinz, Craig Turk, and Dr. Wayne Moffat (Analytical and Instrumentation Laboratory, Department of Chemistry, University of Alberta). The instrument was calibrated using a 1 mg/mL solution of D-10-camphorsulfonic acid. The bandwidth was set at 2.0 nm. Data was collected every 1 nm; each data point represents the average of ten scans. The blank (baseline spectrum of the solvent system) was subtracted from the sample spectra prior to calculating molar ellipticities. Point-by-point integration was performed as a

function of the high voltage readings on the photomultiplier detectors. Results are expressed in units of molar ellipticity (deg cm^2 $dmol^{-1}$) and plotted against the wavelength.

6.1.4.c. NMR

NMR experiments were performed on [^{13}C, ^{15}N]-labeled peptide samples using three spectrometers. In the Department of Chemistry, spectra were recorded on a Varian Inova 600-MHz spectrometer equipped with a triple resonance HCN probe and Z-axis pulsed-field gradients (PFGs). Data acquisition on this instrument was performed with the assistance of Dr. Leah Martin-Visscher (former graduate student) and Mark Miskolzie (NMR Spectroscopy Laboratory, Department of Chemistry, University of Alberta). At the National High Field Nuclear Magnetic Resonance Centre (NANUC, University of Alberta), spectra were recorded by Dr. Ryan McKay on either a Varian Inova 500-MHz spectrometer equipped with a triple resonance HCN probe and Z-axis PFGs or on a Varian Inova 800-MHz spectrometer with a triple-resonance HCN cold probe and Z-axis PFGs.

6.2. Experimental procedures for the structural studies of thuricin CD

6.2.1. Purification of Trn-α and Trn-β

Bacillus thuringiensis DPC 6431 was grown overnight in 10 mL of BHI broth at 37 ºC with shaking (200 rpm). 100 µL of this grown culture was inoculated into another 10 mL of BHI broth and incubated overnight at the same

temperature with shaking. From this second subculture, 1 mL was used to inoculate 1 L of BHI (i.e. to give a 0.1% v/v inoculation), which was then incubated at 37 ºC with shaking for 16 h. The culture was centrifuged at 8,280 ***g*** for 15 min, and both the cell pellet and supernatant were retained.

The culture supernatant was applied to a 2.5 cm × 50 cm column of Amberlite XAD-16 beads (800 m^2/g surface area, 100 Å average pore diameter, Sigma-Aldrich, St Louis, MO). To pack the column, 80 g of the XAD-16 resin was stirred in 100 mL of IPA for 1 h, poured into the column, and rinsed with 2 L of distilled water to remove all traces of IPA. After loading the culture supernatant onto the column at a flow rate of 7.5 mL/min, the column was washed with 500 mL of 30% EtOH (at 7.5 mL/min) and eluted with 500 mL of 70% IPA/ 0.1% TFA (at 10 mL/min).

The cell pellet obtained from centrifugation of the overnight culture was resuspended in 200 mL of 70% IPA/ 0.1% TFA and stirred at 4°C for 4 h. The cells were then centrifuged at 8,280 g for 15 min and the supernatant retained. This supernatant was combined with the IPA elution from the XAD-16 column, and the organic solvent in this pooled fraction was removed by rotary evaporation (Buchi rotary evaporators, Buchi, Flawil, Switzerland). The concentrated material was then applied to a 6 g (20 mL) Strata C18–E solid phase extraction (SPE) column (55 μm, 70 Å, 10 g/60 mL, Phenomenex, Torrance, CA) pre-equilibrated with methanol and water. The column was washed with 2 column volumes of 30% ethanol and eluted with 1.5 column volumes of 70% IPA/ 0.1% TFA. The

material eluted from the C18 column was concentrated down to 15 mL by rotary evaporation, before final purification by HPLC.

RP-HPLC was performed by injecting 1 mL aliquots onto a Vydac C18 RP-HPLC column (Vydac 218TP510: 300 Å pore diameter, 250 mm × 10 mm, 5 μm particle diameter; Grace Davison Discovery Sciences, Deerfield, IL) that was developed on a Varian Prostar Model 210 HPLC using the following method: 40% acetonitrile/ 0.1% TFA to 70% acetonitrile/ 0.1% TFA from 5:00 min to 42:00 min using a flow rate of 3 mL/min. A dual wavelength detector was used to monitor the purification at 220 nm and 280 nm. Trn-α eluted at 28.8 min and Trn-β eluted at 33.3 min. From 1 L of culture in BHI media, an average yield of 2 mg of Trn-α and 4 mg of Trn-β could be obtained.

6.2.2. Activity testing of Trn-α and Trn-β

A well diffusion assay (WDA) was performed to test the activity of Trn-α and Trn-β against an indicator strain. Molten BHI agar (1.5% agar in BHI media) was inoculated to 0.1% with an overnight culture of *Bacillus firmus* LMG 7125 (grown in BHI at 37 ºC while shaking at 200 rpm). This inoculated agar was poured into sterile petri dishes (~ 20 mL per plate) and allowed to solidify. Wells approximately 6 mm in diameter were bored out of the hardened agar using the back end of a flame sterilized glass pipette. For testing, 50 μl of test solutions (i.e. HPLC fractions) were pipetted into each well. The plates were incubated overnight (16-18 h) at 37 ºC. Active fractions appeared as a clear zone around the well where the bacteria were unable to grow. A negative control (65%

acetonitrile/ 0.1% TFA, to mirror the solvent conditions of the HPLC fractions) was also tested and found to have no inhibitory effects on the growth of *B. firmus* LMG 7125.

6.2.3. MS/MS sequencing and MALDI FTICR MS analysis

MS/MS sequencing was performed by Jing Zheng and Dr. Randy Whittal (Mass Spectrometry Facility, Department of Chemistry, University of Alberta) and MALDI FTICR MS was performed by Dr. Randy Whittal. The amino acid sequences of Trnα and Trnβ were analyzed by infusion MS/MS using a Waters Q-TOF Premier mass spectrometer (Waters, Milford, MA) operated in V mode. The Q-TOF was calibrated using the MS/MS of Glu-fibrinopeptide. Samples were introduced using nanospray, and MS/MS was performed on the doubly charged ion of each peptide. During data collection, the collision energy was varied from 5 eV to 75 eV.

The exact masses of Trnα and Trnβ were analyzed by MALDI FTICR MS using a Bruker 9.4T Apex-Qe FTICR (Bruker Daltonics, Billerica, MA). The FTICR was calibrated externally using polyethylene glycol. The MALDI MS of both peptides was performed using sinapinic acid as the matrix.

6.2.4. Production of [^{13}C, ^{15}N]Trn-α and [^{13}C, ^{15}N]Trn-β

B. thuringiensis DPC 6431 subcultured twice in BHI broth was used to inoculate 1 L of [^{13}C, ^{15}N]Celtone-CN (Cambridge Isotopes Laboratories, Andover, MA) at 0.1%, which was then incubated with shaking at 37 °C for 16 h.

The same procedure as described for the purification of unlabeled Trn-α and Trn-β (section 6.2.1.) was used for centrifugation, XAD-16 purification, C-18 SPE column purification, and cell pellet extraction. The pooled 70% IPA/ 0.1% TFA fraction was concentrated by rotary evaporation to ~ 4 mL volume, to which was added 4 mL of acetonitrile acidified with 0.1% TFA. This solution was injected in 1 mL aliquots onto a Vydac C18 RP-HPLC column (Vydac 218TP510; 300 Å pore diameter; 250 mm × 10 mm; 5 μm particle diameter). The column was developed on a Varian Prostar Model 210 HPLC with a gradient of 55% acetonitrile/ 0.1% TFA to 76% acetonitrile/ 0.1% TFA from 5 to 30 min using a flow rate of 3.0 mL/min. [^{13}C, ^{15}N] Trn-α was isolated from a peak with a retention time of 16.9 min, whereas [^{13}C, ^{15}N]Trn-β was isolated from a peak with a retention time of 25.4 min.

To improve the purity of the peptides for NMR studies, each peptide was purified a second time by RP-HPLC. All fractions containing [^{13}C, ^{15}N]Trn-α were pooled and concentrated by rotary evaporation before reinjection into the Vydac column. The column was then developed with a gradient of 52.5% acetonitrile/ 0.1% TFA to 56% acetonitrile/ 0.1% TFA from 5 to 30 min using a flow rate of 4.0 mL/min. [^{13}C, ^{15}N]Trn-α eluted at 19.0 min. All fractions containing [^{13}C, ^{15}N]Trn-β were also concentrated and reinjected into the Vydac column, which was then developed with 61% acetonitrile/ 0.1% TFA to 67% acetonitrile/ 0.1% TFA from 5 to 30 min using a 4.0 mL/min flow rate. [^{13}C, ^{15}N]Trn-β eluted at 15.8 min. Both peptides were lyophilized and stored at -20 °C until use.

6.2.5. Circular dichroism analysis of Trn-α and Trn-β

David Zinz and Dr. Wayne Moffat performed the CD analysis of Trn-α and Trn-β. The purified peptides were each dissolved to in 50% MeOH to give a concentration of 0.5 mg/mL. After collecting spectra on the peptides dissolved in 50% MeOH, TFE was added to the samples in increasing amounts. CD spectra were collected for peptide samples containing 20%, 40%, 60% and 80% TFE (for each addition of TFE, the final concentration of the peptide would decrease, such that the 80% TFE sample had a peptide concentration of 0.1 mg/mL). Little change in the CD spectra was observed for the peptides between the different solvent conditions; therefore the 80% TFE samples were chosen for further analysis. The percent helicity for each peptide in 80% TFE/ 10% MeOH/ 10% H_2O was calculated according to its molar ellipticity at 222 nm using this equation:[121]

$$\text{Percentage helicity} = \frac{-[\theta_{222nm}] + 3000}{39{,}000} \times 100\% \qquad \text{(eq. 1)}$$

6.2.6. NMR spectroscopy of [^{13}C, ^{15}N]Trn-α and [^{13}C, ^{15}N]Trn-β

NMR samples of each peptide were made up to contain ~0.5 mM peptide in CD3OH (Cambridge Isotopes Laboratories) and 100 μM 2,2-dimethyl-2-silapentane-5-sulfonate sodium salt (DSS). NMR spectra were recorded at 25 °C on the Varian Inova 600-MHz spectrometer or the Varian Inova 800-MHz spectrometer. To assign the ^{1}H, ^{13}C, and ^{15}N resonances of Trn-α and Trn-β, a suite of experiments was run on each peptide. **Table 16** and **Table 17** list the

experimental parameters used to acquire the NMR spectra for Trn-α and Trn-β respectively. NMR spectra were processed using the NMRPIPE program.[122] During processing, the data were multiplied in all dimensions by a 90°-shifted sine-bell squared function. Indirect dimensions were doubled, using linear prediction and zero-filling to the nearest power of two, before undergoing Fourier transformation. Data was analyzed using the NMRView program.[123]

Table 16: Experimental parameters used to acquire NMR spectra on [^{13}C, ^{15}N]Trn-α to obtain chemical shift assignments, coupling constants, and NOE restraints.

Exp. Name[a]	Nuclei[b]	x-sw[c]	y-sw	z-sw	x-pts	y-pts	z-pts	Ref
^{13}C-HSQC (full)	^{1}H, ^{13}C	11990	28160		1024	128		
^{15}N-HSQC	^{1}H, ^{15}N	11990	3242		1024	128		124
HNHA	^{1}H, ^{1}H$_{\alpha}$, ^{15}N	11990	6000	2500	1024	110	32	125,126
CBCA(CO)NH	^{1}H, ^{13}C, ^{15}N	11990	16092	3242	1024	64	32	127
HCCH-TOCSY	^{1}H, ^{1}H, ^{13}C	11990	8000	16090	1024	128	34	128
HNCO	^{1}H, ^{13}C(O), ^{15}N	11990	3770	3242	1024	64	32	129-130
rtm-HNCA[d]	^{1}H, ^{13}C, ^{15}N	12001	4526	1702	1024	48	32	129-130
HNCACB	^{1}H, ^{13}C, ^{15}N	11990	16092	3242	1024	64	32	127,130,131
^{13}C-NOESYHSQC	^{1}H, ^{1}H, ^{13}C	11990	9001	16090	1024	128	37	132
^{15}N-NOESYHSQC	^{1}H, ^{1}H, ^{15}N	11990	9000	2400	1024	128	32	133

[a]Experiments were acquired at 800 MHz unless otherwise specified.
[b]The nucleus acquired in each dimension (e.g. 1H,15N indicates hydrogen x, nitrogen y).
[c]x,y,z-pts and sw are the number of complex points and sweep width in each respective dimension (x is the directly detected dimension).
[d]Experiment was acquired at 600MHz.

Table 17: Experimental parameters used to acquire NMR spectra on [^{13}C, ^{15}N]Trn-β to obtain chemical shift assignments, coupling constants, and NOE restraints.

Exp. Name[a]	Nuclei	x-sw	y-sw	z-sw	x-pts	y-pts	z-pts	Ref
^{13}C-HSQC (full)	^{1}H, ^{13}C	12001	21123		1024	200		
^{13}C-HSQC (aliph)	^{1}H, ^{13}C	12001	12068		1024	300		
^{15}N-HSQC	^{1}H, ^{15}N	12001	1944		1024	64		124
HNHA	^{1}H, ^{1}H$_{\alpha}$, ^{15}N	12001	12001	1944	1024	110	32	125,126
CBCA(CO)NH	^{1}H, ^{13}C, ^{15}N,	12001	12070	1944	1024	64	32	127
HCCH-TOCSY	^{1}H, ^{1}H, ^{13}C	12001	6599	12070	1024	100	32	128
HNCO	^{1}H, ^{13}C(O), ^{15}N	12001	3770	1944	1024	32	32	129-130
HNCACB	^{1}H, ^{13}C, ^{15}N	12001	12070	1944	1024	64	32	127,130,131
^{13}C-NOESYHSQC	^{1}H, ^{1}H, ^{13}C	12001	6599	12068	768	100	32	132
^{15}N-NOESYHSQC	^{1}H, ^{1}H, ^{15}N	12001	6599	1944	1024	110	32	133
^{15}N-TOCSYHSQC	^{1}H, ^{1}H, ^{15}N	12001	6599	1944	1024	110	32	133

[a]Experiments were acquired at 600 MHz.

Most of the proton chemical shift assignments were made based on data from the HCCH-TOCSY and ^{13}C-HSQC experiments. Most of the carbon and nitrogen chemical shift assignments were made based on the backbone experiments, including the HNCACB and the CBCA(CO)NH. In the case of Trn-α, the α-carbons of the modified threonines could not be detected by the standard backbone experiments, perhaps due to the downfield nature and slow relaxation times of these quaternary carbons. The standard BioPack (Agilent Inc., USA) pulse sequence ghn_ca.c[127, 129, 130, 134] was altered by Dr. Ryan McKay to allow an optimized search for any modified alpha carbons. The pulse sequence was examined and we found that a shift of the primary carbon carrier position from the standard 56 ppm to 77 ppm should allow the most efficient detection of any atoms that had been modified. The pulse sequence normally maintains a carrier position of 56 ppm throughout the entire experiment and then utilizes shifted laminar

pulses[135] to excite and/or invert the carbonyl resonances with simultaneous nulls in the alpha carbon region. The pulse sequence also uses timed alpha carbon pulses that create nulls in the carbonyl region. In order to execute the carrier position change, the off-resonance shifts for the carbonyl pulses and simultaneous null points for both carbonyl and aliphatic pulses had to be moved. A new shaped pulse was created by modifying the BPmake180CO_Ca macro and testing the new shape with the visualization software PulseTool (Agilent Inc., Santa Clara, CA).

6.2.7. Modification of CYANA program

The structure calculation program, CYANA 2.1,[87] was modified to allow for structure calculations on peptides with sulfur to α-carbon linkages to Ser, Thr, Ala, and Tyr residues. Modification of the program was performed with assistance from Dr. Pascal Mercier, Dr. Leah Martin-Visscher, and Dr. Jeremy Sit. Descriptions of the sulfur-linked residues with L- and D-stereochemistry (see section 2.2.6.a. and Appendix A) were added to the cyana.lib file. As well, the translate.cya file was changed such that references to Ser, Thr, Ala and Tyr would also include references to the modified L- and D-residues (MSER, DSER, MTHR, DTHR, MALA, DALA, MTYR and DTYR).

6.2.8. Structure calculations

The structures of all of the stereoisomers for Trn-α and Trn-β were calculated with CYANA 2.1,[87] using NOE restraints measured from the ^{13}C-NOESYHSQC and ^{15}N-NOESYHSQC experiments and angle restraints obtained from the HNHA experiment and from TALOS.[88] The automatically assigned NOEs were calibrated within CYANA according to their intensities. It was found that use of only automatic NOE assignments maximized the number of NOEs included in the structure calculations. As such, the same NOE peak lists were used for calculating each stereoisomer of a given peptide (Trn-α or Trn-β) and no manual assignments were included in the calculations. After seven rounds of calculation for the Trn-α LLD isomer (10,000 steps per round), a total of 381 cross-peak NOE assignments, 12 $^{3}J_{\mathrm{HNH}\alpha}$ coupling constants, and 38 dihedral angle restraints were used in the final calculation. After seven rounds of calculation for the Trn-β LLD isomer, a total of 313 cross-peak NOE assignments, 19 $^{3}J_{\mathrm{HNH}\alpha}$ coupling constants, and 38 dihedral angle restraints were used in the final round of calculation. The same number of coupling constants and dihedral angle restraints were used for each of the corresponding stereoisomers, while the number of NOE assignments used varied for each stereoisomer. 20 lowest energy conformations were generated for each stereoisomer, with no residues in the disallowed region of the Ramachandran plot. Coordinates for Trn-α (LLD isomer) and Trn-β (LLD isomer) have been deposited in the Protein Data Bank (2l9x and 2la0, respectively) and chemical shift assignments have been deposited in the BioMagResBank (17492 and 17495, respectively). Electrostatic surface

calculations were computed with APBS.[136] All other figures were generated using PyMOL (Schrödinger, Portland, OR).

6.3. Experimental procedures for the structural studies of thurincin H

6.3.1. Purification of thurincin H

A starter culture of *Bacillus thuringiensis* SF361 in 10 mL of tryptic soy broth (TSB) (EMD Chemicals Inc., Darmstadt, Germany) was grown overnight at 30 ºC with shaking (250 rpm.). 1 mL of the starter culture was used to inoculate 1 L of TSB. After growing for 16 h at 30 ºC with shaking (250 rpm), the culture was centrifuged at 11000 ***g*** for 10 min at 4 ºC. The supernatant was applied to a column of Amberlite XAD16 beads following the same procedure described for the purification of Trn-α and Trn-β (section 6.2.1.). The cell pellet was also resuspended and extracted with 70% IPA/ 0.1% TFA as described previously, and the extract was combined with the elution from the XAD16 column for concentration and further purification using a Strata C18–E SPE column (section 6.2.1.). The material eluted from the C18 column was concentrated down to 15 mL by rotary evaporation, before final purification by HPLC. 1 mL aliquots were injected onto a Vydac C18 RP-HPLC column (Vydac 218TP510: 300 Å pore diameter, 250 mm × 10 mm, 5 μm particle diameter; Grace Davison Discovery Sciences, Deerfield, IL) that was developed on a Varian Prostar Model 210 HPLC using the following method: 55 % acetonitrile/ 0.1 % TFA to 68 % acetonitrile/ 0.1% TFA from 5:00 min to 21:40 min using a flow rate of 3 mL/min. thurincin H eluted at 17.1 min. On average, 1 L of TSB culture yields 12 mg of thurincin H.

6.3.2. Activity testing of thurincin H

A spot-on-lawn assay was performed to test the activity of thurincin H against an indicator strain. A 10 mL aliquot of molten soft TSB agar (0.7% agar in TSB media) was inoculated to 0.1% with an overnight culture of *Listeria monocytogenes* ATCC 43256 (grown in TSB at 37 ºC while shaking at 250 rpm). This inoculated agar was poured onto TSB hard agar plates and allowed to solidify. For testing, 10 µl of sample solutions (i.e. HPLC fractions) were on top of the soft agar and allowed to air dry. The plates were incubated overnight (16-18 h) at 37 ºC. Active fractions appeared as a clear zone where the bacteria were unable to grow. A negative control (65% acetonitrile/ 0.1% TFA, to mirror the solvent conditions of the HPLC fractions) was also tested and found to have no inhibitory effects on the growth of *L. monocytogenes* ATCC 43256.

6.3.3. MS/MS sequencing and MALDI FTICR MS analysis

MS/MS sequencing was performed by Jing Zheng and Bela Reiz (Mass Spectrometry Facility, Department of Chemistry, University of Alberta) and MALDI FTICR MS was performed by Dr. Randy Whittal. The amino acid sequence of thurincin H was analyzed using infusion nanoESI MS/MS and MALDI MS/MS. Infusion nanoESI MS/MS was performed on a Waters Q-TOF Premier mass spectrometer operated in V mode. Calibration of the Q-TOF was done using the MS/MS of Glu-fibrinopeptide. Samples were introduced by nanospray, and MS/MS was performed on the triply charged ion of the peptide. During data collection, the collision energy was varied from 5 eV to 75 eV.

MALDI MS/MS was performed on an AB Sciex 4800 MALDI TOF/TOF (AB Sciex, Foster City, CA), using α-cyano-4-hydroxycinnamic acid as the matrix. Calibration was completed using a mixture of standard peptides over the mass range of 700 to 3500 Da.

The exact mass of thurincin H was measured by MALDI FTICR mass spectrometry using a Bruker 9.4T Apex-Qe FTICR. The FTICR was calibrated externally using polyethylene glycol. The MALDI MS of the peptide was performed using 2,5-dihydroxybenzoic acid as the matrix.

6.3.4. Production of [^{13}C, ^{15}N]thurincin H

Test growths of *B. thuringiensis* SF361 in mixtures of [^{13}C, ^{15}N]Celton-CN and TSB media were performed to determine which ratio achieved the best level of labeling while maintaining a high yield. A starter culture (TSB) of the producer strain was used to inoculate (to 0.1%) 10 mL of 9:1, 4:1, 7:3, 3:2, and 1:1 ratios of [^{13}C, ^{15}N]Celton-CN to TSB media, which were then incubated at 30 ºC overnight with shaking (250 rpm). Visual observations on each test culture were then recorded (i.e. whether the culture was cloudy or the bacteria had sporulated and sunk to the bottom of the test tube) before 1 mL of each culture was centrifuged at 13,800 ***g***. The supernatants were analyzed by MALDI-TOF MS to ascertain levels of labeling as well as relative amounts of thurincin H production. It was determined that 4:1 [^{13}C, ^{15}N]Celton-CN to TSB media gave the best compromise for yield and percentage labeling of the peptide.

To produce [^{13}C, ^{15}N]thurincin H in large scale, 1 mL of a starter culture of *B. thuringiensis* SF361 in TSB was used to inoculate 1 L of 80% [^{13}C, ^{15}N]Celtone-CN/ 20% TSB. This culture was incubated for 16 h with shaking (250 rpm) prior to purification using a procedure identical to the purification of unlabeled thurincin H (section 6.3.1.). From 1 L of this mixed media, 8 mg of partially [^{13}C, ^{15}N]-labeled thurincin H was obtained.

6.3.5. Circular dichroism analysis of thurincin H

David Zinz and Craig Turk performed the CD analysis of thurincin H. The peptide was dissolved in 100% MeOH (to mimic NMR solvent conditions) at a concentration of 0.5 mg/mL for CD spectroscopy. Since the CD spectrum gave an unusual trace that differs from the typical spectra observed for alpha helices, beta sheets or random coil peptides, the percent helicity of the peptide was not analyzed.

6.3.6. NMR spectroscopy of [^{13}C, ^{15}N]thurincin H

NMR data was acquired and processed in the same fashion as described in section 6.2.6. Spectra were recorded on either the Varian Inova 500-MHz spectrometer or the Varian Inova 800-MHz spectrometer. **Table 18** lists the experimental parameters used to acquire the NMR spectra for thurincin H. Most of the proton chemical shift assignments were made based on data from the HCCH-TOCSY and ^{13}C-HSQC experiments. Most of the carbon and nitrogen chemical shift assignments were made based on the backbone experiments, including the HNCACB, the CBCA(CO)NH, and the rtm-HNCA.[76] The backbone

NH signals for Ser14 and Leu20 could not be definitively assigned due to spectral overlap.

Table 18: Experimental parameters used to acquire NMR spectra on [^{13}C, ^{15}N]thurincin H to obtain chemical shift assignments, coupling constants, and NOE restraints.

Exp. Name[a]	Nuclei[b]	x-sw[c]	y-sw	z-sw	x-pts	y-pts	z-pts	Ref
^{13}C-HSQC (aliph)	^{1}H, ^{13}C	11990	14079		1024	256		
^{13}C-HSQC (full)	^{1}H, ^{13}C	11990	28160		1024	128		
^{15}N-HSQC	^{1}H, ^{15}N	11990	3242		1024	256		124
HNHA[d]	^{1}H, ^{1}H$_{\alpha}$, ^{15}N	6982	6982	1944	512	64	32	125, 126
CBCA(CO)NH	^{1}H, ^{13}C, ^{15}N	11990	16092	2100	1024	64	32	127
HCCH-TOCSY	^{1}H, ^{1}H, ^{13}C	11990	8000	10000	1024	128	40	128
HNCO	^{1}H, ^{13}C(O), ^{15}N	11990	3770	2000	1024	64	32	127, 129, 130, 134
rtm-HNCA	^{1}H, ^{13}C, ^{15}N	11990	16089	2000	1024	64	32	76, 127, 129, 130, 134, 135
HNCACB	^{1}H, ^{13}C, ^{15}N	11990	16092	2800	1024	80	40	127, 130, 131
^{13}C-NOESYHSQC	^{1}H, ^{1}H, ^{13}C	11990	8000	10000	1024	160	40	132
^{15}N-NOESYHSQC	^{1}H, ^{1}H, ^{15}N	11990	8000	2100	1024	128	44	133
^{15}N-TOCSYHSQC	^{1}H, ^{1}H, ^{15}N	11990	8000	2600	1024	128	30	133

[a]Experiments were acquired at 800 MHz unless otherwise specified.
[b]The nucleus acquired in each dimension (e.g. 1H,15N indicates hydrogen x, nitrogen y).
[c]x,y,z-pts and sw are the number of complex points and sweep width in each respective dimension (x is the directly detected dimension).
[d]Experiment was acquired at 500MHz.

6.3.7. Modification of CYANA program

CYANA 2.1 was again modified to allow for structure calculations on peptides with sulfur to α-carbon linkages to Asn. Modification of the program was performed with assistance from Dr. Pascal Mercier, Dr. Leah Martin-Visscher and Dr. Jeremy Sit. Descriptions of the sulfur-linked Asn with L- and D-stereochemistry (see Appendix B) were added to the cyana.lib file. As well, the

translate.cya file was changed such that references to Asn would also include references to the modified L- and D-residues (MASN and DASN).

6.3.8. Structure calculations

CYANA 2.1 was used to calculate the structures of all the stereoisomers for thurincin H,[87] using NOE restraints measured from the ^{13}C-NOESYHSQC and ^{15}N-NOESYHSQC experiments combined with angle restraints obtained from the HNHA experiment and from TALOS.[88] The automatically assigned NOEs were calibrated within CYANA according to their intensities. The same NOE peak lists were used for the structure calculations of each stereoisomer, following the same procedure as described in section 6.2.8. After seven rounds of calculation for the thurincin H DDDD isomer (10,000 steps per round), a total of 502 cross-peak NOE assignments, 22 $^{3}J_{\mathrm{HNH}\alpha}$ coupling constants, and 20 dihedral angle restraints were used in the final calculation. The same number of coupling constants and dihedral angle restraints were used for each of the corresponding stereoisomers, while the number of automatic NOE assignments varied for each stereoisomer. 20 lowest energy conformations were generated for each stereoisomer. Coordinates for thurincin H (DDDD isomer) have been deposited in the Protein Data Bank (2lbz) and chemical shift assignments have been deposited in the BioMagResBank (17583). Electrostatic surface calculations were computed with APBS.[136] All other figures were generated using PyMOL.

6.4. Experimental procedures for the production and structural elucidation of a double serine mutant of leucocin A

6.4.1. Construction of pMAL.FXA.(C9S, C14S)LeuA

To build a gene for expressing (C9S, C14S)-leucocin A, two long primers with overlapping complimentary sequences were designed by Dr. Marco van Belkum and amplified by PCR. The forward primer, MVB193 (5′-AATATGAGCTCGAACAACAACAACAATAACAATAACAACAACCTCGG GATCGAGGGAAGGAAATACTACGGTAACGGCGTTCACTCTACCAAAT CTGGTTCTTCCG-3′), featured a *Sac*I restriction site (underlined) and encoded for the C-terminus of MBP, the factor Xa (FXA) recognition sequence (in green), as well as the N-terminal region of (C9S, C14S)-leucocin A. The reverse primer, MVB194 (5′-TATATGGATCCTTACCAGAAACCGTTGCCACCGTTCGCCA GACGGTGCACGCCAGCAGAGAACGCTTCACCCCAGTTAACGGAAGAA CCAGATTTGGTAGAGTGAA-3′), featured a *Bam*H1 restriction site (underlined) and the C-terminal region of (C9S, C14S)-leucocin A. The overlapping complimentary sequence in each primer is coloured in red. The PCR reaction (split in 2 × 50 μL) consisted of 10 μL of 10 × PCR buffer, 4 μL of 50 mM $MgSO_4$, 2 μL of 10 mM dNTP mix, 5 μL of MVB193 (20 pmol/μL), 5 μL of MVB194 (20 pmol/μL), 1 μL of Platinum® *Taq* High Fidelity (Invitrogen, Carlsbad, CA) and 73 μL of H_2O. The cycling conditions used were as follows: (1) 5 cycles of 94 °C for 30 s, 56 °C for 30 s, 68 °C for 30 s; (2) return to 94 ºC to begin a sixth cycle.

At the beginning of cycle 6, two short primers, MVB191 (5′-AATATGAGCTCGAACAACAACAA-3′) and MVB192 (5′-TATATGGATCCTTACCAGAAAC-3′), were added to each of the 50 μL reaction mixtures to increase the efficiency of gene amplification. The short primer mix (2 × 3 μL), which consisted of 2 μL of MVB191 (200 pmol/μL), 2 μL of MVB192 (200 pmol/μL), and 2 μL of H_2O, was pipetted into the PCR reaction mixture before continuing for a further 15 cycles of 94 °C for 30 s, 56 °C for 30 s, 68 °C for 30 s, followed by cooling and hold at 4 ºC. Amplification of the DNA was confirmed by agarose gel electrophoresis of 5 μL of the PCR reaction mixture. The 5 μL sample was mixed with 1 μL of 6 × sample buffer (10 mM Tris-HCl pH 7.6, 0.03% bromophenol blue, 0.03% xylene cyanol, 60% glycerol, 60 mM EDTA) and loaded onto a 1.5% agarose gel in tris/borate/EDTA (TBE) buffer stained with SYBR® Safe (Invitrogen). The gel was run at 80 V for 1 h and visualized with a Dark Reader Transilluminator (Clare Chemical Research, Dolores, CO). The remaining PCR product was purified using the QIAquick™ PCR Purification Kit (Qiagen, Mississauga, ON, Canada) following the manufacturer's instructions and dissolved in 50 μL of 10 mM Tris-HCl (pH 8.5).

The PCR product was then cloned into the *Sac*I and *Bam*H1 site of the pMAL-c2X vector (New England Biolabs, Ipswich, MA) by performing a double digestion of the vector and PCR product, followed by ligation. The PCR product was digested with both enzymes as follows: 25 μL of purified PCR product was incubated with 1.5 μL of *Sac*I (Fermentas, Burlington, ON, Canada) and 1.5 μL of *Bam*H1 (Fermentas) in 5 μL of 10 × FastDigest® buffer (Fermentas) and 17 μL of

H_2O for 30 min at 37°C. The pMAL-c2X vector was also digested with both *Sac*I and *Bam*H1 at the same time (1.5 μg of vector DNA dissolved in 25 μL of H_2O was digested using the same conditions as for the digestion of the PCR product). After digestion, the DNA from both reactions was purified using the QIAquick™ PCR Purification Kit, concentrated by ethanol precipitation and dissolved in 5 μL of H_2O. For the ligation reaction, 30-50 ng of PCR product and 30-50 ng of vector DNA were mixed with 1 μL of 5 × Ligase Reaction Buffer (Invitrogen), 0.5 μL of T4 DNA Ligase (Invitrogen) and 2 μL of H_2O and incubated at room temperature for 2.5 h.

After ligation, the reaction mixture was used to transform electrocompetent *E. coli* JM109 cells (prepared by Dr. Marco van Belkum). 2.5 μL of the ice-cold ligation reaction mixture was added to 100 μL of ice-cold *E. coli* JM109 cells, which were then transferred to a pre-chilled electroporation cuvette (0.2 cm gap) and held on ice for 5 mins. The cells were transformed using the Gene Pulser Electroporator at 1.0 kV and 800 Ω resistance. After electroporation, 1 mL of Luria Bertani (LB) broth was added to the cuvette and the resulting cell mixture was transferred to a microcentrifuge tube for incubation at 37 ºC for 1 h. The cells were then streaked onto LB hard agar plates containing 150 μg/mL ampicillin (Aldrich, St. Louis, MO) and incubated at 37 ºC for 24 h.

6.4.2. Screening for desired clones in transformed *E. coli* JM109

After transformation, clones were screened to determine if they contained the desired insert. From the hard agar plate that was streaked with the transformed

cells, several colonies were picked and grown in 10 mL of LB with 150 μg/mL ampicillin (incubated at 37 ºC, shaking at 200 rpm, overnight). 1 mL of each grown culture was then centrifuged at 13,800 ***g*** for 1 min, and the supernatant removed. Following the manufacturer's instructions, the GeneJET™ Plasmid Miniprep Kit (Fermentas) was then used to lyse the cell pellets (through alkaline lysis), and isolate and purify the plasmids by adsorption of the DNA on a silica spin column. After washing, the DNA was eluted from the spin columns using 30 μL of elution buffer (10 mM Tris-HCl, pH 8.5).

The presence of the insert in the isolated plasmid DNA was checked by PCR amplifications. The PCR reaction consisted of 0.5 μL of plasmid DNA, 5 μL of 10 × PCR buffer, 2 μL of $MgSO_4$, 1 μL of 10mM dNTP mix, 0.5 μL of MVB191 (200 pmol/μL), 0.5 μL of MVB192 (200 pmol/μL), 1 μL of Platinum® *Taq* High Fidelity and 40.5 μL of H_2O. The cycling conditions used were as follows: (1) 25 cycles of 94 °C for 30 s, 50 °C for 30 s, 68 °C for 30 s; (2) hold at 4 ºC. An agarose gel was run on 5 μL of the PCR products, confirming the presence of the insert.

The sequence of the insert from the isolated plasmid DNA was also confirmed by sequencing with a BigDye Terminator v3.1 Cycle Sequencing Kit (Applied Biosystems, Carlsbad, CA) followed by electrophoresis on an ABI 3730 DNA Analyzer (Applied Biosystems) at the Molecular Biology Services Unit (Biological Services, University of Alberta). Forward and reverse sequencing reactions consisted of 2 μL of sequencing buffer (200 mM Tris-HCl pH 9, 5 mM $MgCl_2$), 1 μL of primer containing 2 pmol of DNA, 200-300 ng of plasmid DNA,

and 2 μL of BigDye® premix. The forward sequencing reaction used MVB35 (5'-TTTCCCAGTCACGACGTTGT-3') as the primer while the reverse reaction used MVB36 (5'-TCAACGCCGCCAGCGGTC-3'). The reaction mixtures were then subjected to the following PCR conditions: 30 cycles of 96° C for 30 s, 50 °C for 15 s, 60 °C for 60 s. The DNA was then purified and concentrated by sodium acetate / ethanol precipitation by transferring the reaction mixture (10 μL) to a microcentrifuge tube containing 10 μL of water, 2 μL of sodium acetate (3 M, pH 5.2) and 80 μL of 95% EtOH. The mixture was vortexed and incubated at 4 ºC overnight. The precipitated DNA was pelleted by centrifugation (13,800 ***g***, 15 min, 4°C), washed twice with 0.5 mL of ice-cold 70% EtOH and dried under vacuum for ~5 min. Sequences obtained from electrophoresis were inspected manually.

6.4.3. Overexpression and isolation of (C9S, C14S)-leucocin A

The *E. coli* JM109 clone harbouring the pMAL.FXA.(C9S, C14S)LeuA plasmid was grown in 10 mL of LB/ 100 μg/mL ampicillin for 16 h at 37 ºC with shaking (200 rpm). This culture was used to inoculate 1 L of LB/ 100 μg/mL ampicillin to 0.1%, which was incubated at 37 ºC with shaking (200 rpm) until an OD_{600} of 0.5 was reached (typically about 4 hours). The culture was then supplemented with isopropyl β-D-1-thiogalactopyranoside (IPTG) to a final concentration of 0.3 mM and incubated for a further 3 h. The cells were harvested by centrifugation (11,300 ***g***, 20 min, 4 ºC) and frozen and stored at -20 ºC.

The cells were resuspended in 50 mL of ice-cold amylose column buffer (20 mM Tris-HCl pH 7.4, 100 mM NaCl, 1 mM EDTA, 1 mM NaN_3, 1 mM

dithiothreitol (DTT)) containing one Cφmplete EDTA-Free protease inhibitor cocktail tablet (Roche Diagnostic, Indianapolis, IN). Cells were lysed using the cell disrupter (20 kpsi), and centrifuged at 27,200 ***g*** for 30 min at 4 ºC. The supernatant (cleared lysate) was diluted to 300 mL with amylose column buffer and loaded at 1mL/min onto an amylose column (amylose resin from New England Biolabs packed into a 2.5 × 50 cm column at a flow rate of 2 mL/min and washed with amylose column buffer). After loading, the column was washed with 800 mL of amylose column buffer, after which the MBP-fusion protein was eluted by addition of 10 mM maltose to the buffer. Fractions containing the protein (as detected by UV absorbance at 280 nm and by SDS-PAGE) were transferred into dialysis tubing (6 – 8 kDa molecular weight cutoff) and dialyzed against 4 L of H_2O (4 ºC, refreshed 2 times at 2 h each, and a third time for 12 h). The protein solution was frozen, lyophilized and stored at -20 ºC. From 1 L of LB culture, typically 30 mg of lyophilized fusion protein could be obtained.

6.4.4. Factor Xa digestion pilot study

A 1 mg/mL solution of the fusion protein in FXa buffer (20 mM Tris-HCl pH 8.0, 100 mM NaCl, 2 mM $CaCl_2$) was used for this pilot study. 100 μL of this solution was incubated at room temperature for 24 h as a control. Another 200 μL of this solution was incubated with 0.5% FXa (New England Biolabs) at room temperature for 24 h. Samples of the control were saved at 0 h and 24 h for analysis by SDS PAGE and MALDI-TOF MS. Samples of the FXa digest were saved at 2 h, 4 h, 6 h, and 24 h for analysis by SDS PAGE, and at 1 h, 2 h, 3 h, 4 h,

6 h, and 24 h for analysis by MALDI-TOF MS. All MALDI-TOF MS samples were acidified with 0.1% TFA and frozen until analysis. All SDS PAGE samples were mixed with 2 × Laemmli Sample Buffer (BioRad) and frozen until analysis.

MALDI-TOF MS analysis was performed to track the formation of (C9S, C14S)-leucocin A while SDS PAGE was performed to track the cleavage of the fusion protein and appearance of free MBP. For SDS PAGE, the proteins were resolved with 10% (w/v) acrylamide SDS PAGE gels, with 4% stacking gels. Protein samples mixed with the sample buffer were heated at 100 ºC for 5 min prior to loading on the gel. Electrophoresis employed a constant voltage of 90 V for ~ 20 min until the bands had compressed, before increasing the voltage to 180 V for ~ 45 min, until the dye front neared the bottom of the gel. Protein standards (BioRad) were also run to serve as molecular weight markers for comparison with the protein samples. Gels were stained with GelCode Blue stain (Pierce, Rockford, IL) and destained with water. After MALDI-TOF MS and SDS PAGE analysis, it was found that a 2 h digest gave optimum production of (C9S, C14S)-leucocin A while minimizing the amount of degradation products.

6.4.5. Purification of (C9S, C14S)-leucocin A

A large scale FXa digest (5 mg of fusion protein, 0.025 mg FXa, 2 mL FXA buffer) was incubated for 2 h at room temperature, after which the reaction was stopped by adding 2 μL of 4-(2-aminoethyl)benzenesulfonyl fluoride (AEBSF). The digest was immediately injected onto a Phenomenex Luna® C18 RP-HPLC column (100 Å pore diameter; 250 mm × 21.2 mm; 5 μm particle

diameter). The column was developed on the Beckman System Gold HPLC using a gradient of 25% acetonitrile/ 0.1% TFA to 55% acetonitrile/ 0.1% TFA from 5 to 25 min using a flow rate of 10.0 mL/min. (C9S, C14S)-leucocin A eluted at a retention time of 18.1 min. From 1 L of LB culture, 2.5 mg of peptide was obtained. MALDI-TOF MS was used to confirm the identity of the peptide.

6.4.6. Activity testing of (C9S, C14S)-leucocin A

Spot-on-lawn assays were performed to test the activity of (C9S, C14S)-leucocin A against *Carnobacterium maltaromaticum* UAL26, *Carnobacterium divergens* LV13, *Lactococcus lactis* cremoris HP, and *Listeria monocytogenes* ATCC 43256. The same procedure as described in section 6.3.2. was used to carry out the testing, with All Purpose Tween (APT) as the growth media. Wild-type leucocin A was used as the positive control, while H_2O was used as the negative control.

6.4.7. Test growth of *E. coli* JM109 transformants in M9 minimal media

The *E. coli* JM109 clone harbouring the pMAL.FXA.(C9S, C14S)LeuA plasmid was grown in 10 mL of LB/ 100 μg/mL ampicillin for 16 h at 37 ºC with shaking (200 rpm). This culture was used to inoculate 1 L of M9 minimal media / 100 μg/mL ampicillin to 0.1%. M9 minimal media was prepared as follows: for 1 L of media, 200 mL of 5 × M9 salts (0.043 M NaCl, 0.11 M KH_2PO_4 and 0.25 M $Na_2HPO_4 \bullet 7H_2O$) was diluted with 785 mL of H_2O and sterilized; the remaining filter sterilized components (10 mL of 20% glucose, 2.5 mL of 20% $(NH_4)_2SO_4$, 2

mL of 1M $MgSO_4$, 1 mL of 0.1 M $CaCl_2$, 100 μL of 10 mM $FeSO_4$, and 100 μL of 10 mg/mL thiamine) were then added. The inoculated M9 media was incubated at 37 ºC with shaking (200 rpm) until an OD_{600} of 0.5 was reached (21 to 24 h). It was found that growth of the cells in M9 minimal media was much slower than growth in LB. The culture was then supplemented with IPTG to a final concentration of 0.3 mM and incubated for a further 3 h. The cells were harvested by centrifugation (11,300 ***g***, 20 min, 4 ºC) and lysed as described in section 6.4.3. The fusion protein in the cell lysate was purified by amylose affinity chromatography, dialyzed, and lyophilized following the same procedure as in section 6.4.3. Only ~ 3 mg of lyophilized fusion protein was obtained from 1 L of M9 culture.

6.4.8. Transformation of *E. coli* BL21(DE3)

In hopes of improving peptide production in M9 minimal media, the pMAL.FXA.(C9S, C14S)LeuA vector was transformed into *E. coli* BL21(DE3) by heat shock treatment. 50 μL of ice cold competent *E. coli* BL21(DE3) cells (prepared by Dr. Tara Sprules) was mixed with 2 μL of the pMAL.FXA.(C9S, C14S)LeuA vector and incubated on ice for 5 mins. The mixture was then incubated in a water bath at 42 ºC for 90 s, before being chilled on ice for another 2 min. After heat shock treatment, 0.5 mL of LB was added to the cells, which were then incubated at 37 ºC for 1 h. The cells were then streaked onto LB hard agar plates containing 150 μg/mL ampicillin and incubated overnight at 37 ºC.

Clones were screened for the desired insert following the same procedure described in section 6.4.2.

6.4.9. Production of [^{13}C, ^{15}N]-(C9S, C14S)-leucocin A

The *E. coli* BL21(DE3) clone harbouring the pMAL.FXA.(C9S, C14S)LeuA plasmid was grown in 10 mL of LB/ 100 μg/mL ampicillin for 16 h at 37 ºC with shaking (200 rpm). This culture was used to inoculate to 1 L of [^{13}C, ^{15}N]M9 minimal media/ 100 μg/mL ampicillin to 0.1%. [^{13}C, ^{15}N]M9 minimal media was constructed in the same fashion as described in section 6.4.7., but with the use of [U-^{13}C]-D-glucose and $(^{15}NH_4)_2SO_4$ (99% isotopic purity, Cambridge Isotope Laboratories) as the sole carbon and nitrogen sources, respectively. The inoculated [^{13}C, ^{15}N]M9 culture was incubated at 37 ºC with shaking (200 rpm) until an OD_{600} of 0.5 was reached (~ 5 h) before induction with IPTG following the same procedure as described in section 6.4.3. Cell lysis, amylose affinity chromatography, dialysis, FXA cleavage, and HPLC purification were performed as detailed in sections 6.4.3. and 6.4.5. From 1 L of [^{13}C, ^{15}N]M9 culture, 1.9 mg of [^{13}C, ^{15}N]-(C9S, C14S)-leucocin A was obtained. The identity of the peptide was confirmed by MALDI-TOF MS.

6.4.10. NMR spectroscopy of [^{13}C, ^{15}N]-(C9S, C14S)-leucocin A

An NMR sample of [^{13}C, ^{15}N]-(C9S, C14S)-leucocin A (~ 0.5 mM) was dissolved in 9:1 TFE-d_3/H_2O with 100 μM DSS. NMR spectra were recorded at 25 °C on the Varian Inova 600-MHz spectrometer or the Varian Inova 800-MHz

spectrometer. To assign the ^{1}H, ^{13}C, and ^{15}N resonances of (C9S, C14S)-leucocin A, a suite of experiments was run the peptide. **Table 19** lists the experimental parameters used to acquire the NMR spectra. The spectra were processed following the same procedure as described in section 6.2.6.

Table 19: Experimental parameters used to acquire NMR spectra on [^{13}C, ^{15}N]-(C9S, C14S)-leucocin A to obtain chemical shift assignments, coupling constants, and NOE restraints.

Exp. Name[a]	Nuclei[b]	x-sw[c]	y-sw	z-sw	x-pts	y-pts	z-pts	Ref
^{13}C-HSQC (full)	^{1}H, ^{13}C	11990	28155		1024	128		
^{15}N-HSQC[d]	^{1}H, ^{15}N	8385	2429		512	128		124
HNHA	^{1}H, $^{1}H_{\alpha}$, ^{15}N	11990	7198	2400	1024	64	32	125, 126
CBCA(CO)NH[d]	^{1}H, ^{13}C, ^{15}N	8385	12056	2429	512	64	32	127
HCCH-TOCSY	^{1}H, ^{1}H, ^{13}C	11990	8000	16090	1024	160	38	128
HNCO[d]	^{1}H, $^{13}C(O)$, ^{15}N	8385	3770	2429	512	64	32	127, 129, 130, 134
HNCACB[d]	^{1}H, ^{13}C, ^{15}N	8385	12056	2429	512	64	32	127, 130, 131
^{13}C-NOESYHSQC	^{1}H, ^{1}H, ^{13}C	11990	8000	15001	1024	128	32	132
^{15}N-NOESYHSQC	^{1}H, ^{1}H, ^{15}N	11990	8000	2308	1024	120	32	133
^{15}N-TOCSYHSQC	^{1}H, ^{1}H, ^{15}N	11990	10000	2400	1024	128	32	133

[a]Experiments were acquired at 800 MHz unless otherwise specified.
[b]The nucleus acquired in each dimension (e.g. 1H,15N indicates hydrogen x, nitrogen y).
[c]x,y,z-pts and sw are the number of complex points and sweep width in each respective dimension (x is the directly detected dimension).
[d]Experiment was acquired at 600MHz.

6.4.11. Structure calculations

CYANA 2.1 was used to calculate the of (C9S, C14S)-leucocin A,[87] using NOE restraints measured from the ^{13}C-NOESYHSQC and ^{15}N-NOESYHSQC experiments combined with angle restraints obtained from the HNHA experiment and from TALOS.[88] NOEs were calibrated within CYANA according to their

intensities. After seven rounds of calculation (10,000 steps per round), a total of 403 cross-peak NOE assignments, 27 $^{3}J_{\mathrm{HNH}_{\alpha}}$ coupling constants, and 17 dihedral angle restraints were used in the final calculation. Electrostatic surface calculations were computed with APBS.[136] All other figures were generated using PyMOL.

Chapter 7. References

1. Cotter, P. D.; Hill, C.; Ross, R. P. Bacteriocins: Developing innate immunity for food. *Nat. Rev. Microbiol.,* **2005,** *3* (10), 777-788.
2. Nissen-Meyer, J.; Rogne, P.; Oppegård, C.; Haugen, H. S.; Kristiansen, P. E. Structure-function relationships of the non-lanthionine-containing peptide (class II) bacteriocins produced by Gram-positive bacteria. *Curr. Pharm. Biotechnol.,* **2009,** *10* (1), 19-37.
3. Chatterjee, C.; Paul, M.; Xie, L. L.; van der Donk, W. A. Biosynthesis and mode of action of lantibiotics. *Chem. Rev.,* **2005,** *105* (2), 633-683.
4. Martin-Visscher, L. A.; Sprules, T.; Gursky, L. J.; Vederas, J. C. Nuclear magnetic resonance solution structure of PisI, a group B immunity protein that provides protection against the type IIa bacteriocin piscicolin 126, PisA. *Biochemistry,* **2008,** *47* (24), 6427-6436.
5. Kuipers, O. P.; Beerthuyzen, M. M.; Siezen, R. J.; Devos, W. M. Characterization of the nisin gene cluster *nisABTCIPR* of *Lactococcus lactis* - Requirement of expression of the *nisA* and *nisI* genes for development of immunity. *Eur. J. Biochem.,* **1993,** *216* (1), 281-291.
6. Draper, L. A.; Ross, R. P.; Hill, C.; Cotter, P. D. Lantibiotic immunity. *Curr. Protein Pept. Sci.,* **2008,** *9* (1), 39-49.
7. van Belkum, M. J.; Derksen, D. J.; Franz, C.; Vederas, J. C. Structure-function relationship of inducer peptide pheromones involved in bacteriocin production in *Carnobacterium maltaromaticum* and *Enterococcus faecium*. *Microbiology-(UK),* **2007,** *153*, 3660-3666.

8. Quadri, L. E. N. Regulation of class II bacteriocin production by cell-cell signaling. *J. Microbiol.,* **2003,** *41* (3), 175-182.

9. Sun, Z. Z.; Zhong, J.; Liang, X. B.; Liu, J. L.; Chen, X. Z.; Huan, L. D. Novel mechanism for nisin resistance via proteolytic degradation of nisin by the nisin resistance protein NSR. *Antimicrob. Agents Chemother.,* **2009,** *53* (5), 1964-1973.

10. Staron, A.; Finkeisen, D. E.; Mascher, T. Peptide antibiotic sensing and detoxification modules of *Bacillus subtilis*. *Antimicrob. Agents Chemother.,* **2011,** *55* (2), 515-525.

11. Ernst, C. M.; Peschel, A. Broad-spectrum antimicrobial peptide resistance by MprF-mediated aminoacylation and flipping of phospholipids. *Mol. Microbiol.,* **2011,** *80* (2), 290-299.

12. Cotter, P. D.; Hill, C.; Ross, R. P. Bacterial lantibiotics: strategies to improve therapeutic potential. *Curr. Protein Pept. Sci.,* **2005,** *6* (1), 61-75.

13. Martin-Visscher, L. A.; Yoganathan, S.; Sit, C. S.; Lohans, C. T.; Vederas, J. C. The activity of bacteriocins from *Carnobacterium maltaromaticum* UAL307 against Gram-negative bacteria in combination with EDTA treatment. *FEMS Microbiol. Lett.,* **2011,** *317* (2), 152-159.

14. Gao, Y.; van Belkum, M. J.; Stiles, M. E. The outer membrane of Gram-negative bacteria inhibits antibacterial activity of brochocin-C. *Appl. Environ. Microbiol.,* **1999,** *65* (10), 4329-4333.

15. Ganzle, M. G.; Weber, S.; Hammes, W. P. Effect of ecological factors on the inhibitory spectrum and activity of bacteriocins. *Int. J. Food Microbiol.,* **1999,** *46* (3), 207-217.

16. Stevens, K. A.; Sheldon, B. W.; Klapes, N. A.; Klaenhammer, T. R. Nisin treatment for inactivation of *Salmonella* species and other Gram-negative bacteria. *Appl. Environ. Microbiol.,* **1991,** *57* (12), 3613-3615.

17. Yoganathan, S.; Sit, C. S.; Vederas, J. C. Chemical synthesis and biological evaluation of gallidermin-siderophore conjugates. *Org. Biomol. Chem.,* **2011,** *9* (7), 2133-2141.

18. Rea, M. C.; Clayton, E.; O'Connor, P. M.; Shanahan, F.; Kiely, B.; Ross, R. P.; Hill, C. Antimicrobial activity of lacticin 3147 against clinical *Clostridium difficile* strains. *J. Med. Microbiol.,* **2007,** *56* (7), 940-946.

19. Maher, S.; McClean, S. Investigation of the cytotoxicity of eukaryotic and prokaryotic antimicrobial peptides in intestinal epithelial cells in vitro. *Biochem. Pharmacol.,* **2006,** *71* (9), 1289-1298.

20. Gardiner, G. E.; Rea, M. C.; O'Riordan, B.; O'Connor, P.; Morgan, S. M.; Lawlor, P. G.; Lynch, P. B.; Cronin, M.; Ross, R. P.; Hill, C. Fate of the two-component lantibiotic lacticin 3147 in the gastrointestinal tract. *Appl. Environ. Microbiol.,* **2007,** *73* (21), 7103-7109.

21. Dobson, A.; Crispie, F.; Rea, M. C.; O'Sullivan, O.; Casey, P. G.; Lawlor, P. G.; Cotter, P. D.; Ross, P.; Gardiner, G. E.; Hill, C. Fate and efficacy of lacticin 3147-producing *Lactococcus lactis* in the mammalian gastrointestinal tract. *FEMS Microbiol. Ecol.,* **2011,** *76* (3), 602-614.

22. Sit, C. S.; Yoganathan, S.; Vederas, J. C. Biosynthesis of aminovinyl-cysteine-containing peptides and its application in the production of potential drug candidates. *Acc. Chem. Res.,* **2011,** *44* (4), 261-268.

23. Marki, F.; Hanni, E.; Fredenhagen, A.; Vanoostrum, J. Mode of action of the lanthionine-containing peptide antibiotics duramycin, duramycin B and C, and cinnamycin as indirect inhibitors of phospholipase A2. *Biochem. Pharmacol.,* **1991,** *42* (10), 2027-2035.

24. Silkin, L.; Hamza, S.; Kaufman, S.; Cobb, S. L.; Vederas, J. C. Spermicidal bacteriocins: Lacticin 3147 and subtilosin A. *Bioorg. Med. Chem. Lett.,* **2008,** *18* (10), 3103-3106.

25. Sit, C. S.; Vederas, J. C. Approaches to the discovery of new antibacterial agents based on bacteriocins. *Biochem. Cell Biol.,* **2008,** *86* (2), 116-123.

26. Oman, T. J.; van der Donk, W. A. Follow the leader: the use of leader peptides to guide natural product biosynthesis. *Nat. Chem. Biol.,* **2010,** *6* (1), 9-18.

27. Kleanthous, C. Swimming against the tide: progress and challenges in our understanding of colicin translocation. *Nat. Rev. Microbiol.,* **2010,** *8* (12), 843-848.

28. Klaenhammer, T. R. Genetics of bacteriocins produced by lactic acid bacteria. *FEMS Microbiol. Rev.,* **1993,** *12* (1-3), 39-86.

29. Martin-Visscher, L. A.; Gong, X.; Duszyk, M.; Vederas, J. C. The three-dimensional structure of carnocyclin A reveals that many circular

bacteriocins share a common structural motif. *J Biol Chem,* **2009,** *284* (42), 28674-81.

30. Martin-Visscher, L. A.; Belkum, M. J.; Vederas, J. C., Class IIc or circular bacteriocins. In *Prokaryotic Antimicrobial Peptides*, Drider, D.; Rebuffat, S., Eds. Springer New York: 2011; pp 213-236.
31. van Belkum, M. J.; Martin-Visscher, L. A.; Vederas, J. C. Structure and genetics of circular bacteriocins. *Trends in microbiology,* **2011,** *In press*.
32. Kawulka, K. E.; Sprules, T.; Diaper, C. M.; Whittal, R. M.; McKay, R. T.; Mercier, P.; Zuber, P.; Vederas, J. C. Structure of subtilosin A, a cyclic antimicrobial peptide from *Bacillus subtilis* with unusual sulfur to alpha-carbon cross-links: Formation and reduction of alpha-thio-alpha-amino acid derivatives. *Biochemistry,* **2004,** *43* (12), 3385-3395.
33. Lin, Y. H.; Teng, K. L.; Huan, L. D.; Zhong, J. Dissection of the bridging pattern of bovicin HJ50, a lantibiotic containing a characteristic disulfide bridge. *Microbiol. Res.,* **2011,** *166* (3), 146-154.
34. Kabuki, T.; Uenishi, H.; Seto, Y.; Yoshioka, T.; Nakajima, H. A unique lantibiotic, thermophilin 1277, containing a disulfide bridge and two thioether bridges. *J. Appl. Microbiol.,* **2009,** *106* (3), 853-862.
35. Cooper, L. E.; McClerren, A. L.; Chary, A.; van der Donk, W. A. Structure-activity relationship studies of the two-component lantibiotic haloduracin. *Chem. Biol.,* **2008,** *15* (10), 1035-1045.
36. Yoganathan, S.; Vederas, J. C. Fracturing rings to understand lantibiotics. *Chem. Biol.,* **2008,** *15* (10), 999-1001.

37. Kawulka, K.; Sprules, T.; McKay, R. T.; Mercier, P.; Diaper, C. M.; Zuber, P.; Vederas, J. C. Structure of subtilosin A, an antimicrobial peptide from *Bacillus subtilis* with unusual posttranslational modifications linking cysteine sulfurs to alpha-carbons of phenylalanine and threonine. *J. Am. Chem. Soc.,* **2003,** *125* (16), 4726-4727.

38. Siegers, K.; Entian, K. D. Genes involved in immunity to the lantibiotic nisin produced by *Lactococcus lactis* 6F3. *Appl. Environ. Microbiol.,* **1995,** *61* (3), 1082-1089.

39. Engelke, G.; Gutowskieckel, Z.; Kiesau, P.; Siegers, K.; Hammelmann, M.; Entian, K. D. Regulation of nisin biosynthesis and immunity in *Lactococcus lactis* 6F3. *Appl. Environ. Microbiol.,* **1994,** *60* (3), 814-825.

40. Levengood, M. R.; Patton, G. C.; van der Donk, W. A. D. The leader peptide is not required for post-translational modification by lacticin 481 synthetase. *J. Am. Chem. Soc.,* **2007,** *129* (34), 10314-10315.

41. Li, B.; Yu, J. P. J.; Brunzelle, J. S.; Moll, G. N.; van der Donk, W. A.; Nair, S. K. Structure and mechanism of the lantibiotic cyclase involved in nisin biosynthesis. *Science,* **2006,** *311* (5766), 1464-1467.

42. Bierbaum, G.; Sahl, H. G. Lantibiotics: mode of action, biosynthesis and bioengineering. *Curr. Pharm. Biotechnol.,* **2009,** *10* (1), 2-18.

43. Qiao, M. Q.; Immonen, T.; Koponen, O.; Saris, P. E. J. The cellular location and effect on nisin immunity of the NisI protein from *Lactococcus lactis* N8 expressed in *Escherichia coli* and *L. lactis*. *FEMS Microbiol. Lett.,* **1995,** *131* (1), 75-80.

44. Koponen, O.; Takala, T. M.; Saarela, U.; Qiao, M. Q.; Saris, P. E. J. Distribution of the NisI immunity protein and enhancement of nisin activity by the lipid-free NisI. *FEMS Microbiol. Lett.,* **2004,** *231* (1), 85-90.

45. Kuipers, O. P.; Beerthuyzen, M. M.; Deruyter, P.; Luesink, E. J.; Devos, W. M. Autoregulation of nisin biosynthesis in *Lactococcus lactis* by signal transduction. *J. Biol. Chem.,* **1995,** *270* (45), 27299-27304.

46. Hasper, H. E.; Kramer, N. E.; Smith, J. L.; Hillman, J. D.; Zachariah, C.; Kuipers, O. P.; de Kruijff, B.; Breukink, E. An alternative bactericidal mechanism of action for lantibiotic peptides that target lipid II. *Science,* **2006,** *313* (5793), 1636-1637.

47. Hsu, S. T. D.; Breukink, E.; Tischenko, E.; Lutters, M. A. G.; de Kruijff, B.; Kaptein, R.; Bonvin, A.; van Nuland, N. A. J. The nisin-lipid II complex reveals a pyrophosphate cage that provides a blueprint for novel antibiotics. *Nat. Struct. Mol. Biol.,* **2004,** *11* (10), 963-967.

48. Asaduzzaman, S. M.; Sonomoto, K. Lantibiotics: diverse activities and unique modes of action. *J. Biosci. Bioeng.,* **2009,** *107* (5), 475-487.

49. Lubelski, J.; Rink, R.; Khusainov, R.; Moll, G. N.; Kuipers, O. P. Biosynthesis, immunity, regulation, mode of action and engineering of the model lantibiotic nisin. *Cell. Mol. Life Sci.,* **2008,** *65* (3), 455-476.

50. Chan, W. C.; Leyland, M.; Clark, J.; Dodd, H. M.; Lian, L. Y.; Gasson, M. J.; Bycroft, B. W.; Roberts, G. C. K. Structure-activity relationships in the peptide antibiotic nisin: antibacterial activity of fragments of nisin. *FEBS Lett.,* **1996,** *390* (2), 129-132.

51. Rink, R.; Wierenga, J.; Kuipers, A.; Kluskens, L. D.; Driessen, A. J. M.; Kuipers, O. P.; Moll, G. N. Dissection and modulation of the four distinct activities of nisin by mutagenesis of rings A and B and by C-terminal truncation. *Appl. Environ. Microbiol.,* **2007,** *73* (18), 5809-5816.

52. Field, D.; Connor, P. M. O.; Cotter, P. D.; Hill, C.; Ross, R. P. The generation of nisin variants with enhanced activity against specific Gram-positive pathogens. *Mol. Microbiol.,* **2008,** *69* (1), 218-230.

53. Field, D.; Quigley, L.; O'Connor, P. M.; Rea, M. C.; Daly, K.; Cotter, P. D.; Hill, C.; Ross, R. P. Studies with bioengineered nisin peptides highlight the broad-spectrum potency of nisin V. *Microb. Biotechnol.,* **2010,** *3* (4), 473-486.

54. Ross, A. C.; Vederas, J. C. Fundamental functionality: recent developments in understanding the structure-activity relationships of lantibiotic peptides. *J. Antibiot.,* **2011,** *64* (1), 27-34.

55. Field, D.; Hill, C.; Cotter, P. D.; Ross, R. P. The dawning of a 'Golden era' in lantibiotic bioengineering. *Mol. Microbiol.,* **2010,** *78* (5), 1077-1087.

56. Levengood, M. R.; Knerr, P. J.; Oman, T. J.; van der Donk, W. A. In vitro mutasynthesis of lantibiotic analogues containing nonproteinogenic amino acids. *J. Am. Chem. Soc.,* **2009,** *131* (34), 12024-12025.

57. Babasaki, K.; Takao, T.; Shimonishi, Y.; Kurahashi, K. Subtilosin A, a new antibiotic peptide produced by *Bacillus subtilis* 168: isolation, stuctural analysis and biogenesis. *J. Biochem.,* **1985,** *98* (3), 585-603.

58. Shelburne, C. E.; An, F. Y.; Dholpe, V.; Ramamoorthy, A.; Lopatin, D. E.; Lantz, M. S. The spectrum of antimicrobial activity of the bacteriocin subtilosin A. *J. Antimicrob. Chemother.,* **2007,** *59* (2), 297-300.

59. Zheng, G. L.; Yan, L. Z.; Vederas, J. C.; Zuber, P. Genes of the sbo-alb locus of Bacillus subtilis are required for production of the antilisterial bacteriocin subtilosin. *J. Bacteriol.,* **1999,** *181* (23), 7346-7355.

60. Zheng, G. L.; Hehn, R.; Zuber, P. Mutational analysis of the *sbo-alb* locus of *Bacillus subtilis*: identification of genes required for subtilosin production and immunity. *J. Bacteriol.,* **2000,** *182* (11), 3266-3273.

61. Rea, M. C.; Sit, C. S.; Clayton, E.; O'Connor, P. M.; Whittal, R. M.; Zheng, J.; Vederas, J. C.; Ross, R. P.; Hill, C. Thuricin CD, a posttranslationally modified bacteriocin with a narrow spectrum of activity against *Clostridium difficile*. *Proc. Natl. Acad. Sci. U. S. A.,* **2010,** *107* (20), 9352-9357.

62. Fontecave, M.; Atta, M.; Mulliez, E. S-adenosylmethionine: nothing goes to waste. *Trends Biochem.Sci.,* **2004,** *29* (5), 243-249.

63. Sit, C. S.; van Belkum, M. J.; McKay, R. T.; Worobo, R. W.; Vederas, J. C. The 3D solution structure of thurincin H, a bacteriocin with four sulfur to alpha-carbon crosslinks. *Angew. Chem.-Int. Ed.,* **2011,** *Accepted*.

64. Thennarasu, S.; Lee, D. K.; Poon, A.; Kawulka, K. E.; Vederas, J. C.; Ramamoorthy, A. Membrane permeabilization, orientation, and antimicrobial mechanism of subtilosin A. *Chem. Phys. Lipids,* **2005,** *137* (1-2), 38-51.

65. Yamamoto, K.; Xu, J. D.; Kawulka, K. E.; Vederas, J. C.; Ramamoorthy, A. Use of a copper-chelated lipid speeds up NMR measurements from membrane proteins. *J. Am. Chem. Soc.,* **2010,** *132* (20), 6929-6931.

66. Huang, T.; Geng, H.; Miyyapuram, V. R.; Sit, C. S.; Vederas, J. C.; Nakano, M. M. Isolation of a variant of subtilosin A with hemolytic activity. *J. Bacteriol.,* **2009,** *191* (18), 5690-5696.

67. Fimland, G.; Johnsen, L.; Dalhus, B.; Nissen-Meyer, J. Pediocin-like antimicrobial peptides (class IIa bacteriocins) and their immunity proteins: biosynthesis, structure, and mode of action. *Journal of Peptide Science,* **2005,** *11* (11), 688-696.

68. Marugg, J. D.; Gonzalez, C. F.; Kunka, B. S.; Ledeboer, A. M.; Pucci, M. J.; Toonen, M. Y.; Walker, S. A.; Zoetmulder, L. C. M.; Vandenbergh, P. A. Cloning, expression, and nucleotide sequence of genes involved in production of pediocin PA-1, a bacteriocin from *Pediococcus acidilactici* PAC1.0. *Appl. Environ. Microbiol.,* **1992,** *58* (8), 2360-2367.

69. vanBelkum, M. J.; Worobo, R. W.; Stiles, M. E. Double-glycine-type leader peptides direct secretion of bacteriocins by ABC transporters: Colicin V secretion in *Lactococcus lactis*. *Mol. Microbiol.,* **1997,** *23* (6), 1293-1301.

70. Havarstein, L. S.; Diep, D. B.; Nes, I. F. A family of bacteriocin ABC transporters carry out proteolytic processing of their substrates concomitant with export. *Mol. Microbiol.,* **1995,** *16* (2), 229-240.

71. Johnsen, L.; Fimland, G.; Meyer, J. N. The C-terminal domain of pediocin-like antimicrobial peptides (class IIa bacteriocins) is involved in specific

recognition of the C-terminal part of cognate immunity proteins and in determining the antimicrobial spectrum. *J. Biol. Chem.,* **2005,** *280* (10), 9243-9250.

72. Diep, D. B.; Skaugen, M.; Salehian, Z.; Holo, H.; Nes, I. F. Common mechanisms of target cell recognition and immunity for class II bacteriocins. *Proc. Natl. Acad. Sci. U. S. A.,* **2007,** *104* (7), 2384-2389.

73. Derksen, D. J.; Boudreau, M. A.; Vederas, J. C. Hydrophobic interactions as substitutes for a conserved disulfide linkage in the type IIa bacteriocins, leucocin A and pediocin PA-1. *ChemBioChem,* **2008,** *9* (12), 1898-1901.

74. Fimland, G.; Johnsen, L.; Axelsson, L.; Brurberg, M. B.; Nes, I. F.; Eijsink, V. G. H.; Nissen-Meyer, J. A C-terminal disulfide bridge in pediocin-like bacteriocins renders bacteriocin activity less temperature dependent and is a major determinant of the antimicrobial spectrum. *J. Bacteriol.,* **2000,** *182* (9), 2643-2648.

75. Johnsen, L.; Fimland, G.; Eijsink, V.; Nissen-Meyer, J. Engineering increased stability in the antimicrobial peptide pediocin PA-1. *Appl. Environ. Microbiol.,* **2000,** *66* (11), 4798-4802.

76. Sit, C. S.; McKay, R. T.; Hill, C.; Ross, R. P.; Vederas, J. C. The 3D structure of thuricin CD, a two-component bacteriocin with cysteine sulfur to alpha-carbon crosslinks. *J. Am. Chem. Soc.,* **2011,** *133* (20), 7680-7683.

77. Ryan, M. P.; Rea, M. C.; Hill, C.; Ross, R. P. An application in cheddar cheese manufacture for a strain of *Lactococcus lactis* producing a novel

broad-spectrum bacteriocin, lacticin 3147. *Appl. Environ. Microbiol.,* **1996,** *62* (2), 612-619.

78. O'Toole, P. W.; Claesson, M. J. Gut microbiota: Changes throughout the lifespan from infancy to elderly. *Int. Dairy J.,* **2010,** *20* (4), 281-291.

79. Freeman, J.; Bauer, M. P.; Baines, S. D.; Corver, J.; Fawley, W. N.; Goorhuis, B.; Kuijper, E. J.; Wilcox, M. H. The changing epidemiology of *Clostridium difficile* infections. *Clin. Microbiol. Rev.,* **2010,** *23* (3), 529-549.

80. Hubert, B.; Loo, V. G.; Bourgault, A. M.; Poirier, L.; Dascal, A.; Fortin, E.; Dionne, M.; Lorange, M. A portrait of the geographic dissemination of the *Clostridium difficile* North American pulsed-field type 1 strain and the epidemiology of *C. difficile*-associated disease in Quebec. *Clin. Infect. Dis.,* **2007,** *44* (2), 238-244.

81. Pepin, J.; Valiquette, L.; Cossette, B. Mortality attributable to nosocomial *Clostridium difficile*-associated disease during an epidemic caused by a hypervirulent strain in Quebec. *Can. Med. Assoc. J.,* **2005,** *173* (9), 1037-1042.

82. Gravel, D.; Miller, M.; Simor, A.; Taylor, G.; Gardam, M.; McGeer, A.; Hutchinson, J.; Moore, D.; Kelly, S.; Boyd, D.; Mulvey, M.; Canadian Nosocomial, I. Health care-associated *Clostridium difficile* infection in adults admitted to acute care hospitals in Canada: a Canadian nosocomial infection surveillance program study. *Clin. Infect. Dis.,* **2009,** *48* (5), 568-576.

83. MacCannell, D. R.; Louie, T. J.; Gregson, D. B.; Laverdiere, M.; Labbe, A. C.; Laing, F.; Henwick, S. Molecular analysis of *Clostridium difficile* PCR ribotype 027 isolates from Eastern and Western Canada. *J. Clin. Microbiol.,* **2006,** *44* (6), 2147-2152.

84. Musher, D. M.; Aslam, S.; Logan, N.; Nallacheru, S.; Bhaila, I.; Borchert, F.; Hamill, R. J. Relatively poor outcome after treatment of *Clostridium difficile* colitis with metronidazole. *Clin. Infect. Dis.,* **2005,** *40* (11), 1586-1590.

85. Grehan, M. J.; Borody, T. J.; Leis, S. M.; Campbell, J.; Mitchell, H.; Wettstein, A. Durable alteration of the colonic microbiota by the administration of donor fecal flora. *J. Clin. Gastroenterol.,* **2010,** *44* (8), 551-561.

86. Wishart, D. S.; Bigam, C. G.; Holm, A.; Hodges, R. S.; Sykes, B. D. 1H, 13C and 15N random coil NMR chemical shifts of the common amino acids. I. Investigations of nearest-neighbor effects. *J. Biomol. NMR,* **1995,** *5* (1), 67-81.

87. Guntert, P.; Mumenthaler, C.; Wuthrich, K. Torsion angle dynamics for NMR structure calculation with the new program DYANA. *J. Mol. Biol.,* **1997,** *273* (1), 283-298.

88. Cornilescu, G.; Delaglio, F.; Bax, A. Protein backbone angle restraints from searching a database for chemical shift and sequence homology. *J. Biomol. NMR,* **1999,** *13* (3), 289-302.

89. Salvatella, X.; Caba, J. M.; Albericio, F.; Giralt, E. Solution structure of the antitumor candidate trunkamide A by 2D NMR and restrained simulated annealing methods. *J. Org. Chem.,* **2003,** *68* (2), 211-215.

90. Liu, W. T.; Yang, Y. L.; Xu, Y. Q.; Lamsa, A.; Haste, N. M.; Yang, J. Y.; Ng, J.; Gonzalez, D.; Ellermeier, C. D.; Straight, P. D.; Pevzner, P. A.; Pogliano, J.; Nizet, V.; Pogliano, K.; Dorrestein, P. C. Imaging mass spectrometry of intraspecies metabolic exchange revealed the cannibalistic factors of Bacillus subtilis. *Proc. Natl. Acad. Sci. U. S. A.,* **2010,** *107* (37), 16286-16290.

91. Lee, H.; Churey, J. J.; Worobo, R. W. Biosynthesis and transcriptional analysis of thurincin H, a tandem repeated bacteriocin genetic locus, produced by *Bacillus thuringiensis* SF361. *FEMS Microbiol. Lett.,* **2009,** *299* (2), 205-213.

92. Sebei, S.; Zendo, T.; Boudabous, A.; Nakayama, J.; Sonomoto, K. Characterization, N-terminal sequencing and classification of cerein MRX1, a novel bacteriocin purified from a newly isolated bacterium: *Bacillus cereus* MRX1. *J. Appl. Microbiol.,* **2007,** *103* (5), 1621-1631.

93. Chehimi, S.; Delalande, F.; Sable, S.; Hajlaoui, A. R.; Van Dorsselaer, A.; Limam, F.; Pons, A. M. Purification and partial amino acid sequence of thuricin S, a new anti-*Listeria* bacteriocin from *Bacillus thuringiensis*. *Can. J. Microbiol.,* **2007,** *53* (2), 284-290.

94. Ahern, M.; Verschueren, S.; van Sinderen, D. Isolation and characterisation of a novel bacteriocin produced by *Bacillus thuringiensis* strain B439. *FEMS Microbiol. Lett.,* **2003,** *220* (1), 127-131.

95. Gray, E. J.; Di Falco, M.; Souleimanov, A.; Smith, D. L. Proteomic analysis of the bacteriocin thuricin 17 produced by *Bacillus thuringiensis* NEB17. *FEMS Microbiol. Lett.,* **2006,** *255* (1), 27-32.

96. Kamoun, F.; Mejdoub, H.; Aouissaoui, H.; Reinbolt, J.; Hammami, A.; Jaoua, S. Purification, amino acid sequence and characterization of Bacthuricin F4, a new bacteriocin produced by *Bacillus thuringiensis*. *J. Appl. Microbiol.,* **2005,** *98* (4), 881-888.

97. Chehimi, S.; Pons, A. M.; Sable, S.; Hajlaoui, M. R.; Limam, F. Mode of action of thuricin S, a new class IId bacteriocin from *Bacillus thuringiensis*. *Can. J. Microbiol.,* **2010,** *56* (2), 162-167.

98. Lee, H. J.; Churey, J. J.; Worobo, R. W. Antimicrobial activity of bacterial isolates from different floral sources of honey. *Int. J. Food Microbiol.,* **2008,** *126* (1-2), 240-244.

99. Mundo, M. A.; Padilla-Zakour, O. I.; Worobo, R. W. Growth inhibition of foodborne pathogens and food spoilage organisms by select raw honeys. *Int. J. Food Microbiol.,* **2004,** *97* (1), 1-8.

100. Mook, P.; O'Brien, S. J.; Gillespie, I. A. Concurrent conditions and human listeriosis, England, 1999-2009. *Emerg. Infect. Dis,* **2011,** *17* (1), 38-43.

101. Usha, R.; Ramasami, T. Structure and conformation of intramolecularly cross-linked collagen. *Colloid Surf. B-Biointerfaces,* **2005,** *41* (1), 21-24.

102. Ladokhin, A. S.; Selsted, M. E.; White, S. H. CD spectra of indolicidin antimicrobial peptides suggest turns, not polyproline helix. *Biochemistry,* **1999,** *38* (38), 12313-12319.

103. Arnold, G. E.; Day, L. A.; Dunker, A. K. Tryptophan contributions to the unusual circular dichroism of fd bacteriophage *Biochemistry,* **1992,** *31* (34), 7948-7956.

104. Gray, E. J.; Lee, K. D.; Souleimanov, A. M.; Di Falco, M. R.; Zhou, X.; Ly, A.; Charles, T. C.; Driscoll, B. T.; Smith, D. L. A novel bacteriocin, thuricin 17, produced by plant growth promoting rhizobacteria strain *Bacillus thuringiensis* NEB17: isolation and classification. *J. Appl. Microbiol.,* **2006,** *100* (3), 545-554.

105. Lee, K. D.; Gray, E. J.; Mabood, F.; Jung, W. J.; Charles, T.; Clark, S. R. D.; Ly, A.; Souleimanov, A.; Zhou, X. M.; Smith, D. L. The class IId bacteriocin thuricin-17 increases plant growth. *Planta,* **2009,** *229* (4), 747-755.

106. Jung, W. J.; Mabood, F.; Souleimanov, A.; Zhou, X. M.; Jaoua, S.; Kamoun, F.; Smith, D. L. Stability and antibacterial activity of bacteriocins produced by *Bacillus thuringiensis* and *Bacillus thuringiensis* ssp. *kurstaki*. *J. Microbiol. Biotechnol.,* **2008,** *18* (11), 1836-1840.

107. Hastings, J. W.; Stiles, M. E. Antibiosis of *Leuconostoc gelidum* isolated from meat. *J. Appl. Bacteriol.,* **1991,** *70* (2), 127-134.

108. Fregeau Gallagher, N. L.; Sailer, M.; Niemczura, W. P.; Nakashima, T. T.; Stiles, M. E.; Vederas, J. C. Three-dimensional structure of leucocin A in

trifluoroethanol and dodecylphophocholine micelles: spatial location of residues critical for biological activity in type IIa bacteriocins from lactic acid bacteria. *Biochemistry,* **1997,** *36* (49), 15062-15072.

109. Hastings, J. W.; Sailer, M.; Johnson, K.; Roy, K. L.; Vederas, J. C.; Stiles, M. E. Characterization of leucocin A UAL 187 and cloning of the bacteriocin gene from *Leuconostoc gelidum*. *J. Bacteriol.,* **1991,** *173* (23), 7491-7500.
110. van Belkum, M. J.; Stiles, M. E. Molecular characterization of genes involved in the production of the bacteriocin leucocin A from *Leuconostoc gelidum*. *Appl. Environ. Microbiol.,* **1995,** *61* (10), 3573-3579.
111. Wang, Y. J.; Henz, M. E.; Gallagher, N. L. F.; Chai, S. Y.; Gibbs, A. C.; Yan, L. Z.; Stiles, M. E.; Wishart, D. S.; Vederas, J. C. Solution structure of carnobacteriocin B2 and implications for structure-activity relationships among type IIa bacteriocins from lactic acid bacteria. *Biochemistry,* **1999,** *38* (47), 15438-15447.
112. Sprules, T.; Kawulka, K. E.; Gibbs, A. C.; Wishart, D. S.; Vederas, J. C. NMR solution structure of the precursor for carnobacteriocin B2, an antimicrobial peptide from *Carnobacterium piscicola* - implications of the alpha-helical leader section for export and inhibition of type IIa bacteriocin activity. *Eur. J. Biochem.,* **2004,** *271* (9), 1748-1756.
113. Uteng, M.; Hauge, H. H.; Markwick, P. R. L.; Fimland, G.; Mantzilas, D.; Nissen-Meyer, J.; Muhle-Goll, C. Three-dimensional structure in lipid micelles of the pediocin-like antimicrobial peptide sakacin P and a sakacin

P variant that is structurally stabilized by an inserted C-terminal disulfide bridge. *Biochemistry,* **2003,** *42* (39), 11417-11426.

114. Haugen, H. S.; Fimland, G.; Nissen-Meyer, J.; Kristiansen, P. E. Three-dimensional structure in lipid micelles of the pediocin-like antimicrobial peptide curvacin A. *Biochemistry,* **2005,** *44* (49), 16149-16157.
115. Kaur, K.; Andrew, L. C.; Wishart, D. S.; Vederas, J. C. Dynamic relationships among type IIa bacteriocins: Temperature effects on antimicrobial activity and on structure of the C-terminal amphipathic alpha helix as a receptor-binding region. *Biochemistry,* **2004,** *43* (28), 9009-9020.
116. Derksen, D. J.; Stymiest, J. L.; Vederas, J. C. Antimicrobial leucocin analogues with a disulfide bridge replaced by a carbocycle or by noncovalent interactions of allyl glycine residues. *J. Am. Chem. Soc.,* **2006,** *128* (44), 14252-14253.
117. Kazazic, M.; Nissen-Meyer, J.; Fimland, G. Mutational analysis of the role of charged residues in target-cell binding, potency and specificity of the pediocin-like bacteriocin sakacin P. *Microbiology-(UK),* **2002,** *148*, 2019-2027.
118. Chen, Y. H.; Ludescher, R. D.; Montville, T. J. Electrostatic interactions, but not the YGNGV consensus motif, govern the binding of pediocin PA-1 and its fragments to phospholipid vesicles. *Appl. Environ. Microbiol.,* **1997,** *63* (12), 4770-4777.
119. Fimland, G.; Pirneskoski, J.; Kaewsrichan, J.; Jutila, A.; Kristiansen, P. E.; Kinnunen, P. K. J.; Nissen-Meyer, J. Mutational analysis and membrane-

interactions of the beta-sheet-like N-terminal domain of the pediocin-like antimicrobial peptide sakacin P. *BBA-Proteins Proteomics,* **2006,** *1764* (6), 1132-1140.

120. Dai, Y. Q.; Whittal, R. M.; Li, L. Two-layer sample preparation: A method for MALDI-MS analysis of complex peptide and protein mixtures. *Anal. Chem.,* **1999,** *71* (5), 1087-1091.
121. Morrow, J. A.; Segall, M. L.; Lund-Katz, S.; Phillips, M. C.; Knapp, M.; Rupp, B.; Weisgraber, K. H. Differences in stability among the human apolipoprotein E isoforms determined by the amino-terminal domain. *Biochemistry,* **2000,** *39* (38), 11657-11666.
122. Delaglio, F.; Grzesiek, S.; Vuister, G. W.; Zhu, G.; Pfeifer, J.; Bax, A. NMRPipe - A multidimensional spectral processing system based on Unix pipes. *J. Biomol. NMR,* **1995,** *6* (3), 277-293.
123. Johnson, B. A.; Blevins, R. A. NMRView - A computer program for the visualization and analysis of NMR data. *J. Biomol. NMR,* **1994,** *4* (5), 603-614.
124. Kay, L. E.; Keifer, P.; Saarinen, T. Pure absorption gradient enhanced heteronuclear single quantum correlation spectroscopy with improved sensitivity. *J. Am. Chem. Soc.,* **1992,** *114* (26), 10663-10665.
125. Kuboniwa, H.; Grzesiek, S.; Delaglio, F.; Bax, A. Measurement of HN-H alpha J couplings in calcium-free calmodulin using new 2D and 3D water-flip-back methods. *J. Biomol. NMR,* **1994,** *4* (6), 871-878.

126. Vuister, G. W.; Bax, A. Quantitative J correlation: a new approach for measuring homonuclear three-Bond J(HNH.alpha.) coupling constants in 15N-enriched proteins. *J. Am. Chem. Soc.,* **1993,** *115* (17), 7772-7777.

127. Muhandiram, D. R.; Kay, L. E. Gradient enhanced triple resonance three-dimensional NMR experiments with improved sensitivity. *J. Magn. Reson. Ser. B,* **1994,** *103* (3), 203-216.

128. Sattler, M.; Schwendinger, M. G.; Schleucher, J.; Griesinger, C. Novel strategies for sensitivity enhancement in heteronuclear multidimensional NMR experiments employing pulsed-field gradients. *J. Biomol. NMR,* **1995,** *6* (1), 11-22.

129. Ikura, M.; Kay, L. E.; Bax, A. A novel approach for sequential assignment of ^{1}H, ^{13}C, and ^{15}N spectra of larger proteins: heteronuclear triple-resonance three-dimensional NMR spectroscopy. Application to calmodulin. *Biochemistry,* **1990,** *29* (19), 4659-4667.

130. Kay, L. E.; Xu, G. Y.; Yamazaki, T. Enhanced-sensitivity triple-resonance spectroscopy with minimal H_2O saturation. *J. Magn. Reson. Ser. A,* **1994,** *109* (1), 129-133.

131. Wittekind, M.; Mueller, L. HNCACB, a high-sensitivity 3D NMR experiment to correlate amide-proton and nitrogen resonances with the alpha-carbon and beta-carbon resonances in proteins. *J. Magn. Reson. Ser. B,* **1993,** *101* (2), 201-205.

132. Pascal, S. M.; Muhandiram, D. R.; Yamazaki, T.; Forman-Kay, J. D.; Kay, L. E. Simultaneous acquisition of ^{15}N- and ^{13}C-edited NOE spectra of proteins dissolved in H2O. *J. Magn. Reson. Ser. B,* **1994,** *103* (2), 197-201.

133. Zhang, O. W.; Kay, L. E.; Olivier, J. P.; Forman-Kay, J. D. Backbone ^{1}H and ^{15}N resonance assignments of the N-terminal SH3 domain of drk in folded and unfolded states using enhanced-sensitivity pulsed-field gradient NMR techniques. *J. Biomol. NMR,* **1994,** *4* (6), 845-858.

134. Grzesiek, S.; Bax, A. Improved 3D triple-resonance NMR techniques applied to a 31 kDa protein. *J. Magn. Reson.,* **1992,** *96* (2), 432-440.

135. Patt, S. L. Single-frequency-shifted and multiple-frequency-shifted laminar pulses. *J. Magn. Reson.,* **1992,** *96* (1), 94-102.

136. Baker, N. A.; Sept, D.; Joseph, S.; Holst, M. J.; McCammon, J. A. Electrostatics of nanosystems: Application to microtubules and the ribosome. *Proc. Natl. Acad. Sci. U. S. A.,* **2001,** *98* (18), 10037-10041.

Appendix A. Thuricin CD NMR data and CYANA files

Table A1: ^{1}H Chemical shift assignments of Trn-α

	HN	Hα	Hβ	others
Gly 1		3.70		
Asn 2	8.41	4.70	2.99, 2.80	δNH_2 7.65, 7.01
Ala 3	8.94	3.91	1.36	
Ala 4	8.18	3.98	1.44	
Cys 5	7.84	4.04	3.73, 3.21	
Val 6	7.60	3.39	2.10	γCH_3 0.99, 0.86
Ile 7	7.74	3.52	1.71	γCH_2 1.56, 1.12, γCH_3 0.76, δCH_3 0.75
Gly 8	8.02	3.22, 2.79		
Cys 9	8.98	4.03	3.17, 2.89	
Ile 10	8.02	3.47	1.78	γCH_2 1.80, 0.96, γCH_3 0.75, δCH_3 0.73
Gly 11	8.40	3.69, 3.53		
Ser 12	7.86	4.10	4.03, 3.85	
Cys 13	8.25	3.64	3.22, 2.90	
Val 14	8.32	3.55	2.16	γCH_3 0.98, 0.87
Ile 15	7.87	3.89	1.94	γCH_2 1.59, 1.32, γCH_3 0.91, δCH_3 0.80
Ser 16	7.26	4.51	4.09, 3.65	
Glu 17	8.04	3.92	2.35, 2.26	γCH_2 2.38
Gly 18	8.46	4.23, 3.45		
Ile 19	7.80	3.87	1.96	γCH_2 1.57, 1.21, γCH_3 0.89, δCH_3 0.87
Gly 20	8.25	4.04, 3.72		
Ser 21	8.07	**none**	3.99, 3.73	
Leu 22	7.82	4.01	1.69, 1.55	γCH 1.64, δCH_3 0.89, 0.82
Val 23	7.38	4.02	2.10	γCH_3 0.91, 0.87
Gly 24	8.65	4.31, 3.75		
Thr 25	7.50	**none**	4.05	γCH_3 1.36
Ala 26	8.02	4.05	1.43	
Phe 27	8.39	4.10	3.20	
Thr 28	8.24	**none**	4.11	γCH_3 1.19
Leu 29	7.89	4.04	1.75, 1.56	γCH 1.59, δCH_3 0.86, 0.76
Gly 30	7.64	3.60, 3.94		

Table A2: ^{1}H Chemical shift assignments of Trn-β

	HN	**Hα**	**Hβ**	**others**
Gly 1		3.62, 3.54		
Trp 2	8.54	4.39	3.32, 3.26	
Val 3	7.70	3.34	1.75	γCH$_3$ 0.71, 0.45
Ala 4	7.33	4.03	1.31	
Cys 5	7.72	4.24	3.33, 2.95	
Val 6	8.18	3.54	2.03	γCH$_3$ 0.97, 0.89
Gly 7	7.95	3.76		
Ala 8	8.14	4.07	1.47	
Cys 9	8.95	3.86	3.16, 2.91	
Gly 10	8.54	3.85, 3.57		
Thr 11	7.88	3.77	4.10	γCH$_3$ 1.17
Val 12	7.51	3.60	1.95	γCH$_3$ 1.05, 0.91
Cys 13	9.01	3.66	4.38, 2.94	
Leu 14	8.16	4.02	1.86, 1.59	γCH 1.72, δCH$_3$ 0.85, 0.84
Ala 15	8.17	4.08	1.50	
Ser 16	7.54	4.56	4.32, 3.77	
Gly 17	8.10	4.00, 3.84		
Gly 18	8.48	4.41, 3.38		
Val 19	7.60	3.81	2.16	γCH$_3$ 1.13, 0.99
Gly 20	8.50	4.28, 3.49		
Thr 21	7.90	**none**	4.43	γCH$_3$ 1.18
Glu 22	8.64	3.78	1.85	γCH$_2$ 2.24
Phe 23	7.50	4.27	3.07	
Ala 24	8.62	4.01	1.67	
Ala 25	8.32	**none**	1.83	
Ala 26	7.66	4.27	1.63	
Ser 27	8.32	3.93	4.14, 3.90	
Tyr 28	8.20	**none**	3.16, 2.62	
Phe 29	7.78	4.17	3.39, 2.91	
Leu 30	7.75	4.30	1.80, 1.56	γCH 1.71, δCH$_3$ 0.89, 0.85

Table A3: Nitrogen and carbon chemical shift assignments of Trn-α

	N	**Cα**	**Cβ**	**others**
Gly 1		43.02		
Asn 2	116.19	52.95	44.00	δN 110.07
Ala 3	124.80	55.22	18.04	
Ala 4	117.86	54.93	17.60	
Cys 5	114.45	61.76	30.67	
Val 6	118.51	67.55	31.62	Cγ 22.28, 20.67
Ile 7	116.84	64.43	37.58	Cγ 28.74, Cγ' 16.61, Cδ 11.89
Gly 8	106.66	46.35		
Cys 9	120.79	61.20	31.45	
Ile 10	118.16	65.76	37.74	Cγ 29.14, Cγ' 16.86, Cδ 12.79
Gly 11	105.49	47.34		
Ser 12	114.76	62.07	63.38	
Cys 13	119.79	61.65	30.24	
Val 14	118.23	66.45	31.60	Cγ 22.35, 20.75
Ile 15	116.98	58.30	37.81	Cγ 28.26, Cγ' 16.91, Cδ 12.73
Ser 16	110.89	56.97	62.91	
Glu 17	115.69	56.94	26.03	Cγ 32.66
Gly 18	104.50	45.62		
Ile 19	120.60	63.18	37.92	Cγ 28.23, Cδ 12.23
Gly 20	105.00	45.71		
Ser 21	121.09	73.68	67.63	
Leu 22	117.25	58.70	41.82	Cγ 27.04, Cδ 24.08, 23.13
Val 23	112.58	63.10	32.26	Cγ 20.78, 20.61
Gly 24	110.17	48.76		
Thr 25	110.49	75.19	76.91	Cγ 18.00
Ala 26	106.63	55.63	17.41	
Phe 27	116.55	62.78	39.31	
Thr 28	119.76	78.49	76.89	Cγ 20.03
Leu 29	115.79	55.88	42.02	Cγ 27.24, Cδ 24.63, 21.86
Gly 30	105.58	43.00		

Table A4: Nitrogen and carbon chemical shift assignments of Trn-β

	N	Cα	Cβ	others
Gly 1		43.16		
Trp 2	120.68	60.01	29.58	
Val 3	119.57	65.54	31.40	Cγ 20.99, 20.59
Ala 4	120.57	54.11	17.97	
Cys 5	114.69	60.61	30.51	
Val 6	118.32	66.96	31.38	Cγ 22.19, 20.68
Gly 7	105.40	46.83		
Ala 8	125.67	55.49	17.81	
Cys 9	114.70	60.63	30.26	
Gly 10	104.53	47.85		
Thr 11	114.89	67.49	68.69	Cγ 20.96
Val 12	119.93	66.55	31.26	Cγ 22.57, 21.57
Cys 13	120.35	63.57	29.54	
Leu 14	118.84	58.46	41.75	Cγ 27.12, Cδ 24.05, 23.55
Ala 15	120.71	54.86	17.94	
Ser 16	105.94	57.11	64.15	
Gly 17	109.60	46.59		
Gly 18	103.44	44.28		
Val 19	120.36	65.72	31.97	Cγ 21.84, 20.64
Gly 20	102.20	46.13		
Thr 21	125.22	76.05	77.14	Cγ 20.45
Glu 22	116.10	60.04	27.88	Cγ 32.46
Phe 23	115.95	59.99	39.09	
Ala 24	119.30	55.81	19.18	
Ala 25	121.59	70.19	28.07	
Ala 26	119.47	36.37	17.22	
Ser 27	114.10	62.68	62.99	
Tyr 28	129.27	76.08	45.01	
Phe 29	110.81	60.47	39.72	
Leu 30	118.79	54.08	42.13	Cγ 26.95, Cδ 24.76, 22.55

Table A5: NOE correlations between the Cys and modified residues of Trn-α

Trn-α NOE signals	Conclusion
Cys 13 Hβ2 ↔ Ser 21 Hβ1 Cys 13 Hβ2 ↔ Ser 21 Hβ2 Cys 13 Hα ↔ Ser 21 Hβ2	α-thio bridge between Cys 13 and Ser 21
Thr 25 HN ↔ Cys 9 Hβ2 Cys 9 Hβ2 ↔ Thr 25 Hγ21	α-thio bridge between Cys 9 and Thr 25
Thr 28 HN ↔ Cys 5 Hβ1 Thr 28 HN ↔ Cys 5 Hβ2	α-thio bridge between Cys 5 and Thr 28

Table A6: NOE correlations between the Cys and modified residues of Trn-β

Trn-β NOE signals	Conclusion
Thr 21 Hβ ↔ Cys 13 Hβ1 Cys 13 Hα ↔ Thr 21 HN	α-thio bridge between Cys 13 and Thr 21
Ala 25 Hβ ↔ Cys 9 Hβ2 Cys 9 Hβ1 ↔ Ala 25 Hβ Cys 9 Hβ2 ↔ Ala 25 Hβ	α-thio bridge between Cys 9 and Ala 25
Tyr 28 Hβ1 ↔ Cys 5 Hβ2 Cys 5 Hβ1 ↔ Tyr 28 Hβ2 Cys 5 Hβ2 ↔ Tyr 28 Hβ2	α-thio bridge between Cys 5 and Tyr 28

```
RESIDUE  MALA      4   13    3   12
   1 OMEGA    0    0    0.0000    2    1    3    4    0
   2 PHI      0    0    0.0000    1    3    5   11    0
   3 CHI1     0    0    0.0000    3    5    7    8   10
   4 PSI      0    0    0.0000    3    5   11   13    0
   1 C    C_BYL    0    0.0000    0.0000    0.0000    0.0000    2    3    0    0    0
   2 O    O_BYL    0    0.0000   -0.6700    0.0000   -1.0322    1    0    0    0    0
   3 N    N_AMI    0    0.0000    1.3290    0.0000    0.0000    1    4    5    0    0
   4 H    H_AMI    0    0.0000    1.8069   -0.0007    0.8553    3    0    0    0    0
   5 CA   C_ALI    0    0.0000    2.0929   -0.0011   -1.2414    3    7   11    0    0
   6 QB   PSEUD    0    0.0000    0.9384   -0.1665   -2.7175    0    0    0    0    0
   7 CB   C_ALI    0    0.0000    1.1594   -0.1351   -2.4354    5    8    9   10    0
   8 HB1  H_ALI    0    0.0000    0.1776    0.2265   -2.1659    7    0    0    0    6
   9 HB2  H_ALI    0    0.0000    1.5440    0.4465   -3.2598    7    0    0    0    6
  10 HB3  H_ALI    0    0.0000    1.0938   -1.1729   -2.7259    7    0    0    0    6
  11 C    C_BYL    0    0.0000    2.9378    1.2621   -1.3672    5   12   13    0    0
  12 O    O_BYL    0    0.0000    2.4397    2.3166   -1.7634   11    0    0    0    0
  13 N    N_AMI    0    0.0000    4.2169    1.1488   -1.0273   11    0    0    0    0
```

Figure A1. A description of modified alanine with L-stereochemistry (MALA) that was added to the residue library of CYANA.

```
RESIDUE  DALA      4   13    3   12
   1 OMEGA    0    0    0.0000    2    1    3    4    0
   2 PHI      0    0    0.0000    1    3    5   11    0
   3 CHI1     0    0    0.0000    3    5    7    8   10
   4 PSI      0    0    0.0000    3    5   11   13    0
   1 C    C_BYL    0    0.0000    0.0000    0.0000    0.0000    2    3    0    0    0
   2 O    O_BYL    0    0.0000    0.6700    0.0000   -1.0322    1    0    0    0    0
   3 N    N_AMI    0    0.0000   -1.3290    0.0000    0.0000    1    4    5    0    0
   4 H    H_AMI    0    0.0000   -1.8069   -0.0007    0.8553    3    0    0    0    0
   5 CA   C_ALI    0    0.0000   -2.0929   -0.0011   -1.2414    3    7   11    0    0
   6 QB   PSEUD    0    0.0000   -0.9384   -0.1665   -2.7175    0    0    0    0    0
   7 CB   C_ALI    0    0.0000   -1.1594   -0.1351   -2.4354    5    8    9   10    0
   8 HB1  H_ALI    0    0.0000   -0.1776    0.2265   -2.1659    7    0    0    0    6
   9 HB2  H_ALI    0    0.0000   -1.5440    0.4465   -3.2598    7    0    0    0    6
  10 HB3  H_ALI    0    0.0000   -1.0938   -1.1729   -2.7259    7    0    0    0    6
  11 C    C_BYL    0    0.0000   -2.9378    1.2621   -1.3672    5   12   13    0    0
  12 O    O_BYL    0    0.0000   -2.4397    2.3166   -1.7634   11    0    0    0    0
  13 N    N_AMI    0    0.0000   -4.2169    1.1488   -1.0273   11    0    0    0    0
```

Figure A2. A description of modified alanine with D-stereochemistry (DALA) that was added to the residue library of CYANA.

```
RESIDUE  MTHR      6   17    3   16
   1 OMEGA    0    0    0.0000    2    1    3    4    0
   2 PHI      0    0    0.0000    1    3    5   15    0
   3 CHI1     0    0    0.0000    3    5    6    9   14
   4 CHI21    0    0    0.0000    5    6    9   10   10
   5 CHI22    0    0    0.0000    5    6   11   12   14
   6 PSI      0    0    0.0000    3    5   15   17    0
   1 C    C_BYL    0    0.0000    0.0000    0.0000    0.0000    2    3    0    0    0
   2 O    O_BYL    0    0.0000   -0.6693    0.0000   -1.0338    1    0    0    0    0
   3 N    N_AMI    0    0.0000    1.3295    0.0000    0.0000    1    4    5    0    0
   4 H    H_AMI    0    0.0000    1.8063    0.0008    0.8561    3    0    0    0    0
   5 CA   C_ALI    0    0.0000    2.0938    0.0000   -1.2409    3    6   15    0    0
   6 CB   C_ALI    0    0.0000    3.3532   -0.8793   -1.1250    5    8   10   12    0
   7 HB   H_ALI    0    0.0000    3.3321   -1.6176   -1.9139    6    0    0    0    0
   8 QG2  PSEUD    0    0.0000    4.9118    0.1565   -1.3122    0    0    0    0    0
   9 OG1  O_HYD    0    0.0000    3.3686   -1.5486    0.1408    6   10    0    0    0
  10 HG1  H_OXY    0    0.0000    4.2121   -1.3956    0.5736    9    0    0    0    0
  11 CG2  C_ALI    0    0.0000    4.6139   -0.0416   -1.2768    6   12   13   14    0
  12 HG21 H_ALI    0    0.0000    4.3455    1.0012   -1.3599   11    0    0    0    8
  13 HG22 H_ALI    0    0.0000    5.1453   -0.3488   -2.1652   11    0    0    0    8
  14 HG23 H_ALI    0    0.0000    5.2453   -0.1825   -0.4126   11    0    0    0    8
  15 C    C_BYL    0    0.0000    1.2475   -0.4956   -2.4079    5   16   17    0    0
  16 O    O_BYL    0    0.0000    0.7354   -1.6152   -2.3854   15    0    0    0    0
  17 N    N_AMI    0    0.0000    1.1045    0.3443   -3.4277   15    0    0    0    0
```

Figure A3. A description of modified threonine with L-stereochemistry (MTHR) that was added to the residue library of CYANA.

```
RESIDUE  DTHR      6   17    3   16
   1 OMEGA    0    0    0.0000    2    1    3    4    0
   2 PHI      0    0    0.0000    1    3    5   15    0
   3 CHI1     0    0    0.0000    3    5    6    9   14
   4 CHI21    0    0    0.0000    5    6    9   10   10
   5 CHI22    0    0    0.0000    5    6   11   12   14
   6 PSI      0    0    0.0000    3    5   15   17    0
   1 C    C_BYL    0    0.0000    0.0000    0.0000    0.0000    2    3    0    0    0
   2 O    O_BYL    0    0.0000    0.6693    0.0000   -1.0338    1    0    0    0    0
   3 N    N_AMI    0    0.0000   -1.3295    0.0000    0.0000    1    4    5    0    0
   4 H    H_AMI    0    0.0000   -1.8063    0.0008    0.8561    3    0    0    0    0
   5 CA   C_ALI    0    0.0000   -2.0938    0.0000   -1.2409    3    6   15    0    0
   6 CB   C_ALI    0    0.0000   -3.3532   -0.8793   -1.1250    5    8   10   12    0
   7 HB   H_ALI    0    0.0000   -3.3648   -1.3844   -0.1697    6    0    0    0    0
   8 QG2  PSEUD    0    0.0000   -4.9118    0.1565   -1.3122    0    0    0    0    0
   9 OG1  O_HYD    0    0.0000   -3.3252   -1.8576   -2.1703    6   10    0    0    0
  10 HG1  H_OXY    0    0.0000   -3.3232   -2.7374   -1.7854    9    0    0    0    0
  11 CG2  C_ALI    0    0.0000   -4.6139   -0.0416   -1.2768    6   12   13   14    0
  12 HG21 H_ALI    0    0.0000   -4.3455    1.0012   -1.3599   11    0    0    0    8
  13 HG22 H_ALI    0    0.0000   -5.1453   -0.3488   -2.1652   11    0    0    0    8
  14 HG23 H_ALI    0    0.0000   -5.2453   -0.1825   -0.4126   11    0    0    0    8
  15 C    C_BYL    0    0.0000   -1.2475   -0.4956   -2.4079    5   16   17    0    0
  16 O    O_BYL    0    0.0000   -0.7354   -1.6152   -2.3854   15    0    0    0    0
  17 N    N_AMI    0    0.0000   -1.1045    0.3443   -3.4277   15    0    0    0    0
```

Figure A4. A description of modified threonine with D-stereochemistry (DTHR) that was added to the residue library of CYANA.

```
RESIDUE   MTYR     6   27    3   26
   1 OMEGA    0    0    0.0000    2    1    3    4    0
   2 PHI      0    0    0.0000    1    3    5   25    0
   3 CHI1     0    0    0.0000    3    5    6   13   24
   4 CHI2     0    0    0.0000    5    6   13   14   24
   5 CHI6     0    0    0.0000   16   18   23   24   24
   6 PSI      0    0    0.0000    3    5   25   27    0
   1 C    C_BYL    0    0.0000    0.0000    0.0000    0.0000    2    3    0    0    0
   2 O    O_BYL    0    0.0000   -0.6703    0.0000   -1.0328    1    0    0    0    0
   3 N    N_AMI    0    0.0000    1.3283    0.0000    0.0000    1    4    5    0    0
   4 H    H_AMI    0    0.0000    1.8067    0.0012    0.8552    3    0    0    0    0
   5 CA   C_ALI    0    0.0000    2.0926    0.0007   -1.2417    3    6   25    0    0
   6 CB   C_ALI    0    0.0000    3.0946   -1.1550   -1.2490    5    7    8   13    0
   7 HB2  H_ALI    0    0.0000    3.7086   -1.0846   -2.1335    6    0    0    0    9
   8 HB3  H_ALI    0    0.0000    3.7232   -1.0829   -0.3735    6    0    0    0    9
   9 QB   PSEUD    0    0.0000    3.7159   -1.0838   -1.2535    0    0    0    0    0
  10 QD   PSEUD    0    0.0000    2.3703   -2.6769   -1.2423    0    0    0    0   12
  11 QE   PSEUD    0    0.0000    1.3124   -4.8971   -1.2330    0    0    0    0   12
  12 QR   PSEUD    0    0.0000    1.8414   -3.7873   -1.2373    0    0    0    0    0
  13 CG   C_VIN    0    0.0000    2.4445   -2.5201   -1.2433    6   14   21    0    0
  14 CD1  C_ARO    0    0.0000    2.5614   -3.3621   -0.1441   13   15   16    0    0
  15 HD1  H_ARO    0    0.0000    3.1267   -3.0292    0.7144   14    0    0    0   10
  16 CE1  C_ARO    0    0.0000    1.9698   -4.6105   -0.1345   14   17   18    0    0
  17 HE1  H_ARO    0    0.0000    2.0716   -5.2509    0.7293   16    0    0    0   11
  18 CZ   C_VIN    0    0.0000    1.2489   -5.0319   -1.2323   15   19   23    0    0
  19 CE2  C_ARO    0    0.0000    1.1182   -4.2145   -2.3356   18   20   21    0    0
  20 HE2  H_ARO    0    0.0000    0.5541   -4.5449   -3.1953   19    0    0    0   11
  21 CD2  C_ARO    0    0.0000    1.7144   -2.9684   -2.3370   13   19   21    0    0
  22 HD2  H_ARO    0    0.0000    1.6144   -2.3257   -3.1998   21    0    0    0   10
  23 OH   O_HYD    0    0.0000    0.6577   -6.2745   -1.2276   18   24    0    0    0
  24 HH   H_OXY    0    0.0000    0.4800   -6.5407   -0.3224   23    0    0    0    0
  25 C    C_BYL    0    0.0000    1.1680   -0.1054   -2.4506    5   26   27    0    0
  26 O    O_BYL    0    0.0000    1.6224   -0.3027   -3.5762   25    0    0    0    0
  27 N    N_AMI    0    0.0000   -0.1313    0.0279   -2.2068   25    0    0    0    0
```

Figure A5. A description of modified tyrosine with L-stereochemistry (MTYR) that was added to the residue library of CYANA.

```
RESIDUE   DTYR     6   27    3   26
   1 OMEGA    0    0    0.0000    2    1    3    4    0
   2 PHI      0    0    0.0000    1    3    5   25    0
   3 CHI1     0    0    0.0000    3    5    6   13   24
   4 CHI2     0    0    0.0000    5    6   13   14   24
   5 CHI6     0    0    0.0000   16   18   23   24   24
   6 PSI      0    0    0.0000    3    5   25   27    0
   1 C    C_BYL    0    0.0000    0.0000    0.0000    0.0000    2    3    0    0    0
   2 O    O_BYL    0    0.0000    0.6703    0.0000   -1.0328    1    0    0    0    0
   3 N    N_AMI    0    0.0000   -1.3283    0.0000    0.0000    1    4    5    0    0
   4 H    H_AMI    0    0.0000   -1.8067    0.0012    0.8552    3    0    0    0    0
   5 CA   C_ALI    0    0.0000   -2.0926    0.0007   -1.2417    3    6   25    0    0
   6 CB   C_ALI    0    0.0000   -3.0946   -1.1550   -1.2490    5    7    8   13    0
   7 HB2  H_ALI    0    0.0000   -3.7086   -1.0846   -2.1335    6    0    0    0    9
   8 HB3  H_ALI    0    0.0000   -3.7232   -1.0829   -0.3735    6    0    0    0    9
   9 QB   PSEUD    0    0.0000   -3.7159   -1.0838   -1.2535    0    0    0    0    0
  10 QD   PSEUD    0    0.0000   -2.3703   -2.6769   -1.2423    0    0    0    0   12
  11 QE   PSEUD    0    0.0000   -1.3124   -4.8971   -1.2330    0    0    0    0   12
  12 QR   PSEUD    0    0.0000   -1.8414   -3.7873   -1.2373    0    0    0    0    0
  13 CG   C_VIN    0    0.0000   -2.4445   -2.5201   -1.2433    6   14   21    0    0
  14 CD1  C_ARO    0    0.0000   -2.5614   -3.3621   -0.1441   13   15   16    0    0
  15 HD1  H_ARO    0    0.0000   -3.1267   -3.0292    0.7144   14    0    0    0   10
  16 CE1  C_ARO    0    0.0000   -1.9698   -4.6105   -0.1345   14   17   18    0    0
  17 HE1  H_ARO    0    0.0000   -2.0716   -5.2509    0.7293   16    0    0    0   11
  18 CZ   C_VIN    0    0.0000   -1.2489   -5.0319   -1.2323   15   19   23    0    0
  19 CE2  C_ARO    0    0.0000   -1.1182   -4.2145   -2.3356   18   20   21    0    0
  20 HE2  H_ARO    0    0.0000   -0.5541   -4.5449   -3.1953   19    0    0    0   11
  21 CD2  C_ARO    0    0.0000   -1.7144   -2.9684   -2.3370   13   19   21    0    0
  22 HD2  H_ARO    0    0.0000   -1.6144   -2.3257   -3.1998   21    0    0    0   10
  23 OH   O_HYD    0    0.0000   -0.6577   -6.2745   -1.2276   18   24    0    0    0
  24 HH   H_OXY    0    0.0000   -0.4800   -6.5407   -0.3224   23    0    0    0    0
  25 C    C_BYL    0    0.0000   -1.1680   -0.1054   -2.4506    5   26   27    0    0
  26 O    O_BYL    0    0.0000   -1.6224   -0.3027   -3.5762   25    0    0    0    0
  27 N    N_AMI    0    0.0000    0.1313    0.0279   -2.2068   25    0    0    0    0
```

Figure A6. A description of modified tyrosine with D-stereochemistry (DTYR) that was added to the residue library of CYANA.

```
GLY 1
TRP
VAL
ALA
CYSS
VAL
GLY
ALA
CYSS
GLY
THR
VAL
CYSS
LEU
ALA
SER
GLY
GLY
VAL
GLY
DTHR
GLU
PHE
ALA
MALA
ALA
SER
MTYR
PHE
LEU 30
link SG 5 CA 28
link SG 9 CA 25
link SG 13 CA 21
```

Figure A7. An example of a complete sequence file used in the structure calculations of a Trn-β stereoisomer. Instructions for forming the thioether bridges between residues 5 and 28, 9 and 25, and 13 and 21 appear at the end of the sequence.

Appendix B. Thurincin H MS, NMR data and CYANA files

Table B1: MS/MS sequencing results for thurincin H[a]

$[b+H]^+$	$[b-H]^-$	$[b+Na]^+$	b ion #	y ion #	$[y+H]^+$	$[y-H]^-$	$[y+Na]^+$	Sequence
302			2	30		3022	3045	W
403			3	29				T
506			4	28				C
692			5	27				W
779			6	26				S
882			7	25				C
995			8	24				L
1095	1092		9	23				V
1197		1780	10	22		2025*	2067	C
1269			11	21				A
1340			12	20	1871	1869	1893	A
1443			13	19		1798		C
1530			14	18		1694		S
1611*			15	17				V
1758			16	16				E
1871		1893	17	15		1380	1404	L
1984	1982	2006	18	14	1269			L
	2094	2118	19	13		1154		N-2
			20	12	1044	1042		L
		2330	21	11			1177	V
	2405	2429	22	10	831	829		T-2
		2500	23	9	732	730	754	A
	2547	2571	24	8				A
	2646	2670	25	7	590	588		T-2
			26	6	491	489		G
	2774		27	5			513	A
	2859	2883	28	4	363	361		S-2
			29	3	278			T
			30	2	177			A
			31	1				S

[a] $[b+H]^+$ and $[y+H]^+$ fragments were obtained from infusion nanoESI MS/MS. All other fragments were obtained by MALDI MS/MS.
*Represents an ion that has lost H_2O

Table B2: ^{1}H Chemical shift assignments of thurincin H

	HN	**Hα**	**Hβ**	**others**
Asp 1		4.28	3.07, 3.00	
Trp 2	8.95	4.42	3.29, 3.18	
Thr 3	7.42	3.86	4.01	γCH_3 0.74
Cys 4	7.75	4.12	3.25, 2.63	
Trp 5	7.80	4.24	3.24, 3.15	$\zeta_3 CH$ 6.88, $\varepsilon_3 CH$ 7.51
Ser 6	7.83	4.05	3.71	
Cys 7	7.20	4.02	3.61, 2.88	
Leu 8	7.80	4.03	1.85, 1.54	γCH 1.93, δCH_3 1.00, 0.92
Val 9	7.74	3.77	2.18	γCH_3 1.04, 1.00
Cys 10	7.24	4.04	3.67, 2.80	
Ala 11	7.88	3.98	1.42	
Ala 12	7.76	4.12	1.40	
Cys 13	7.22	4.21	3.48, 3.01	
Ser 14	NA[a]	4.08	3.83, 3.77	
Val 15	7.89	4.00	2.07	γCH_3 0.92, 0.89
Glu 16	7.94	4.29	2.25, 1.91	γCH_2 2.43
Leu 17	7.76	4.07	1.72, 1.45	γCH 1.61, δCH_3 0.83, 0.77
Leu 18	8.39	3.91	1.61, 1.59	γCH 1.67, δCH_3 0.89, 0.83
Asn 19	8.28	**none**	3.23, 3.13	δNH_2 7.79, 6.86
Leu 20	NA[a]	4.03	1.84, 1.38	γCH 1.84, δCH_3 0.87, 0.83
Val 21	7.71	3.73	2.95	γCH_3 1.08, 1.00
Thr 22	8.37	**none**	4.80	γCH_3 1.16
Ala 23	8.25	4.06	1.44	
Ala 24	7.77	3.94	1.45	
Thr 25	8.55	**none**	4.88	γCH_3 1.12
Gly 26	8.15	3.91, 3.72		
Ala 27	7.72	3.93	1.42	
Ser 28	8.07	**none**	4.34, 3.93	
Thr 29	7.78	3.77	3.89	γCH_3 0.14
Ala 30	7.47	4.25	1.32	
Ser 31	7.48	4.39	3.83, 3.71	

[a]NA = not assigned. Due to spectral overlap, a chemical shift could not be definitively assigned to the HN proton of Ser 14 or Leu 20.

Table B3: Nitrogen and carbon chemical shift assignments of thurincin H

	N	**Cα**	**Cβ**	**others**
Asp 1		52.45	37.74	
Trp 2	124.89	59.56	29.04	
Thr 3	110.91	63.64	68.67	Cγ 20.79
Cys 4	117.94	57.77	33.48	
Trp 5	118.46	60.13	28.59	
Ser 6	114.29	61.82	62.65	
Cys 7	117.11	57.33	32.29	
Leu 8	119.59	57.65	42.11	Cγ 27.55, Cδ 24.64, 23.21
Val 9	115.04	64.70	31.59	Cγ 20.83, 19.76
Cys 10	117.29	56.92	31.99	
Ala 11	120.23	54.19	17.64	
Ala 12	116.66	53.02	17.87	
Cys 13	116.10	55.90	32.40	
Ser 14	NA[a]	58.71	63.63	
Val 15	116.08	63.65	32.40	Cγ 20.97, 19.95
Glu 16	118.50	55.54	27.55	Cγ 32.09
Leu 17	117.30	57.73	42.16	Cγ 26.73, Cδ 24.73, 22.84
Leu 18	121.98	58.23	40.99	Cγ 27.09, Cδ 23.80, 23.60
Asn 19	119.19	67.09	41.15	Nδ 113.27
Leu 20	NA[a]	57.80	41.86	Cγ 27.01, Cδ 25.43, 22.03
Val 21	117.02	65.52	31.69	Cγ 20.84. 20.73
Thr 22	123.63	72.36	71.53	Cγ 18.91
Ala 23	123.96	54.75	18.18	
Ala 24	120.52	55.24	18.03	
Thr 25	120.36	72.43	70.91	Cγ 18.32
Gly 26	108.18	46.35		
Ala 27	124.80	55.60	17.89	
Ser 28	116.43	72.67	65.27	
Thr 29	112.95	63.88	69.13	Cγ 20.51
Ala 30	122.01	52.16	18.79	
Ser 31	111.40	57.42	64.22	

[a]NA = not assigned. Due to spectral overlap, a chemical shift could not be definitively assigned to the amide nitrogen of Ser 14 or Leu 20.

Table B4: NOEs between the Cys and modified residues of thurincin H

NOE signals	Conclusion
Cys 13 Hβ1 ↔ Asn 19 HN Cys 13 Hβ2 ↔ Asn 19 HN	α-thio bridge between Cys 13 and Asn 19
Cys 10 HA ↔ Thr 22 HN Cys 10 Hβ2 ↔ Thr 22 HN	α-thio bridge between Cys 10 and Thr 22
Cys 7 Hβ1 ↔ Thr 25 HN Cys 7 Hβ2 ↔ Thr 25 HN	α-thio bridge between Cys 7 and Thr 25
Cys 4 Hβ1 ↔ Ser 28 HN Cys 4 Hβ2 ↔ Ser 28 HN	α-thio bridge between Cys 4 and Ser 28

```
RESIDUE   MASN     5   18    3   17
   1 OMEGA    0    0    0.0000    2    1    3    4    0
   2 PHI      0    0    0.0000    1    3    5   16    0
   3 CHI1     0    0    0.0000    3    5    6   10   15
   4 CHI2     0    0    0.0000    5    6   10   11   15
   5 PSI      0    0    0.0000    3    5   16   18    0
   1 C    C_BYL    0    0.0000    0.0000    0.0000    0.0000    2    3    0    0    0
   2 O    O_BYL    0    0.0000   -0.6697    0.0000   -1.0319    1    0    0    0    0
   3 N    N_AMI    0    0.0000    1.3291    0.0000    0.0000    1    4    5    0    0
   4 H    H_AMI    0    0.0000    1.8075    0.0012    0.8553    3    0    0    0    0
   5 CA   C_ALI    0    0.0000    2.0934   -0.0012   -1.2421    3    6   16    0    0
   6 CB   C_ALI    0    0.0000    2.0044   -1.3706   -1.9187    5    7    8   10    0
   7 HB2  H_ALI    0    0.0000    2.5478   -2.0934   -1.3275    6    0    0    0    9
   8 HB3  H_ALI    0    0.0000    0.9686   -1.6684   -1.9812    6    0    0    0    9
   9 QB   PSEUD    0    0.0000    1.7585   -1.8807   -1.6536    0    0    0    0    0
  10 CG   C_BYL    0    0.0000    2.5875   -1.3628   -3.3186    6   11   12    0    0
  11 OD1  O_BYL    0    0.0000    3.3707   -2.2405   -3.6817   10    0    0    0    0
  12 ND2  N_AMI    0    0.0000    2.2072   -0.3683   -4.1122   10   13   14    0    0
  13 HD21 H_AMI    0    0.0000    1.5805    0.2955   -3.7553   12    0    0    0   15
  14 HD22 H_AMI    0    0.0000    2.5684   -0.3393   -5.0227   12    0    0    0   15
  15 QD2  PSEUD    0    0.0000    2.0745   -0.0219   -4.3890    0    0    0    0    0
  16 C    C_BYL    0    0.0000    1.5897    1.0814   -2.1918    5   17   18    0    0
  17 O    O_BYL    0    0.0000    0.3881    1.2025   -2.4288   16    0    0    0    0
  18 N    N_AMI    0    0.0000    2.5174    1.8651   -2.7325   16    0    0    0    0
```

Figure B1. A description of modified asparagine with L-stereochemistry (MASN) that was added to the residue library of CYANA.

```
RESIDUE   DASN     5   18    3   17
   1 OMEGA    0    0    0.0000    2    1    3    4    0
   2 PHI      0    0    0.0000    1    3    5   16    0
   3 CHI1     0    0    0.0000    3    5    6   10   15
   4 CHI2     0    0    0.0000    5    6   10   11   15
   5 PSI      0    0    0.0000    3    5   16   18    0
   1 C    C_BYL    0    0.0000    0.0000    0.0000    0.0000    2    3    0    0    0
   2 O    O_BYL    0    0.0000    0.6697    0.0000   -1.0319    1    0    0    0    0
   3 N    N_AMI    0    0.0000   -1.3291    0.0000    0.0000    1    4    5    0    0
   4 H    H_AMI    0    0.0000   -1.8075    0.0012    0.8553    3    0    0    0    0
   5 CA   C_ALI    0    0.0000   -2.0934   -0.0012   -1.2421    3    6   16    0    0
   6 CB   C_ALI    0    0.0000   -2.0044   -1.3706   -1.9187    5    7    8   10    0
   7 HB2  H_ALI    0    0.0000   -2.5478   -2.0934   -1.3275    6    0    0    0    9
   8 HB3  H_ALI    0    0.0000   -0.9686   -1.6684   -1.9812    6    0    0    0    9
   9 QB   PSEUD    0    0.0000   -1.7585   -1.8807   -1.6536    0    0    0    0    0
  10 CG   C_BYL    0    0.0000   -2.5875   -1.3628   -3.3186    6   11   12    0    0
  11 OD1  O_BYL    0    0.0000   -3.3707   -2.2405   -3.6817   10    0    0    0    0
  12 ND2  N_AMI    0    0.0000   -2.2072   -0.3683   -4.1122   10   13   14    0    0
  13 HD21 H_AMI    0    0.0000   -1.5805    0.2955   -3.7553   12    0    0    0   15
  14 HD22 H_AMI    0    0.0000   -2.5684   -0.3393   -5.0227   12    0    0    0   15
  15 QD2  PSEUD    0    0.0000   -2.0745   -0.0219   -4.3890    0    0    0    0    0
  16 C    C_BYL    0    0.0000   -1.5897    1.0814   -2.1918    5   17   18    0    0
  17 O    O_BYL    0    0.0000   -0.3881    1.2025   -2.4288   16    0    0    0    0
  18 N    N_AMI    0    0.0000   -2.5174    1.8651   -2.7325   16    0    0    0    0
```

Figure B2. A description of modified asparagine with D-stereochemistry (DASN) that was added to the residue library of CYANA.

```
4     CYSS  SG    28    DSER  CA    1.6   5.00E+00
7     CYSS  SG    25    DTHR  CA    1.6   5.00E+00
10    CYSS  SG    22    DTHR  CA    1.6   5.00E+00
13    CYSS  SG    19    DASN  CA    1.6   5.00E+00
```

Figure B3. The lower limit constraints files of a thurincin H isomer [columns 1 to 6 define the residue numbers, names and specific atoms involved in the S-Cα linkage, column 7 defines the bond length constraint in Å, and column 8 gives the weighting function of the constraint].

```
4     CYSS  SG    28    DSER  CA    2.0   5.00E+00
7     CYSS  SG    25    DTHR  CA    2.0   5.00E+00
10    CYSS  SG    22    DTHR  CA    2.0   5.00E+00
13    CYSS  SG    19    DASN  CA    2.0   5.00E+00
```

Figure B4. The upper limit constraints files of a thurincin H isomer [columns 1 to 6 define the residue numbers, names and specific atoms involved in the S-Cα linkage, column 7 defines the bond length constraint in Å, and column 8 gives the weighting function of the constraint].

```
ASP 1
TRP
THR
CYSS
TRP
SER
CYSS
LEU
VAL
CYSS
ALA
ALA
CYSS
SER
VAL
GLU
LEU
LEU
DASN
LEU
VAL
DTHR
ALA
ALA
DTHR
GLY
ALA
DSER
THR
ALA
SER 31
link SG 4 CA 28
link SG 7 CA 25
link SG 10 CA 22
link SG 13 CA 19
```

Figure B5. An example of a complete sequence file used in the structure calculations of a thurincin H stereoisomer. Instructions for forming the thioether bridges between residues 4 and 28, 7 and 25, 10 and 22, and 13 and 19 appear at the end of the sequence.

Appendix C. (C9S, C14S)-leucocin A NMR data

Table C1: ^{1}H Chemical shift assignments of (C9S, C14S)-leucocin A

	HN	Hα	Hβ	others
Lys 1		3.91	1.80	γCH_2 1.32, 1.28, δCH_2 1.68, εCH_2 2.95
Tyr 2	8.17	4.60	2.99, 2.93	
Tyr 3	7.73	4.51	3.08, 2.81	
Gly 4	6.90	3.95, 3.71		
Asn 5	7.98	4.74	2.86	δNH_2 7.20, 6.40
Gly 6	8.22	4.03, 3.91		
Val 7	7.80	3.90	2.09	γCH_3 0.94, 0.89
His 8	8.19	4.66	3.36, 3.26	εCH 8.35
Ser 9	8.24	4.50	4.05, 3.94	
Thr 10	8.06	4.33	4.37	γCH_3 1.30
Lys 11	8.19	4.28	1.92, 1.86	γCH_2 1.52, 1.47, δCH_2 1.69, εCH_2 2.96
Ser 12	8.03	4.35	3.99, 3.91	
Gly 13	8.21	3.96		
Ser 14	8.03	4.45	4.04, 3.96	
Ser 15	7.93	4.40	4.06, 3.95	
Val 16	7.71	3.97	2.04	γCH_3 1.00, 0.84
Asn 17	7.91	4.67	2.90, 2.85	δNH_2 7.21, 6.35
Trp 18	8.04	4.43	3.40, 3.37	ε_1NH 9.27, ζ_2CH 7.29, η_2CH 7.55, ζ_3CH 7.20
Gly 19	8.30	3.90, 3.81		
Glu 20	8.20	4.11	2.28, 2.15	γCH_2 2.62, 2.49
Ala 21	8.01	4.08	1.49	
Phe 22	8.81	4.18	2.92, 2.75	δCH 7.06, εCH 7.25, ζCH 7.14
Ser 23	8.22	4.10	4.13, 4.03	
Ala 24	8.44	4.14	1.53	
Gly 25	8.05	3.88, 3.77		
Val 26	8.10	3.62	1.91	γCH_3 0.76, 0.70
His 27	8.00	4.19	3.25	εCH 8.38
Arg 28	8.08	4.12	2.00	γCH_2 1.75, 1.63, δCH_2 3.17, 3.13, η_2NH_2 7.02, 6.87
Leu 29	8.06	4.13	1.84, 1.62	γCH 1.75, δCH_3 0.89, 0.86
Ala 30	8.23	4.17	1.41	
Asn 31	7.81	4.76	2.95, 2.80	δNH_2 7.31, 6.35
Gly 32	8.04	3.98, 3.88		
Gly 33	8.17	4.00, 3.81		
Asn 34	7.77	4.71	2.83, 2.76	δNH_2 7.06, 6.13
Gly 35	7.89	3.81, 3.68		
Phe 36	7.57	4.56	3.02, 2.90	
Trp 37	7.46	4.77	3.36, 3.27	δ_1CH 7.22, ε_1NH 9.38, ζ_3CH 7.10

Table C2: Nitrogen and carbon chemical shift assignments of (C9S, C14S)-leucocin A

	N	Cα	Cβ	others
Lys 1		55.95	33.00	Cγ 23.69, Cδ 28.69, Cε 42.04
Tyr 2	121.54	58.15	38.95	
Tyr 3	122.16	58.04	38.87	
Gly 4	106.65	45.51		
Asn 5	116.58	53.58	38.36	Cγ 176.66, Nδ 108.24
Gly 6	107.53	45.91		
Val 7	120.39	64.62	31.98	Cγ 20.36, 20.15
His 8	118.14	56.64	28.51	Cε 135.26
Ser 9	114.73	59.53	63.76	
Thr 10	114.70	63.49	69.65	Cγ 20.41
Lys 11	121.37	57.80	32.24	Cγ 24.62, Cδ 28.65, Cε 42.26
Ser 12	114.40	59.91	63.39	
Gly 13	109.23	46.16		
Ser 14	114.47	59.82	63.63	
Ser 15	116.55	60.14	63.42	
Val 16	121.14	64.40	32.34	Cγ 20.70, 20.06
Asn 17	118.86	54.68	38.39	Cγ 176.42, Nδ 108.19
Trp 18	120.73	60.38	29.03	$N\varepsilon_1$ 125.36, $C\zeta_2$ 113.98, $C\eta_2$ 120.56, $C\zeta_3$ 126.25
Gly 19	105.36	47.18		
Glu 20	121.58	58.95	27.96	Cγ 32.53
Ala 21	122.40	55.35	17.50	
Phe 22	119.67	61.00	39.07	Cδ 132.89, Cε 131.09, Cζ 131.27
Ser 23	113.32	61.47	62.96	
Ala 24	125.73	55.58	17.47	
Gly 25	106.13	47.04		
Val 26	120.74	66.33	31.58	Cγ 21.61, 20.23
His 27	115.11	59.52	27.57	Cε 135.54
Arg 28	119.05	59.08	29.76	Cγ 27.32, Cδ 43.16, $N\eta_2$ 123.39
Leu 29	120.21	57.43	42.06	Cγ 26.82, Cδ 23.98, 22.56
Ala 30	120.61	53.83	17.87	
Asn 31	114.61	53.46	38.97	Cγ 177.34, Nδ 108.75
Gly 32	106.96	45.96		
Gly 33	107.13	45.49		
Asn 34	116.98	53.00	38.81	Cγ 176.66, Nδ 108.44
Gly 35	106.85	45.11		
Phe 36	118.64	57.97	39.52	
Trp 37	119.62	56.07	29.25	$C\delta_1$ 129.49, $N\varepsilon_1$ 126.09, $C\zeta_3$ 126.44